Dr. David Carlson
Editor
Earth System Science Data

January 11, 2021

Dear Dr. Carlson,

Subject: Revision and resubmission of manuscript #essd-2020-151

Thank you for reviewing our manuscript. We also appreciate Drs. Tomeu Rigo and Rebecca Adams-Selin for their thoughtful comments and suggestions. We have carefully reviewed the comments and have revised the manuscript accordingly. Our responses are given in a point-by-point manner below. We have also attached a version of the manuscript and supplement with trackable changes and hope the revised manuscript is suitable for publication.

Please address all correspondence concerning this manuscript to me (jianfeng.li@pnnl.gov).

Thanks again for your time.

Sincerely,

Jianfeng Li
Atmospheric Sciences and Global Change Division
Pacific Northwest National Laboratory
Richland, Washington, US, 99354

Response to Reviewer #1: Dr. Tomeu Rigo

Thank you for your careful and thorough reading of this manuscript and your thoughtful comments and suggestions. Our responses follow your comments (in *Italics*).

General comments:

The authors present a new methodology for identifying mesoscale convective systems based on the combination of three different sources: satellite imagery, weather radar volumetric mosaics and rainfall charts obtained from the merging of radar estimation and rain gauge values. The work results interesting but there are some points that should be solved before its accepting. One is the large number of typos associated with the table and figures references (what is S1, S2, …?).

Reply:

Thanks. Table Sx or Figure Sx means figures or tables in the supplement. There is a supplement attached to the main manuscript.

Second one is conceptual, and more important to me: when the authors define isolated deep convection, they do not refer in any case to supercells. Besides, while the limitations of the methodology about the spatial and temporal scales are minimized in the case of MCS (because of their extent and duration), the part of isolated convection does not look like solved as clearly. I think that the authors should try to explain better the limitations (if exists) about this issue or, at least, explain why the results are not affected by this point.

Reply:

Thank you for your comments. When we defined IDC, it was actually non-MCS convection events, consisting of many different types of deep convection, as we explained in Lines 295 – 300 in the revised main manuscript. Supercell is another topic. The well-known characteristics of supercells include hook echoes, bounded weak-echo regions, and the presence of strong rotation updrafts (Lynn, 2002; Naylor et al., 2012). Rotation recognition (or rotation-related variables, such as vertical vorticity, low-level-shear, azimuthal shear, etc.) is necessary for the automatic identification of supercells (Lakshmanan and Smith, 2009; Lynn, 2002; Smith et al., 2012; Stumpf et al., 1998). The source datasets used in this study do not contain Doppler velocities or environmental wind fields and cannot be used to calculate rotation. Besides, rotation is not involved in the current FLEXTRKR algorithm, making FLEXTRKR unable to recognize supercells. Here, we need to emphasize that there are no direct relationships between MCS/IDC and supercell. Both MCS and IDC events may show supercell features sometimes during their lifetimes. The advantage of our data product is that it provides detailed information of each MCS/IDC track, such as the location, time, and a series of convective feature characteristics (area, echo intensity, echo-top height, etc.) of the track. Users of the data product can further identify supercell features of the track by incorporating rotation datasets.

A limitation in the identification of IDC is related to the temporal resolution. The 1-hour temporal resolution is enough for MCSs, as they are generally large and long-lived. However, some IDC events associated with weak convection can be shorter than 1 hour,

which can not be resolved by our data product. We discussed the temporal resolution limitation in Section 4.3 (Lines 658 – 683 in the revised main manuscript). We found that, from the perspective of precipitation, the IDC events with PF lifetimes shorter than 1 hour might be much less important than those IDC events identified in our data product, and the missing of the IDC events with PF lifetime shorter than 1 hour should have little impact on our results.

Finally, the number of results is excessive and, in my opinion, deviates the attention about the main objective of the research: the application of the new methodology. On the contrary, they do not compare their results with other methodologies, which are easy to find and can verify the lines provided by the current manuscript. In the next lines, the authors will find more detailed comments regarding some other points.

Reply:

Thank you for your suggestions. The manuscript's primary purpose is to introduce a new data product useful to the Earth science community, which is the aim of the ESSD journal. The methodology to produce the data product is just part of the data product introduction. The uncertainties, validation/assessment, and potential usage and applications of the data product are also parts of the data product introduction. We indeed show some results in Section 3. However, those results are straightforward and can be easily obtained from the data product. The primary purpose of Section 3 is to validate the quality of the data product and confirm that the data product is consistent with our definitions and general knowledge. Section 3.2, about precipitation characteristics from different sources, is also an example of the potential applications of

the data product. Therefore, we'd like to keep these results except that we have revised some discussions about convection intensity in Lines 374 – 383 and 387 – 393 to make the sentences more understandable. We agree with you that we should add some comparisons between our results with other studies, further validating the data product. We have compared our results with other studies in Lines 346 – 349, 366 – 368, 385 – 386, 435 – 437, 442 – 445, 498 – 500, 509 – 517, 558 – 560, and 569 – 572 in the revised main manuscript.

Abstract

Acronyms (MCS, IDC, FLEXTRKR), references (Li et al., 2020) and web pages (http://dx.doi.org/10.25584/1632005) are not frequent and preferable not included in abstracts. Do you consider strictly necessary for the understanding of the text to maintain them? In my opinion, at least the last sentence should be removed

Reply:

Thank you for your suggestions. We have deleted "FLEXTRKR" in Line 17 in the revised main manuscript since the acronym was only used once there, but we'd like to keep "MCS" and "IDC" in the abstract as they were used several times. Using the acronyms can simplify the abstract. For the last sentence, the doi link and reference is a requirement of the ESSD journal.

Introduction

Although Doswell et al (1996) is still one of the reference paper in this field, there are

many more recent research manuscripts that are noticeable to include in the L46-61 paragraph, for instance:

- *Brooks, H. E., Doswell III, C. A., & Kay, M. P. (2003). Climatological estimates of local daily tornado probability for the United States. Weather and Forecasting, 18(4), 626-640.*
- *Taszarek, M., Allen, J. T., Púčik, T., Hoogewind, K. A., & Brooks, H. E. (2020). Severe Convective Storms across Europe and the United States. Part II: ERA5 Environments Associated with Lightning, Large Hail, Severe Wind, and Tornadoes. Journal of Climate, 33(23), 10263-10286.*

Reply:

Thank you for your suggestions. Brooks et al. (2003) investigated the climatological distributions of tornado occurrence over the contiguous United States. Taszarek et al. (2020) investigated meteorological environments associated with lightning, large hail, severe wind, and tornadoes. Both studies used severe weather hazards as proxies of thunderstorms, confirming the relationship between the weather hazards and deep convection. We have cited both papers in Lines 50 – 51 in the revised main manuscript. Besides, we have also cited another study from Koehler (2020) in Line 50 in the revised main manuscript, which examined the climatological distributions of lightning flashes and thunderstorm days over the contiguous United States.

L62-70: "deep convection" is repeated five times in the same paragraph. Please, modify the text using other options

Reply:

Thanks. We have deleted “deep convection” in Lines 64 and 70 and made some changes to the paragraph. Now those sentences are as follows.

‘The crucial roles of deep convection motivate the need for more accurate and comprehensive datasets to improve understanding and modeling of this process and its impacts. To this end, datasets with information on the location and time of occurrence, intensity, and other properties of deep convection are necessary to understand and quantify its impacts on the hydrologic cycle, severe weather hazards, large-scale circulations, etc. While field campaign data can provide detailed information on deep convection properties, they are limited in space-time coverage for statistical analysis. A corresponding reliable long-term dataset is undoubtedly useful for model evaluation and development (Prein et al., 2017; Yang et al., 2017).’

L75-76: when you introduce IDC, are you including supercells? If the answer is yes, can you confirm that all the sentences that following this are true? In special, I disagree with the points about the higher rain rates, larger echo top heights, and greater ice masses.

Reply:

Thank you for your comments. The definitions of IDC and MCS in Rowe et al. (2011) and Rowe et al. (2012) are similar to our study, based on precipitation feature (different from PF in our study) major axis length and aspect ratio between the major axis and the minor axis. In their studies, IDC is defined as a track with precipitation feature major

axis length < 100 km and aspect ratio less than 5:1; while an MCS is defined as a track with precipitation feature major axis length > 100 km. In short, their definition depends on the size and shape of convective areas but not rotation, which cannot be used to identify supercells, as we mentioned above. Since the results of Rowe et al. (2011) and Rowe et al. (2012) were only based on the North American Monsoon Experiment (NAME) in the summer of 2004, to be more accurate, we change 'can' to 'may' in Line 77 in the revised main manuscript so that the results are not representative of all cases.

Again, lines 80 and 82 depend on if you consider supercells or not in the IDC database

Reply:

Thank you for your comments. The conclusion that MCSs might be associated with more favorable environmental conditions is based on the results of Rowe et al. (2012). Their definitions of IDC and MCS have been described above briefly. French and Parker (2008) compared isolated supercells and MCSs, but their MCSs also showed supercell features. It is consistent with our previous point: supercells can be isolated or embedded in MCSs. We cannot separate supercell in our data product based on the algorithms and source datasets used in this study. To be more accurate, we have changed the sentence as follows (Lines 81 – 87 in the revised main manuscript).

'Rowe et al. (2012) also suggested that the enhanced rainfall from MCSs might be associated with more favorable environmental conditions, such as higher convective available potential energy (CAPE) and wind shear. CAPE and wind shear can impose

different impacts on the initiation and evolution of IDC and MCSs (French and Parker, 2008).'

L103-104: "We produce the data product"?

Reply:

We have combined the two sentences into one as follows (Lines 104 – 113 in the revised main manuscript).

'The data product is developed by applying an updated Flexible Object Tracker (FLEXTRKR) algorithm (Feng et al., 2018; Feng et al., 2019) and the Storm Labeling in Three Dimensions (SL3D) algorithm (Starzec et al., 2017) to the NCEP (National Centers for Environmental Prediction) / CPP (the Climate Prediction Center) L3 4 km Global Merged IR V1 brightness temperature (T_b) dataset (Janowiak et al., 2017), the 3-D Gridded NEXRAD Radar (Gridrad) dataset (Homeyer and Bowman, 2017), the NCEP Stage IV precipitation dataset (Lin and Mitchell, 2005), and melting level heights from ERA5 (ECMWF, 2018).'

Source datasets and algorithms

L120-121: "We only use the hourly Tb data in the FLEXTRKR algorithm discussed below, as all other datasets are only available at an hourly interval" Do you think that this time resolution could have any influence in the results?

Reply:

We discussed the limitations of the temporal resolution in Section 4.3 (Lines 658 – 683). We missed some short-duration (< 1 hour) convective events due to the 1-hour resolution of the data product. If all source datasets were at a resolution of 30 minutes, we would identify some IDC events shorter than 1 hour. Then, the data product would be somewhat different from the current one. Suppose we only used the half-hour T_b data but still used the hourly precipitation and reflectivity datasets in the FLEXTRKR algorithm. In that case, the results might also be different, but the difference should be much smaller than the former case with all half-hour source datasets. The reason is that T_b is only used to identify CCS in FLEXTRKR, and the confirmation of MCS and IDC still needs precipitation and reflectivity data.

Figure 1: Maybe you should include a small map of the whole American continent and a box for the zoomed area shown in the current caption

Reply:

We have added another subplot in Figure 1 showing the whole North American continent and a red box indicating the data product domain. Please see Lines 218 – 226 in the revised main manuscript.

L202 (and many more): you cite "table S1" in the text, but I was not able finding this table in your manuscript.

Reply:

Table Sx or Figure Sx means figures or tables in the supplement. There is a supplement

attached to the main manuscript.

Para 283-288: according to these lines, maybe you should change the label of "IDC" category.

Reply:

Thank you for your suggestions. At the very beginning, we tried to use "non-MCS deep convection," which is the exact meaning of these convective events. But considering that we plan to add hurricanes on the basis of the data product in other studies, we need to assign a specific name to them. We also thought about the term "quasi-isolated deep convection," which Bigelbach et al. (2014) used to separate stronger air mass thunderstorms, multicell clusters, and supercells from weak convection and MCSs. However, "quasi" means "apparently but not really," which can not represent those isolated thunderstorms in our data product. Finally, we decided to use "isolated deep convection" following the idea of Rowe et al. (2011) and Rowe et al. (2012), which used isolated convection to distinguish smaller convection events from MCSs, similar to our data product. Since we mentioned the limitation of the term "IDC" in the manuscript, we'd like to keep it after careful considerations.

In figure 2(b), it seems that there are more categories that the maximum number of the legend. Is this it?

Reply:

Yes. There are too many small clouds, and it is hard to assign a distinct color to each cloud. It is better to assign a constant color to those smaller clouds to show those larger clouds clearly.

Results

This section results too much extend and hard to follow (because its density and the large number of interesting results). However, I miss the comparison of your results with other works such:

Fritsch, J. M., R. J. Kane, and C. R. Chelius, 1986: The Contribution of Mesoscale Convective Weather Systems to the Warm-Season Precipitation in the United States. J. Climate Appl. Meteor., 25, 1333–1345, https://doi.org/10.1175/1520-0450(1986)025<1333:TCOMCW>2.0.CO;2.

Or the cited:

Haberlie, A. M., and W. S. Ashley, 2019: A Radar-Based Climatology of Mesoscale Convective Systems in the United States. J. Climate, 32, 1591–1606, https://doi.org/10.1175/JCLI-D-18-0559.1.

Geerts, B. (1998). Mesoscale convective systems in the southeast United States during 1994–95: A survey. Weather and Forecasting, 13(3), 860-869.

Then, my suggestion is reducing the results to the most interesting one (for instance, the percentage of contributing rainfall for each type) and comparing with the others works. This is also because the goal of the paper is to present the methodology, but not the

"climatology". Then, the authors could have the opportunity of publishing the climatological results in another manuscript.

Reply:

Thank you for your suggestions. We have compared our results with other studies in Lines 346 – 349, 366 – 368, 385 – 386, 435 – 437, 442 – 445, 498 – 500, 509 – 517, 558 – 560, and 569 – 572 in the revised main manuscript.

As mentioned above, the primary purpose of the manuscript is to introduce a new data product. Those results in Section 3 are used to validate the quality of the data product and confirm that the data product is consistent with our definitions and general knowledge. Section 3.2, about precipitation characteristics from different sources, is also an example of the potential applications of the data product. Therefore, we'd like to keep these results except that we have revised some discussions about convection intensity in Lines 374 – 383 and 387 – 393 to make the sentences more understandable.

Uncertainties of the data product

About lines 540-549: there are many more radar errors that can affect NEXRAD or other network, e.g. beam blockage, false echoes related with EM interferences, solar interferences, volumetric conus influence, among others. Have they considered or they can appear in the volumes?

Reply:

When we talked about potential low-quality observations, we meant a summary of those

small errors well-mitigated by the quality control approach from Homeyer and Bowman (2017) (http://gridrad.org/software.html), including false echoes related to electromagnetic interferences and solar interferences.

We think you meant the cone of silence when you mentioned 'volumetric conus influence.' The cone of silence and beam blockage is related to the missing radar data discussed in section 4.2 (Lines 647 – 657 in the revised main manuscript), as no data are available under the impact of the cone of silence and beam blockage. According to the explanation of Homeyer and Bowman (2017), many errors in the native NEXRAD level-2 observations that propagate into the Gridrad 3.1 data can be largely reduced through the quality control approach, but not completely. Therefore, there are still uncertainties in the radar reflectivity data we used for SL3D and FLEXTRKR. That is why we think that using three different datasets in the FLEXTRKR and SL3D algorithms could improve our identification of MCS and IDC than using a single dataset.

L566-567: "we identify the most robust MCS/IDC events satisfying all the criteria based on the three datasets" Which percentage of data satisfies the whole set of criteria?

Reply:

Annually (2004 – 2017), we identified 802,633 tracks based on CCS (brightness temperature T_b), and finally, we obtained 45,800 MCS and IDC tracks. Therefore, 5.7% of the CCS tracks satisfy all the criteria.

About Stage IV: do you think that geo-statistics contribute to the error, at the time of

generating the final product?

Reply:

We think you meant the 'erroneous precipitation' hours in Lines 618 – 624 in the revised main manuscript. We are not sure where the error is from. We contacted the NCEP Stage IV team for help, but they did not know the root cause of the issue either. We suspect that maybe NEXRAD Level-II data (reflectivity, radial velocity, etc.) were not well-filtered and processed in Stage I (the first step of Stage IV). Then the errors were transferred to the following steps to generate Stage IV. Geo-statistics may cause the spread of the errors to larger areas.

L584-586: The sentence "Most grid cells in the US have less than 2% missing hours, which should have a negligible impact on the data product." Is, at least, debatable. According to figure 5, it is difficult finding pixels with more than 170 hours of rainfall per year (combining both maps). This is less than 2% of the yearly hours (8760). If most of those missing hours coincide with a part of the rainfall period, the results changing notably. Please, explain better this point.

Reply:

Thank you for your comments. However, Figure 7 (the old Figure 5) cannot be compared with Figure S10 (the old Figure S12) directly, as Figure 7 and Figure S10 use different criteria. Firstly, according to the caption, Figure 7 shows the number of hours per year when any MCS/IDC events produce > 1 mm hourly accumulated rainfall in a grid cell, while Figure S10 is about missing values (not related to precipitation amount

thresholds). If we exclude the limitation of > 1 mm hourly accumulated rainfall and count the number of hours when any MCS/IDC clouds overpass the grid cell, we can obtain Figure R1.

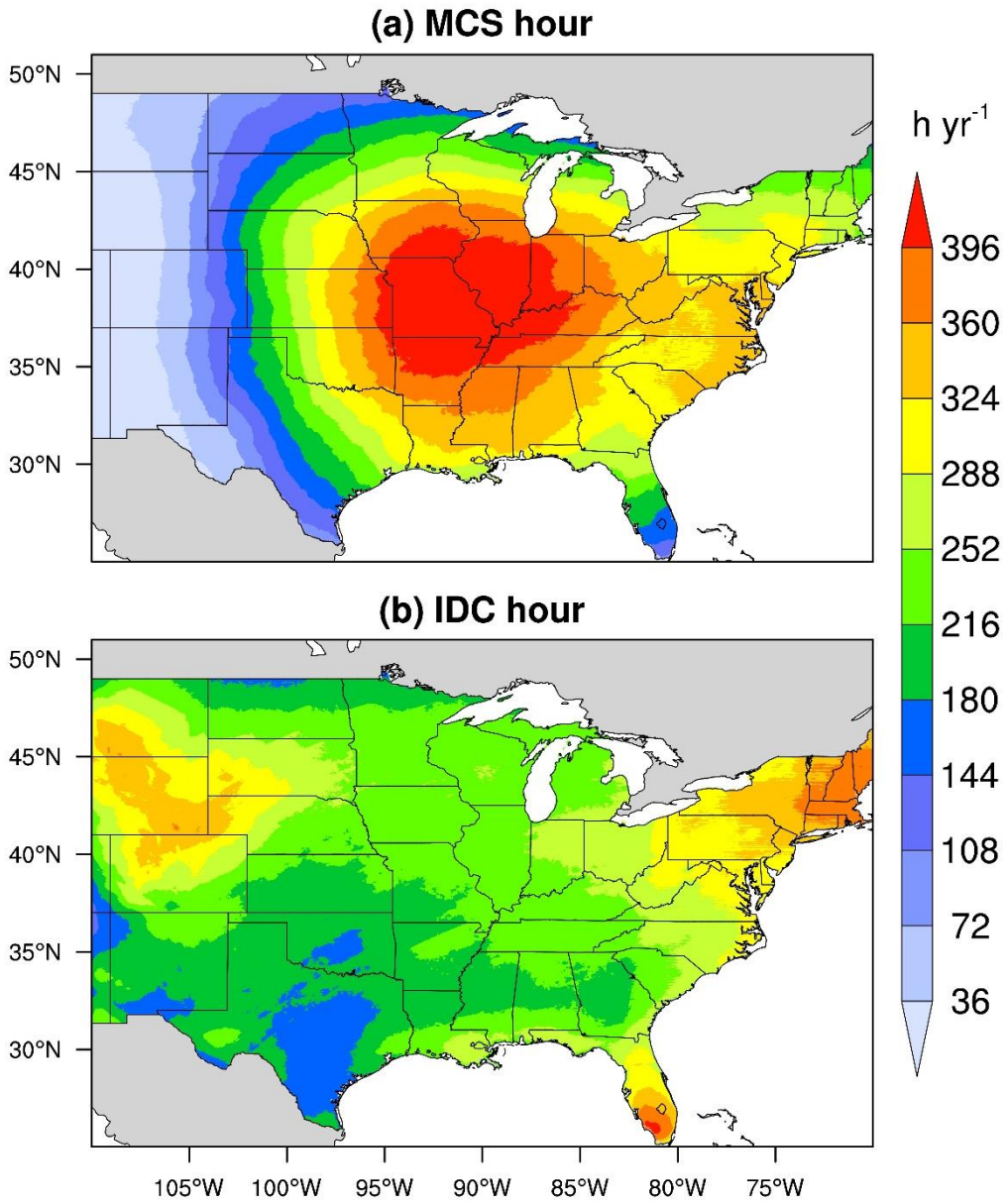

Figure R1. Spatial distributions of annual mean MCS/IDC hours for 2004 – 2017. (a) is for MCS, and (b) is for IDC. The annual mean MCS/IDC hour of a grid cell is the number of hours per year when any MCS/IDC clouds overpass the grid cell.

Secondly, Figure 7 shows the results satisfying all the criteria based on three types of observations, not just precipitation. That is to say, we excluded those 716 hours not

passing the T_b criteria in Lines 632 – 635 in the revised main manuscript in Figure 7. However, when we plotted Figure S10, we included those 716 hours in the denominator to exclude the impact of missing T_b on the missing precipitation calculation. If we exclude those 716 hours and only count the number of hours with missing precipitation in the rest hours with T_b satisfying the criteria in Lines 632 – 635, we can obtain Figure R2, which can be compared to Figure R1. Now we find that most grids only have about 40 – 60 missing precipitation hours per year, while MCS/IDC hours in Figure R1 are mostly above 400 per year, much higher than the values in Figure R2. Anyway, we agree with you that the 40-60 missing precipitation hours can still affect the MCS/IDC results if all these hours coincide with a part of the rainfall period. However, that is an extreme case and unlikely to happen. We find that missing precipitation generally occurs continuously in space. For example, from 2004-03-03T07:00:00Z to 2004-03-03T12:00:00Z, all precipitation data are missing over the data product domain. Therefore, they only affect our identification of MCS and IDC during a short period and should have little impact on our final climatological results from the perspective of time length.

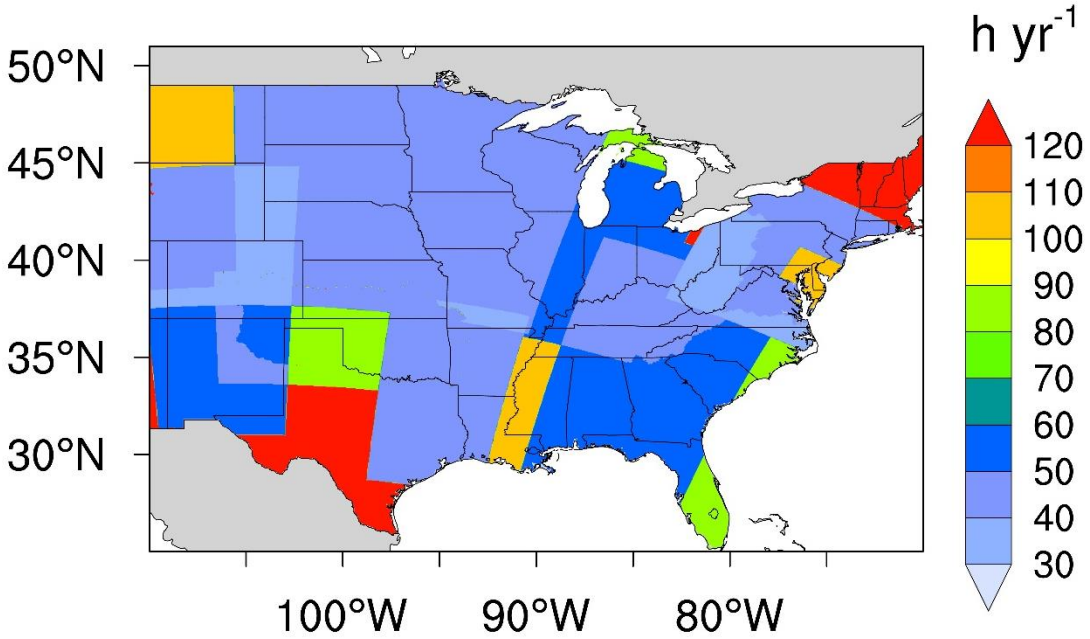

Figure R2. The distribution of the number of hours with missing precipitation per year between 2004 and 2017. Those 716 hours not satisfying the T_b criteria in Lines 572 – 576 are not included in the calculation.

L647: What is for you "most of the important MCS"?

Reply:

Here, we meant MCSs with the most precipitation, which can be derived from the sentence in Lines 706 – 707 in the revised main manuscript: 'The fraction of MCS precipitation only increases by 6% (from 45% to 51%), compared to the almost doubling of MCS number (from 454 to 857).' It means that the increased MCSs contribute little to the total MCS precipitation. To be more accurate, we have added 'with heavy precipitation' in Lines 708 – 709 in the revised main manuscript. The sentence now is as follows.

'The fraction of MCS precipitation only increases by 6% (from 45% to 51%), compared to the almost doubling of MCS number (from 454 to 857), suggesting the MCS

definition in the original data product is capable of capturing most of the important MCSs with heavy precipitation.’

References:

Brooks, H. E., Doswell III, C. A., and Kay, M. P.: Climatological estimates of local daily tornado probability for the United States, Weather and Forecasting, 18, 626-640, https://doi.org/10.1175/1520-0434(2003)018<0626:CEOLDT>2.0.CO;2, 2003.

French, A. J., and Parker, M. D.: The initiation and evolution of multiple modes of convection within a meso-alpha-scale region, Weather and forecasting, 23, 1221-1252, https://doi.org/10.1175/2008WAF2222136.1, 2008.

Homeyer, C. R., and Bowman, K. P.: Algorithm Description Document for Version 3.1 of the Three-Dimensional Gridded NEXRAD WSR-88D Radar (GridRad) Dataset, available at http://gridrad.org/pdf/GridRad-v3.1-Algorithm-Description.pdf, 23, 2017.

Koehler, T. L.: Cloud-to-Ground Lightning Flash Density and Thunderstorm Day Distributions over the Contiguous United States Derived from NLDN Measurements: 1993–2018, Monthly Weather Review, 148, 313-332, https://doi.org/10.1175/MWR-D-19-0211.1, 2020.

Lakshmanan, V., and Smith, T.: Data mining storm attributes from spatial grids, Journal of Atmospheric and Oceanic Technology, 26, 2353-2365, https://doi.org/10.1175/2009JTECHA1257.1, 2009.

Lynn, R. J.: The WDSS-II supercell identification and assessment algorithm, 21st Conference on Severe Local Storms, 2002,

Naylor, J., Gilmore, M. S., Thompson, R. L., Edwards, R., and Wilhelmson, R. B.: Comparison of objective supercell identification techniques using an idealized cloud model, Monthly weather review, 140, 2090-2102, https://doi.org/10.1175/MWR-D-11-00209.1, 2012.

Rowe, A. K., Rutledge, S. A., and Lang, T. J.: Investigation of microphysical processes occurring in isolated convection during NAME, Monthly weather review, 139, 424-443, https://doi.org/10.1175/2010MWR3494.1, 2011.

Rowe, A. K., Rutledge, S. A., and Lang, T. J.: Investigation of microphysical processes occurring in organized convection during NAME, Monthly weather review, 140, 2168-2187, https://doi.org/10.1175/MWR-D-11-00124.1, 2012.

Smith, B. T., Thompson, R. L., Grams, J. S., Broyles, C., and Brooks, H. E.: Convective modes for significant severe thunderstorms in the contiguous United States. Part I: Storm classification and climatology, Weather and Forecasting, 27, 1114-1135, https://doi.org/10.1175/WAF-D-11-00115.1, 2012.

Stumpf, G. J., Witt, A., Mitchell, E. D., Spencer, P. L., Johnson, J., Eilts, M. D., Thomas, K. W., and Burgess, D. W.: The National Severe Storms Laboratory mesocyclone detection algorithm for the WSR-88D, Weather and Forecasting, 13, 304-326, https://doi.org/10.1175/1520-0434(1998)013<0304:TNSSLM>2.0.CO;2, 1998.

Taszarek, M., Allen, J. T., Púčik, T., Hoogewind, K. A., and Brooks, H. E.: Severe convective storms across Europe and the United States. Part II: ERA5 environments associated with

lightning, large hail, severe wind, and tornadoes, J. Clim., 33, 10263-10286, https://doi.org/10.1175/JCLI-D-20-0346.1, 2020.

Response to Reviewer #2: Dr. Rebecca Adams-Selin

Thank you for your careful and thorough reading of this manuscript and your thoughtful comments and suggestions. Our responses follow your comments (in *Italics*).

This article details the development of a highly useful convective climatology for the eastern two-thirds of the continental U.S. Considerable effort is expended explaining the datasets used, potential sources of error and mitigation strategies, and the complex processing steps involved. Future applications for the dataset are described. I am concerned about the design of the algorithm not separating organized from unorganized isolated convection, potentially leading to impacts in the precipitation intensity calculations. Pending responses to my comments enumerated below, I recommend acceptance bending major revisions.

Major comments:

1. *The IDC category is potentially lumping unorganized isolated convection in with highly organized isolated convection such as supercells. I can certainly see the authors' points that MCSs are larger systems than all IDC, and thereby should result in larger transport, circulation, and accumulated precipitation impacts (e.g., Lines 80-82), but citation of a few studies in the literature to that effect would be useful so as to not argue from intuition alone.*

Reply:

We had references for the larger transport and circulation effects of MCSs than IDC in Lines 75 – 77 in the revised main manuscript and have added another reference from

Bigelbach et al. (2014). We think you meant the sentence in Lines 85 – 87 in the revised main manuscript: 'Compared to IDC, MCSs tend to occur in more favorable environmental conditions, such as higher convective available potential energy (CAPE) and wind shear (French and Parker, 2008), potentially making them more conducive to hazardous weather.' We have changed this sentence with more details. We intended to emphasize the different environmental conditions associated with MCS and IDC, but the old sentence misrepresents the results of Rowe et al. (2012) and French and Parker (2008). Now the sentences are as follows.

'Rowe et al. (2012) also suggested that the enhanced rainfall from MCSs might be associated with more favorable environmental conditions, such as higher convective available potential energy (CAPE) and wind shear. CAPE and wind shear can impose different impacts on the initiation and evolution of IDC and MCSs (French and Parker, 2008).'

Severer precipitation impacts can also be reflected by our citation of Rowe et al. (2012).

> *Regarding severe weather, however, including tornados and large hail, MCSs are not the primary generators. Instead, supercells are (e.g., Wurman et al. 2011 BAMS). Furthermore, supercells are increasingly recognized as producers of heavy and extreme rainfall (e.g., Hitchens and Brooks 2013 AR; Smith et al. 2001 JHM). The conflation of two dynamical storm classes when evaluating the impacts of IDCs has potential impacts on the authors' discussion of precipitation intensities (e.g., Figs.3, S9; Sections 3.2.1, 3.2.2). The precipitation intensity distribution for IDC events is in all likelihood a bimodal distribution, containing output from isolated*

non-supercells and supercells (e.g., Hitchens and Brooks 2013 AR).

Can the authors examine the IDC portion of their climatology to determine if there is indeed a bimodal distribution captured within? If not, why do the authors think that the FLEXTRKR algorithm failed to capture heavy/extreme rain events from supercells?

Is it possible to add an additional class to the FLEXTRKR algorithm to detect supercells specifically? How likely is it that supercells will be classified as IDC within this climatology? Supercells do frequently grow upscale into an MCS (e.g., Reif and Bluestein 2017): in such a situation, would the entire storm track be classified as an MCS in this climatology? How would these "misclassifications" impact the results?

Reply:

Thank you for your suggestions. However, a supercell is defined from another perspective but not based on the size and duration of convective systems used to separate MCS from IDC in this study. Supercell characteristics include hook echoes, bounded weak-echo regions, and the presence of strong rotation updrafts (Lynn, 2002; Naylor et al., 2012). Rotation recognition (or rotation-related variables, such as vertical vorticity, low-level-shear, azimuthal shear, etc.) is necessary for the automatic identification of supercells (Lakshmanan and Smith, 2009; Lynn, 2002; Smith et al., 2012; Stumpf et al., 1998). Therefore, the current FLEXTRKR algorithm cannot identify supercells. Also, high spatiotemporal-resolution radar radial velocity data are

needed to calculate rotation-related variables. Gridrad V3.1 only provides hourly reflectivity data. So, the source datasets used in our study is not sufficient to identify supercells either. We find that the Multi-Radar Multi-Sensor radar dataset mentioned below provides half-hourly rotation data, which can be used for supercell identification by using corresponding algorithms.

Since supercell is defined differently, there are no direct relationships between MCS/IDC and supercell. That is to say, both MCS and IDC events can contain supercell features sometimes during their lifetimes (French and Parker, 2008). Supercell can exist in both the MCS and IDC categories in our data product. Our examination of MCS/IDC hourly rain rate probability density functions (PDFs) does not show a significant bimodal shape (Figure R3). The interesting point is that although the PDF shapes between MCS and IDC are very similar, MCS PDF shows slightly larger values in high rain rates, reflecting relatively more pixels with larger rain rates for MCSs. Figure R3 does not mean that supercells do not have higher precipitation intensities than non-supercells. Since supercells only account for a small portion of all convective events, mixing them with other IDC/MCS events in a single PDF would conceal the feature of supercells. We need a supercell PDF to display its uniqueness compared to other convective systems, similar to what Hitchens and Brooks (2013) did.

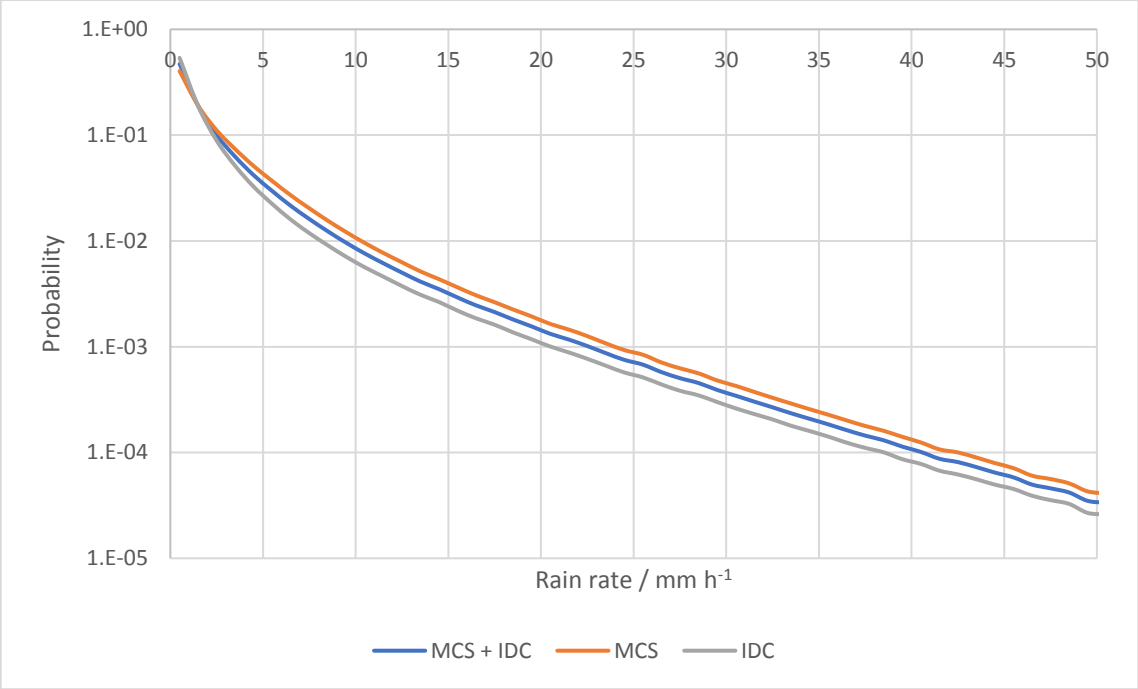

Figure R3. PDFs of pixel-level hourly rain rates for MCS and IDC events during 2004 – 2017. The orange line is for MCS, the gray line is for IDC, and the blue line is for MCS + IDC. We do not consider rain rates larger than 51 mm h^{-1} in this figure. However, the number of those pixels with rain rates > 51 mm h^{-1} only accounts for about 0.03% of the total number. Excluding them should have little impact on the PDFs.

As we mentioned, the current FLEXTRKR algorithm cannot detect supercells by merely adding a supercell class. To identify supercells, we need to add rotation-related variables in FLEXTRKR and make some other changes to the algorithm. Theoretically, FLEXTRKR can be used to detect supercells if enough contents are added. However, this is not necessary. The advantage of our data product is that we store a lot of information for each MCS/IDC track. Supercells can be further identified by combining our data product with other datasets. For example, we know the location and time information of an MCS in our data product. The Multi-Radar Multi-Sensor radar dataset can provide rotation data over the location during the time of that MCS. We can determine whether the MCS shows supercell features or not based on the coincident rotation data (may need some calculations, derivations, and coding). It is much easier

than modifying FLEXTRKR.

For the last question, the answer much depends on the researchers and the purposes. In the study of Hitchens and Brooks (2013), they defined hours as instances of supercell thunderstorms if a storm showed supercell features at that hour. If the FLEXTRKR could identify supercell features, we would define an MCS/IDC track as supercell if it showed supercell features at any time during its lifetime. Or we could set some fraction thresholds: an MCS was defined as a supercell track only when the fraction of hours showing supercell features was larger than a threshold. Ultimately, this depends on the specific purpose of the research. Our data product is not intended for supercell research specifically.

2. *I had trouble following exactly how the SL3D algorithm output was incorporated into the climatology. Given its introduction at the start of section 2.2 I had first assumed its classifications were important to the FLEXTRKR algorithm in identifying the CCFs and PFs. After reading I'm no longer convinced it is used in that effort at all, but instead just incorporated into the climatology after the fact. How are the five SL3D categories, listed in lines 221-222, used to identify the CCFs and PFs (if they are)? If not, how are those categories used? On a display note, how does the data shown in Fig. 2e correspond to the five categories listed?*

Reply:

Thank you for your comments. The usage of the SL3D outputs can be reflected in the definitions of CCF and PF (Lines 238 – 243 in the revised main manuscript). CCF is a

continuous updraft/convective area with precipitation > 0 mm h^{-1}, and PF is a continuous updraft/convective/precipitating-stratiform area with precipitation > 1 mm h^{-1}. Here, updraft (convective updraft), convective, precipitating-stratiform are the categories from SL3D (Table S2). The SL3D algorithm can determine the type of radar echo (five categories or missing value) of each pixel in Figure 2e (we have added explanations to the values in Figure 2e in Lines 327 – 328 in the revised main manuscript: 1, convective updraft; 2, convective; 3, precipitating stratiform; 4, non-precipitating stratiform; 5, anvil). Therefore, after we identify a CCS track, we know the echo type (five categories) and Stage IV hourly precipitation of all the pixels in the CCS track at any time. Among these pixels, we identify continuous areas satisfying specific criteria, such as CCFs and PFs. That is to say, the convective/stratiform status is from SL3D outputs, which is necessary for the FLEXTRKR algorithm to determine MCS and IDC tracks.

3. *How is rain rate calculated? Is it based on assumed Z-R relationships from the GridRad data (which introduces a host of problems), or is it calculated by subtracting accumulated Stage-IV rainfall at successive hours? If calculated by subtracting rainfall accumulations, that has the unfortunately side effect of evenly distributing rainfall over the full hour, lessening peak intensities that occur over shorter periods of time. Given the temporal resolution of the datasets used here, that issue can't be avoided, but the authors should include a few sentences qualifying their discussion on precipitation intensity (beyond the issues already noted in major comments #1.)*

Reply:

Thank you for your comments. All precipitation values and associated variables are derived from the Stage-IV data, which represents hourly accumulated precipitation. As the temporal resolution of all the source datasets and the MCS/IDC data product is 1 hour, we do not need to make any subtractions to Stage-IV rainfall at consecutive hours. Rain rate or precipitation intensity just denote mean hourly precipitation. Anyway, we agree with you that the 1-hour resolution may reduce peak precipitation intensities occurring in minutes. However, since Sections 3.1 and 3.2 talks about climatological mean characteristics, we do not expect the sub-hour heterogeneity will affect the results in Sections 3.1 and 3.2. We mentioned the limitation of the 1-hour temporal resolution in Section 4.3 from the perspective of Gridrad reflectivity, which only includes reflectivities within ± 3.8 minutes of each hour. Considering the 1-hour temporal resolution of our study, we cannot find a suitable place to add discussions about the sub-hour precipitation variations.

4. *Figures S1 and S5 are key to understanding the descriptions in the text and should be moved to the main article.*

Reply:

Thanks. We have moved the two figures to the main manuscript (Figures 3 and 4). All figure numberings have been changed accordingly in the revised main manuscript and supplement.

Minor comments:

- *Lines 39-45: This is a nice summary of the wide-reaching impacts of deep convection. On a minor note, should multiple citations within one reference be provided in chronological order?*

Reply:

Thanks. According to the reference format of ESSD on https://www.earth-system-science-data.net/submission.html#references, in-text citations can be sorted chronologically or alphabetically or based on relevance, depending on the author's preference. There is no specific requirement for it. References listed at the end of the manuscript should be sorted alphabetically under the first author's name, except for those with the same first author. Our current in-text citation format follows the rule of reference listing at the end of the manuscript.

- *Line 49: "deep convection associated thunderstorms" –> deep convective thunderstorms*

Reply:

Have corrected. Please see Line 51 in the revised main manuscript.

- *Line 201: Is the "nearestst*od" *method essentially nearest neighbor? A brief one-line description would be helpful.*

Reply:

Yes. There are two types of nearest neighbor methods in the ESMF regrid module:

"neareststod" and "nearestdtos." The "neareststod" method maps each destination point to the closest source point, while the "nearestdtos" method maps each source point to the destination point. In the "nearestdtos" approach, it is noteworthy that some destination points may not be mapped to any source points, which cannot be used in our study. We have added a sentence to explain the "neareststod" method in Lines 187 – 188 in the revised main manuscript, just as follows.

'The "neareststod" method maps each destination point to the closest source point.'

- *Lines 229-231: A few sentences describing, theoretically, how CCFs and PFs differ, and what kind of features each of these is intended to represent, would be helpful. It wasn't always clear to me why essentially two separate datasets were being developed.*

Reply:

As defined in Lines 238 – 243 in the revised main manuscript, CCF is a continuous updraft/convective area with precipitation > 0 mm h^{-1}, and PF is a continuous updraft/convective/precipitating-stratiform area with precipitation > 1 mm h^{-1}. The difference between PF and CCF can be clarified in Figure 3 in Lines 336 – 337 in the revised main manuscript. In the last row of Figure 3, the red color indicates CCF, and the green color indicates PF. Theoretically, PF represents areas with significant precipitation (> 1 mm h^{-1}), while CCF represents convective cores. They are somewhat spatiotemporally overlapped, as generally convective cores have substantial precipitation. There is another variable used in the definition: intense convective cell,

which is convective cells with column maximum reflectivity ≥ 45 dBZ and precipitation > 1 mm h^{-1} (pink areas in Figure 3) (Lines 271 – 272 in the revised main manuscript), representing the strongest convection activity (other values may be used in other studies, such as 40 dBZ in Bigelbach et al. (2014)). In the definition of MCS, we use PF and intense convective cells, while in the definition of IDC, we use PF and CCF. PF is intended to denote the size of a convective system. However, PF cannot be used solely in the MCS/IDC definitions, as PF may contain no convective precipitation but just stratiform precipitation. Intense convective cells and CCF are used to confirm that a track is convective. Specifically, intense convective cells are also used in the MCS definition to ensure that the MCS convection activity is strong enough. Our idea of using two different types of variables to separate different convective systems is similar to Bigelbach et al. (2014), which used an areal variable to represent the size of the convective object and a reflectivity threshold to confirm convection. A similar definition approach was also found in Geerts (1998).

Now the question is whether we can only use CCF or intense convective cells to define MCS and IDC. The answer is Yes. Rowe et al. (2011) and Rowe et al. (2012) used cell features to separate MCS and IDC events. Their cells required reflectivity (the only dataset used in their tracking algorithm) to be larger than 35 or 45 dBZ, which are similar to convective cores in our study. In their studies, IDC is defined as a track with cell major axis length < 100 km and aspect ratio less than 5:1; while an MCS is defined as a track with cell major axis length > 100 km. However, this kind of definition may be problematic in some cases when multiple convective cores of an MCS are somewhat separated by weaker precipitating stratiform clouds, making it unable to satisfy the size

criterion. The significant large precipitating-stratiform area associated with some convective systems, especially for MCSs (Parker and Johnson, 2000), may cause CCF or intense convective cells unable to represent the actual sizes of the convective systems. Since there are no precise definitions of MCS or IDC and many studies used different source datasets and definition criteria, using CCF or intense convective cell solely in the MCS or IDC definition is practically possible, but the limitations should be understood.

Finally, CCS is another variable to determine the size of the convective systems in our study. However, cold-top upper-level clouds do not always contain precipitation, and CCS cannot represent the size of the precipitating area. So, we used CCS and PF together in the definition. This is another reason why we use several different variables in the definition of MCS and IDC: we hope to minimize the false identification of MCS and IDC events by combining different datasets.

We have added some explanations about our purposes to use PF, CCF, and intense convective cells in the updated FLEXTRKR algorithm in Lines 239 – 240, 242 – 243, and 272 in the revised main manuscript.

- *Lines 290-293, Fig. 2: I was only able to understand the descriptions of the pixel-level information by reading the caption of Fig. 2. I'd move the description in the caption into the text and expand lines 290-293 by referencing each subfigure individually.*

Reply:

Thank you for your suggestions. We have added more detailed explanations to Figures

2f-2i in Lines 302 – 311 in the revised main manuscript. Now, the sentences are as follows.

'Figures 2f – 2i give an example of the pixel-level MCS/IDC information at 2005-07-04T03:00:00Z. Figure 2f displays the spatial coverages of MCS/IDC tracks at that time at pixel scale and the corresponding unique numbers of these tracks. From Figure 2f, we know whether a pixel belongs to an MCS/IDC track and the number of the track if the pixel belongs to a track. We can further determine whether the track is an MCS or IDC event from Figure 2g, which shows the types (MCS or IDC) of the tracks in Figure 2f at the pixel scale. Figures 2h and 2i are similar to Figures 2f and 2g, respectively. The difference is that Figures 2h and 2i only show pixels with precipitation > 1 mm h^{-1} in that hour.'

- *Lines 345-346, 349, 356, 358: Six different proxies for convective intensity are used in a small section: convective precipitation area, convective 20-dBZ echo-top height, area with column max reflectivity >= 45DBZ, max 30-dBZ echo-top height, max 40-dBZ echo-top height, mean convective 20-DBZ echo-top height. Why are all these different proxies are being used – do the underlying results differ? I'd find it easier to read if the convective intensity results were all discussed in the frame of one proxy.*

Reply:

By using multiple variables, we just wanted to confirm that our results are robust. In addition, we hoped to separate the strongest convective activity (area with column max

reflectivity ≥ 45DBZ and max 40-dBZ echo-top height) from the mean convective activity (convective 20-dBZ echo-top height). Since the original sentences are confusing, we have made some changes in Lines 363 – 364, 374 – 383, and 387 – 393, and only used convective 20-dBZ echo-top height as the proxy for mean convective intensity. Table 1 (Line 404 in the revised main manuscript) and Table S5 (Line 89 in the revised supplement) have been updated accordingly.

- *Lines 363-370: While Section 3.2 is a good application of the climatology product, it isn't "a detailed examination of the 3D evolutions of MCS/IDC events."*

Reply:

No, it isn't. Section 3.2 is just an example of the potential applications of the data product, as we mentioned in Line 400 in the revised main manuscript. The data product can be useful in a variety of other studies, although we only show some direct results from the data product in this study. In fact, although Section 3.1 also shows some results related to MCS and IDC, it is more intended to be used to verify our data product, to ensure the MCS and IDC climatological characteristics consistent with our algorithm definitions and general knowledge. Therefore, we summarize the potential applications of the data product in Lines 395 – 400 in the revised main manuscript. Lines 400 – 402 is used to connect with Section 3.2.

- *Line 391-393: Instead of using "stratiform" as the name for all precipitation not associated with MCSs or IDCs, I suggest the phrase "non-convective". "Stratiform" is confusing as there is stratiform rain within both MCSs and IDCs.*

Reply:

Thank you for your suggestions. We have changed “stratiform” in Section 3.2 and Section 4 to “non-convective” (NC) accordingly, as well as figures and tables in the revised main manuscript and supplement. Besides, we have added another sentence in Lines 426 – 428 in the revised main manuscript discussing the limitation of NC precipitation, possibly containing some convective-associated rain. We think adding this sentence can make the definition more accurate, although we also discussed the limitation in Section 3.2.3 and Section 4.

- *Lines 451, 460, 466: Discussion of Figure S9 happens before that of Figure S8.*

Reply:

Thank you for your suggestions. Figures S6 (the old Figure S8) and S7 (the old Figure S9) first appeared in Line 493 with the correct order. In this sentence, we wanted to keep precipitation amounts and fractions together (because precipitation fractions are calculated from precipitation amounts), so we put S6 before S7. We understand that we first discussed Figure S7 in detail to make the paragraph easy and fluent. However, we had a summarized sentence at the beginning of the paragraph and intended to discuss these figures together. Therefore, we want to keep the current figure order.

- *Lines 565-567: Can the authors elaborate how each dataset is incorporated into the CCF/PF and CCS criteria listed in Section 2.2?*

Reply:

As defined in Lines 238 – 243 and 249 in the revised main manuscript, CCF is a continuous updraft/convective area with precipitation > 0 mm h^{-1}, PF is a continuous updraft/convective/precipitating-stratiform area with precipitation > 1 mm h^{-1}, and CCS is generally a continuous area with T_b < 241 K (exceptions and details are discussed in Lines 248 – 257 in the revised main manuscript). As mentioned above, all the precipitation values are from Stage-IV, not related to Gridrad reflectivity at all in this study. Gridrad only provides reflectivity Z_H, and satellite infrared T_b dataset only provides T_b. Therefore, we can understand which datasets are used based on their definitions. CCS is mainly based on the satellite T_b dataset. We use "mainly" is because, as demonstrated in Lines 254 – 257 in the revised main manuscript, CCSs sharing the same coherent precipitation feature (different from PF) are connected, and the coherent precipitation feature is defined based on reflectivity. PF, firstly, is related to Stage IV precipitation dataset, as it requires precipitation > 1 mm h^{-1}. Secondly, updraft/ convective/precipitating-stratiform categories are from the SL3D algorithm (Lines 229 – 232 in the revised main manuscript), and SL3D is based on Gridrad reflectivity and ERA5 melting-level heights (Lines 232 – 233 in the revised main manuscript). Therefore, PF is defined based on Stage IV, Gridrad, and ERA5 datasets. CCF is similar to PF, since it is also related to SL3D categories and precipitation. Because all these datasets are at the same grids, we are able to handle them simultaneously, such as finding continuous areas satisfying specific criteria, e.g. CCS, CCF, and PF. After finding out CCS/CCF/PFs, we can calculate their characteristics, such as area, major axis length, rain rate, aspect ratio, etc.

- *Line 613: Instead of individual NEXRAD radar data, could the Multi-Radar Multi-*

Sensor radar dataset be used? (https://www.nssl.noaa.gov/projects/mrms/)

Reply:

Just to be clear, the GridRad radar dataset used in our study is a mosaic of all the NEXRAD radar data east of the Rocky Mountains, but not "individual radar data." Based on the parameter "3D Mosaic Levels" shown on https://mrms.nssl.noaa.gov/qvs/product_viewer/, the Multi-Radar Multi-Sensor radar dataset can be used by the SL3D and FLEXTRKR algorithms after re-gridding. The Multi-Radar Multi-Sensor radar dataset has a resolution of 1 km and 2 minutes, covering 33 vertical levels from 0.5 km to 19 km, which is better than the Gridrad 3.1 dataset used in our study. In addition, the Multi-Radar Multi-Sensor data also contains rotation, which can be used for supercell identification.

- *Line 633: Section 3.2.2 –> Section 2.2.2*

Reply:

Thanks. We have corrected it. Please see Line 694 in the revised main manuscript

- *Section 4.4: I appreciate the authors' testing of the MCS and IDC definition criteria and discussion of that criteria's impact on classified precipitation. I would recommend the authors urge caution of future researchers using this dataset to examine transport or large-scale circulation impacts without conducting their own, similar analysis.*

Reply:

Thank you for your suggestions. We have added a relevant sentence in Lines 744 – 749 in the revised main manuscript. The sentence is as follows.

‘Lastly, although our sensitivity test in Section 4.4 shows that precipitation characteristics are similar between two different sets of MCS/IDC definition criteria, we still recommend users conduct further sensitivity tests and examine the impact of different definition criteria on the results if the data product is applied to other studies, such as the effects of MCS and IDC events on atmospheric circulation, environmental conditions associated with the initiation and evolution of MCS and IDC events, and MCS/IDC associated weather hazards.’

References:

Bigelbach, B., Mullendore, G., and Starzec, M.: Differences in deep convective transport characteristics between quasi‐isolated strong convection and mesoscale convective systems using seasonal WRF simulations, J. Geophys. Res.-Atmos., 119, 11,445-411,455, https://doi.org/10.1002/2014JD021875, 2014.

French, A. J., and Parker, M. D.: The initiation and evolution of multiple modes of convection within a meso-alpha-scale region, Weather and forecasting, 23, 1221-1252, https://doi.org/10.1175/2008WAF2222136.1, 2008.

Geerts, B.: Mesoscale convective systems in the southeast United States during 1994–95: A survey, Weather and Forecasting, 13, 860-869, https://doi.org/10.1175/1520-0434(1998)013<0860:MCSITS>2.0.CO;2, 1998.

Hitchens, N. M., and Brooks, H. E.: Preliminary investigation of the contribution of supercell thunderstorms to the climatology of heavy and extreme precipitation in the United States, Atmospheric research, 123, 206-210, https://doi.org/10.1016/j.atmosres.2012.06.023, 2013.

Lakshmanan, V., and Smith, T.: Data mining storm attributes from spatial grids, Journal of Atmospheric and Oceanic Technology, 26, 2353-2365, https://doi.org/10.1175/2009JTECHA1257.1, 2009.

Lynn, R. J.: The WDSS-II supercell identification and assessment algorithm, 21st Conference on Severe Local Storms, 2002,

Naylor, J., Gilmore, M. S., Thompson, R. L., Edwards, R., and Wilhelmson, R. B.: Comparison of objective supercell identification techniques using an idealized cloud model, Monthly weather review, 140, 2090-2102, https://doi.org/10.1175/MWR-D-11-00209.1, 2012.

Parker, M. D., and Johnson, R. H.: Organizational modes of midlatitude mesoscale convective systems, Monthly weather review, 128, 3413-3436, https://doi.org/10.1175/1520-0493(2001)129<3413:OMOMMC>2.0.CO;2, 2000.

Rowe, A. K., Rutledge, S. A., and Lang, T. J.: Investigation of microphysical processes occurring in isolated convection during NAME, Monthly weather review, 139, 424-443, https://doi.org/10.1175/2010MWR3494.1, 2011.

Rowe, A. K., Rutledge, S. A., and Lang, T. J.: Investigation of microphysical processes occurring in organized convection during NAME, Monthly weather review, 140, 2168-2187, https://doi.org/10.1175/MWR-D-11-00124.1, 2012.

Smith, B. T., Thompson, R. L., Grams, J. S., Broyles, C., and Brooks, H. E.: Convective modes for significant severe thunderstorms in the contiguous United States. Part I:

Storm classification and climatology, Weather and Forecasting, 27, 1114-1135, https://doi.org/10.1175/WAF-D-11-00115.1, 2012.

Stumpf, G. J., Witt, A., Mitchell, E. D., Spencer, P. L., Johnson, J., Eilts, M. D., Thomas, K. W., and Burgess, D. W.: The National Severe Storms Laboratory mesocyclone detection algorithm for the WSR-88D, Weather and Forecasting, 13, 304-326, https://doi.org/10.1175/1520-0434(1998)013<0304:TNSSLM>2.0.CO;2, 1998.

A high-resolution unified observational data product of mesoscale convective systems and isolated deep convection in the United States for 2004 – 2017

Jianfeng Li[1*], Zhe Feng[1], Yun Qian[1*], L. Ruby Leung[1]

[1] Atmospheric Sciences and Global Change Division, Pacific Northwest National Laboratory, Richland, Washington

* *Correspondence to* Jianfeng Li (jianfeng.li@pnnl.gov) and Yun Qian (yun.qian@pnnl.gov)

Abstract

Deep convection possesses markedly distinct properties at different spatiotemporal scales. We present an original high-resolution (4 km, hourly) unified data product of mesoscale convective systems (MCSs) and isolated deep convection (IDC) in the United States east of the Rocky Mountains and examine their climatological characteristics from 2004 to 2017. The data product is produced by applying an updated ~~FLEXTRKR (~~Flexible Object Tracker~~)~~ algorithm to hourly satellite brightness temperature, radar reflectivity, and precipitation datasets. Analysis of the data product shows that MCSs are much larger and longer-lasting than IDC, but IDC occurs about 100 times more frequently than MCSs, with a mean convective intensity comparable to that of MCSs. Hence both MCS and IDC are essential contributors to precipitation east of the Rocky Mountains, although their precipitation shows significantly different spatiotemporal characteristics. IDC precipitation concentrates in summer in the Southeast with a peak in the late afternoon, while MCS precipitation is significant in all seasons, especially for spring and summer in the Great Plains. The spatial distribution of MCS precipitation amounts varies by seasons, while diurnally, MCS precipitation generally peaks during nighttime except in the Southeast. Potential uncertainties and limitations of the data product are also discussed. The data product is useful for investigating the atmospheric environments and physical processes associated with different types of convective systems, quantifying the impacts of convection on hydrology, atmospheric chemistry, and severe weather events, and evaluating and improving the representation of convective processes in weather and climate models. The data product is available at http://dx.doi.org/10.25584/1632005 (Li et al., 2020).

1 Introduction

In the atmosphere, deep convection refers to thermally driven turbulent mixing that displaces air parcels from the lower atmosphere to the troposphere above 500 hPa (Davison, 1999), leading to the development of convective storms. The heavy rain-rates associated with deep convection can significantly affect the water cycle (Hu et al., 2020) and other aspects such as soil erosion (Nearing et al., 2004), surface water quality (Carpenter et al., 2018; Motew et al., 2018), and managed and unmanaged ecosystems (Angel et al., 2005; Derbile and Kasei, 2012; Rosenzweig et al., 2002) that are essential elements of the biogeochemical cycle. By redistributing heat, mass, and momentum within the atmosphere, deep convection also has important effects on atmospheric chemistry (Anderson et al., 2017; Andreae et al., 2001; Choi et al., 2014; Grewe, 2007; Thompson et al., 1997; Twohy et al., 2002), large-scale environments (Houze Jr, 2004; Piani et al., 2000; Stensrud, 1996, 2013; Wang, 2003), and radiation balance (Feng et al., 2011; Zhang et al., 2017).

Besides its effects on the energy, water, and biogeochemical cycles, deep convection also has more direct societal impacts. As a significant source of natural hazards such as tornadoes, hail, wind gusts, lightning, and flash flooding, deep convection poses critical threats to human life and property (Brooks et al., 2003; Doswell III et al., 1996; Koehler, 2020; Taszarek et al., 2020). During 1950 – 1994, deep convection ~~associated~~ thunderstorms produced 47% of annual rainfall and up to 72% of summer rainfall on average east of the Rocky Mountains (Changnon, 2001b). During the same period, both the number of severe thunderstorms and deep convection precipitation has increased in most regions of the contiguous United States (CONUS) (Changnon, 2001a, b; Groisman et al., 2004). Folger and Reed (2013) found that hazards

associated with thunderstorms accounted for 57% of annual insured catastrophe losses since 1953. Since the 1980s, the inflation-adjusted economic losses due to convective storms increased from about $5 billion to about $20 billion in the recent decade (https://www.iii.org/fact-statistic/facts-statistics-tornadoes-and-thunderstorms). With warmer temperatures, the environments of hazardous convective weather are projected to become more frequent in the future (Diffenbaugh et al., 2013; Seeley and Romps, 2015), although few robust trends have emerged in the recent decades (Houze Jr et al., 2019; Tippett et al., 2015).

The crucial roles of deep convection motivate the need for more accurate and comprehensive datasets ~~of deep convection~~ to improve understanding and modeling of this process and its impacts. To this end, datasets with information on the location and time of occurrence, intensity, and other properties of deep convection are necessary to understand and quantify its impacts on the hydrologic cycle, severe weather hazards, large-scale circulations, etc. While field campaign data can provide detailed information on deep convection properties, they are limited in space-time coverage for statistical analysis. A corresponding reliable long-term dataset ~~of deep convection~~ is undoubtedly useful for model evaluation and development (Prein et al., 2017; Yang et al., 2017).

Deep convection can exist as isolated convective storms or organized storms with mesoscale structures. A mesoscale convective system (MCS) is an aggregate of convective storms organized into a larger and longer-lived system, which is the largest type of deep convection. Due to their much longer duration and broader spatial coverage, MCSs generally have stronger and longer-lasting influences on large-scale circulations than isolated deep convection (IDC) events (Bigelbach et al., 2014; Stensrud, 1996, 2013). MCSs ~~can~~ may also

produce higher rain rates, larger echo top heights, and greater water and ice masses than IDC (Rowe et al., 2011, 2012). The enhanced rain rates in MCSs might be caused by larger amounts of ice falling out and melting, higher amounts of liquid water below the melting level, and higher concentrations of smaller drops (Rowe et al., 2011, 2012). Rowe et al. (2012) also suggested that the enhanced rainfall from MCSs might be associated with more favorable environmental conditions, such as higher convective available potential energy (CAPE) and wind shear. CAPE and wind shear can impose different impacts on the initiation and evolution of IDC and MCSs (French and Parker, 2008). ~~Compared to IDC, MCSs tend to occur in more favorable environmental conditions, such as higher convective available potential energy (CAPE) and wind shear (French and Parker, 2008), potentially making them more conducive to hazardous weather.~~

Considering the significant differences between IDC and MCS events, a reliable long-term dataset not only describing the characteristics of deep convection but also separating IDC events from MCSs is useful. With the deployment of operational remote sensing platforms such as geostationary satellites and ground-based radar network several decades ago, scientists have developed numerical algorithms to automatically detect deep convective systems and track their evolutions over large areas and for long durations on the basis of continuous measurements from remote sensors (Cintineo et al., 2013; Feng et al., 2011; Feng et al., 2012; Futyan and Del Genio, 2007; Geerts, 1998; Hodges and Thorncroft, 1997; Liu et al., 2007; Machado et al., 1998). Objective tracking of deep convection has been applied to geostationary satellite data (Cintineo et al., 2013; Sieglaff et al., 2013; Walker et al., 2012) and Next Generation Weather Radar (NEXRAD) data (Haberlie and Ashley, 2019; Pinto et al., 2015) in the United States (US) over different periods. However, a long-term climatological data product of MCS and IDC events over the CONUS has heretofore not been developed.

Here, building on the work by Feng et al. (2019), which developed an algorithm for MCS tracking and a dataset for MCSs for eastern CONUS, we produce a unified high-resolution data product of both MCS and IDC events and analyze their characteristics east of the Rocky Mountains for 2004 – 2017. The data product is developed by applying an updated Flexible Object Tracker (FLEXTRKR) algorithm (Feng et al., 2018; Feng et al., 2019) and the Storm Labeling in Three Dimensions (SL3D) algorithm (Starzec et al., 2017) ~~using~~ to the NCEP (National Centers for Environmental Prediction) / CPP (the Climate Prediction Center) L3 4 km Global Merged IR V1 brightness temperature (T_b) dataset (Janowiak et al., 2017), the 3-D Gridded NEXRAD Radar (Gridrad) dataset (Homeyer and Bowman, 2017), the NCEP Stage IV precipitation dataset (Lin and Mitchell, 2005), and melting level heights from ERA5 (ECMWF, 2018)~~. We produce the data product by applying an updated Flexible Object Tracker (FLEXTRKR) algorithm (Feng et al., 2018; Feng et al., 2019) and the Storm Labeling in Three Dimensions (SL3D) algorithm (Starzec et al., 2017) to the datasets mentioned above~~. Section 2 describes the updated FLEXTRKR and SL3D algorithms in detail, as well as the source datasets used by the algorithms. In Section 3, we first compare the climatological characteristics between MCS and IDC events based on the MCS/IDC data product. Then, as an application of the data product, we examine the spatiotemporal precipitation characteristics of MCS and IDC events. In Section 4, we discuss the uncertainties and limitations of the data product. Section 5 provides the availability information of the data product. Finally, we summarize the study in Section 6.

2 Source datasets and algorithms

2.1 Source datasets

2.1.1 Merged 4-km Infrared brightness temperature dataset

In this study, we identify cold clouds associated with MCSs and IDC by using the NOAA NCEP/CPP L3 half-hourly 4 km Global Merged IR V1 infrared T_b data for 2004 – 2017 (Janowiak et al., 2017). The dataset is a combination of various geostationary IR satellites with parallax correction and viewing angle correction, therefore, providing continuous coverage globally from 60°S – 60°N with a horizontal resolution of about 4 km and a temporal resolution of 0.5 hours (Janowiak et al., 2001). We only use the hourly T_b data in the FLEXTRKR algorithm discussed below, as all other datasets are only available at an hourly interval.

2.1.2 Three-dimensional Gridded NEXRAD Radar (Gridrad) dataset

Gridrad is an hourly 3-D radar reflectivity (Z_H) mosaic combining individual NEXRAD radar observations to a Cartesian gridded dataset, with a horizontal resolution of 0.02° × 0.02° and a vertical resolution of 1 km. The dataset covers 115° W to 69° W in longitude, 25° N to 49° N in latitude, and 1 to 24 km in altitude above sea level (ASL). Homeyer and Bowman (2017) produced the dataset by applying a four-dimensional binning procedure to merge level-2 Z_H data from 125 National Weather Service (NWS) NEXRAD weather radars to Gridrad grid boxes at analysis times. Only the level-2 observations within 300 km of each radar and 3.8 minutes of the analysis time were used in the binning procedure. The Gridrad Z_H was the weighted average of the level-2 observations within the Gridrad grid boxes to reduce the potential loss of information. The weight calculation of each level-2 observation followed a Gaussian scheme in both space

and time. Observation weight was negatively correlated with the distance of the observation from the source radar and the time difference between the observation and analysis time. The Gridrad dataset provides the total weight of the level-2 observations within each Gridrad grid box, which is useful for quality control. In addition, the number of level-2 radar observations (N_{obs}) and the number of level-2 radar observations with echoes (N_{echo}) within each Gridrad grid box around analysis times (± 3.8 min) are also available in the Gridrad dataset.

We obtain the Gridrad datasets between 2004 and 2017 from NCAR/UCAR Research Data Archive (RDA) (https://rda.ucar.edu/datasets/ds841.0/, last access: Jan 2, 2020). Following the quality control criteria of Homeyer and Bowman (2017) (http://gridrad.org/software.html, last access: Jan 22, 2020), we remove potential low-quality observations, scanning artifacts, and non-meteorological echoes from biological scatters and artifacts. Then we regrid Gridrad Z_H onto the 4 km satellite Merged IR grids by using the "bilinear" method from the Earth System Modeling Framework (ESMF) Python module (https://www.earthsystemcog.org/projects/esmpy/) as follows.

First, we convert the Gridrad logarithmic reflectivity Z_H to linear reflectivity ($Z^{'}$: $mm^6\ m^{-3}$). We then set $Z^{'}$ in grid boxes with radar observations but no echoes ($N_{obs} > 0$, but Z_H = NAN; NAN, Not-A-Number) to 0 ($Z^{'} = 0$). Here the physical interpretation is that NEXRAD scans those grid boxes, but no detectable hydrometers return any echo. The primary motivation of this procedure is to avoid the reduction of the number of valid reflectivity values after re-gridding, as the ESMF bilinear method treats destination point as NAN as long as there is one NAN value in the source points. A common scenario is at the edge between hydrometeor echoes and clear air. Setting $Z^{'}$ of those grid boxes having radar observations but no echoes to NAN would cause all

surrounding destination points to become NAN even though all other source points have valid $Z^{'}$ values, which would reduce the number of re-gridded valid Z_H ($Z_H \neq$ NAN) by about 20% for 2004 – 2017. After the "bilinear" re-gridding of $Z^{'}$, we convert the linear reflectivity $Z^{'}$ back to the logarithmic reflectivity Z_H. And we set Z_H equal to NAN for those grid boxes with $Z^{'}$ equal to 0. Now the NAN values are acceptable and won't affect the SL3D algorithm and FLEXTRKR algorithm discussed below.

2.1.3 NCEP Stage IV precipitation dataset

The NCEP Stage IV precipitation dataset provides hourly rain accumulations over polar stereographic grids across the CONUS with a resolution of 4.76 km at 60°N since 2002. The dataset is a mosaic of precipitation estimates from 12 River Forecast Centers (RFCs) over the CONUS (Stage IV data in Alaska and Puerto Rico are archived separately) (Lin and Mitchell, 2005; Nelson et al., 2016). Each RFC produces its precipitation estimates through a combination of radar and rain gauge data based on the multisensory precipitation estimator (MPE) algorithm (for most RFCs), P3 algorithm (for Arkansas-Red basin RFC), or Mountain Mapper algorithm (for California-Nevada, Northwest, and Colorado-basin RFCs with missing radar-derived estimates) (Nelson et al., 2016). Some manual quality control steps are conducted to remove bad radar and gauge data before radar-gauge merging (Lin and Mitchell, 2005; Nelson et al., 2016). The Stage IV dataset has been widely used as a basis to evaluate model simulations, satellite precipitation estimates, and radar precipitation estimates (Davis et al., 2006; Gourley et al., 2011; Kalinga and Gan, 2010; Lopez, 2011; Yuan et al., 2008). Here, we obtain the hourly Stage IV precipitation for 2004 –- 2017 from the NCAR/UCAR RDA (https://rda.ucar.edu/datasets/ds507.5/, last access: Dec 28, 2019). We regrid the original Stage

IV precipitation from polar stereographic grids to the 4 km satellite Merged IR grids by using the "nearestdtod" method from the ESMF 'NCL' module (https://www.ncl.ucar.edu/Applications/ESMF.shtml). The "nearestdtod" method maps each destination point to the closest source point.

2.1.4 ERA5 melting level dataset

Melting hydrometeors produce intense radar echoes in a horizontal layer about 0.5 km thick located just below the 0°C level (melting level), which is known as "bright band" (Giangrande et al., 2008; Steiner et al., 1995). The bright-band signatures are often pronounced for stratiform precipitation, while convective precipitation produces well-defined vertical cores of maximum reflectivity, diluting bright-band signals (Giangrande et al., 2008; Steiner et al., 1995). Therefore, the SL3D algorithm that is described below examines Z_H above the melting level to avoid the false identification of stratiform rain as convective (Starzec et al., 2017). In this study, we use the hourly melting level heights from the ERA5 reanalysis dataset.

ERA5, as the successor to ERA-Interim, contains many modeling improvements and more observations based on 4D-Var data assimilation using Cycle 41r2 of the Integrated Forecasting System (IFS) at the European Centre for Medium-Range Weather Forecasts (ECMWF). ERA5 provides hourly estimates of atmospheric variables at a horizontal resolution of 31 km and 137 vertical levels from the surface to 0.01 hPa from 1979 to the present (Hersbach et al., 2019). We obtain ERA5 "Zero degree level" (melting level heights above ground) for 2004 – 2017 and "Orography" (geopotential at the ground surface) from the Climate Data Store (CDS) disks (ECMWF, 2018) (last access: Jan 24, 2020). The CDS archived ERA5 variables have been interpolated to regular latitude/longitude grids with a resolution of 0.25° × 0.25°. We calculate

207 melting level heights ASL from "Zero degree level" and "Orography" (divided by 9.80665 m s^{-2}
208 to obtain ground surface height). Finally, we regrid the hourly 0.25° melting level heights ASL
209 to the 4-km satellite Merged IR grids by using the ESMF "neareststod" method.

210 We summarize the basic information of the four types of source datasets in Table S1. And,
211 we define our data product domain as 110°W – 70°W in longitude and 25°N – 51°N in latitude
212 (Figure 1), which covers the US east of the Rocky Mountains and excludes the western US. The
213 domain coverage takes into consideration the availability of the GridRad radar dataset, the
214 relatively scarce radar coverage over the Rocky Mountains, and associated uncertainties in radar-
215 based Stage IV precipitation estimates in complex terrains (Nelson et al., 2016). As shown in
216 Figure 1a, we further define four regions in the domain following Feng et al. (2019): Northern
217 Great Plains (NGP), Southern Great Plains (SGP), Southeast (SE), and Northeast (NE).

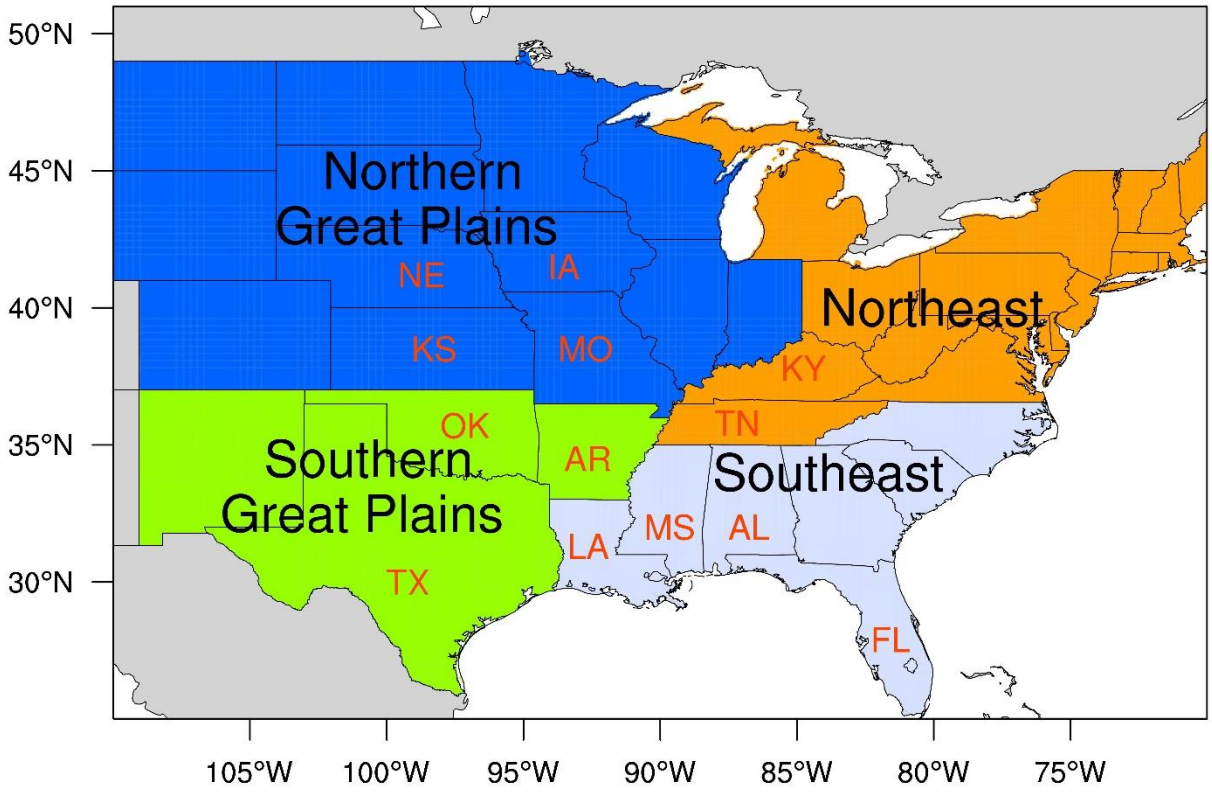

218

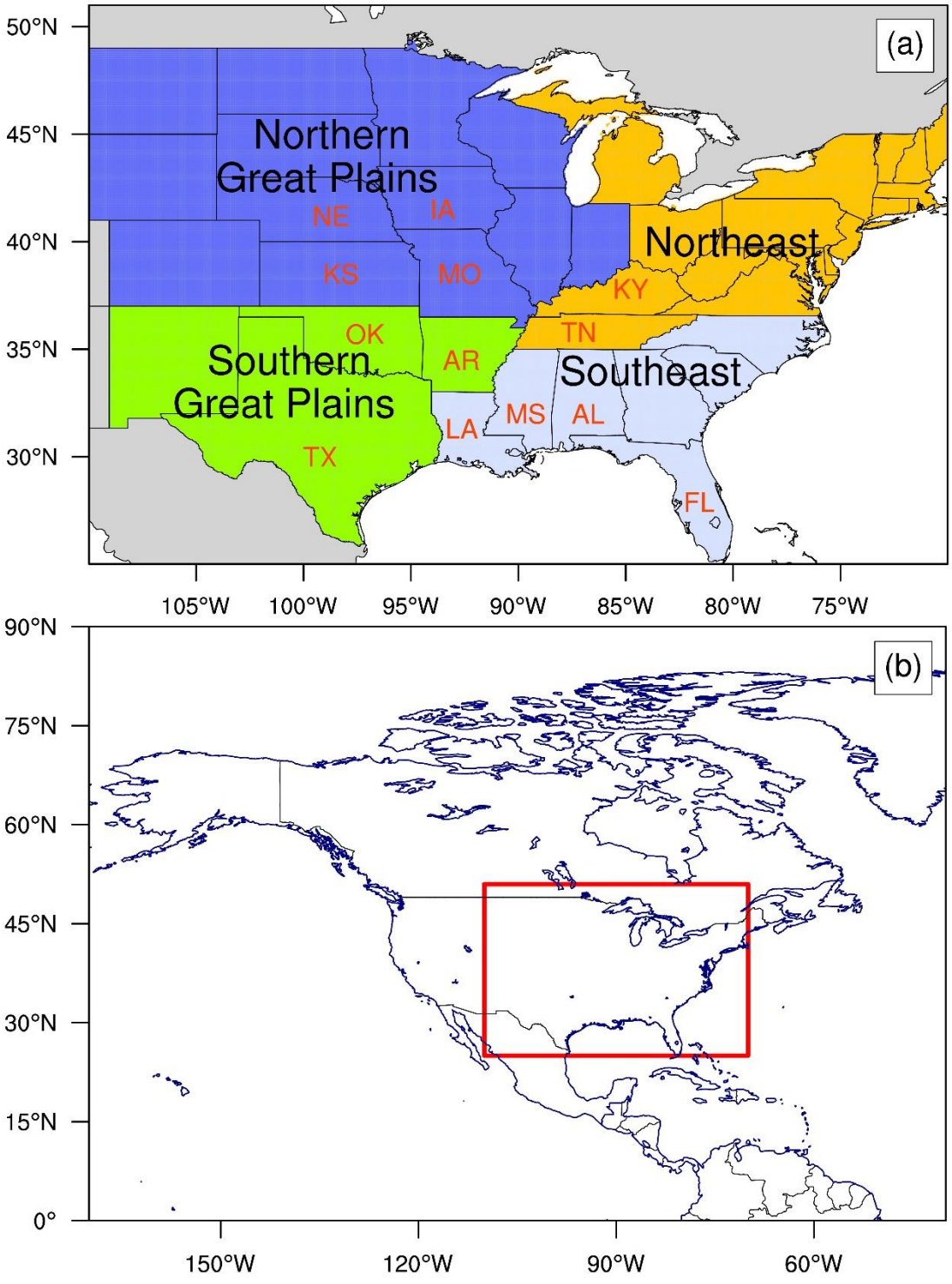

Figure 1. (a) Data product domain and region definitions. Blue shading denotes the Northern Great Plains (NGP), green-yellow shading denotes the Southern Great Plains (SGP), light steel blue shading denotes the Southeast (SE), and orange shading denotes the Northeast (NE). The locations of some US states within each region are also labeled. TX is for Texas, OK for Oklahoma, KS for Kansas, NE for Nebraska, IA for Iowa, MO for Missouri, AR for Arkansas,

LA for Louisiana, MS for Mississippi, AL for Alabama, TN for Tennessee, KY for Kentucky, and FL for Florida. (b) The location of the data product domain (red box) in North America.

2.2 Algorithm description

2.2.1 SL3D algorithm

The SL3D algorithm exploits Gridrad Z_H to classify each grid column with radar echoes into five categories: convective, precipitating stratiform, non-precipitating stratiform, anvil, and convective updraft (Starzec et al., 2017). SL3D identifies these five categories successively following the criteria listed in Table S2. We run the SL3D algorithm for 2004 – 2017 by using the re-gridded ERA5 melting level heights and Gridrad Z_H dataset described in Section 2.1. Figure 2e shows an example of the SL3D classification results based on Gridrad Z_H (Figure 2d) at 2005-07-04T03:00:00Z. A sizeable convective system with intense radar echoes and precipitation is observed in Kansas, and many isolated convection events are also observed in the Southeast. The SL3D classification results will be used in the following FLEXTRKR algorithm to identify convective core features (CCFs, continuous updraft/convective areas with precipitation > 0 mm h^{-1}, which are used to indicate the existence of convective activity in the IDC definition; red regions in Figure ~~S1~~3) and precipitation features (PFs, continuous updraft/convective/precipitating-stratiform areas with precipitation > 1 mm h^{-1}; green areas in Figure ~~S1~~3, which are used to denote the sizes of convective systems in the MCS and IDC definitions).

2.2.2 MCS/IDC identification and tracking

The FLEXTRKR algorithm was first developed and used by Feng et al. (2019) to track MCSs. In this study, we further update the algorithm so that it can identify and track MCS and IDC events simultaneously.

Figure ~~S1~~ 3 displays the schematic of FLEXTRKR (Feng et al., 2019). The first step is to identify cold cloud systems (CCSs; continuous areas with T_b < 241 K) at each hour by applying a multiple T_b threshold "detect and spread" approach (Futyan and Del Genio, 2007). We search for cold cloud cores with T_b < 225 K and spread the cold cloud cores to contiguous areas with T_b < 241 K. Cloud systems that do not contain a cold cloud core but with T_b < 241 K are also labeled as long as they can form continuous areas with at least 64 km^2 (4 pixels). In addition, as described in Feng et al. (2019), CCSs that share the same coherent precipitation feature are combined as a single CCS. A coherent precipitation feature is defined as continuous areas with smoothed Z_H at 2 km > 28 dBZ (if Z_H is not available at 2 km, use Z_H at 3 km instead if it is available) (Feng et al., 2019). We use a 5 × 5 pixel moving window to smooth Z_H. Figure 2b shows an example of the CCSs identified in the first step based on T_b at 2005-07-04T03:00:00Z. "Cloud 1" in Figure 2b corresponds to a large area of low T_b in the central US (Figure 2a).

In step 2, CCSs between two consecutive hours are linked if their spatial overlaps are > 50%. "Linked" means the CCSs are considered to be from the same cloud systems. FLEXTRKR produces tracks by extending the link between two consecutive time steps to the entire tracking period, as shown in Figure ~~S1~~3. Each track represents the lifecycle of a cloud system. We calculate a series of CCS summary statistics associated with each track, such as CCS-based lifetime of the track (the duration of the track when CCSs are present), CCS area, CCS major

axis length, CCS propagation speed, etc. Besides, SL3D classification (Figure 2e) and Stage IV precipitation (Figures 2c) within the tracked CCS are associated with the tracks and their merges and splits (described below). Then, we can obtain CCF and PF statistics of each track, such as convective and stratiform area, precipitation intensity and coverage, radar-derived echo-top heights, PF major axis length, CCF major axis length, intense convective cells (convective cells with column maximum reflectivity ≥ 45 dBZ and precipitation > 1 mm h^{-1}; pink areas in Figure S13, which are used to indicate intense convective activity in the following MCS definition), etc.

Merging and splitting refer to situations when two or more CCSs are linked to one CCS between consecutive hours (Figures S12 and S23). A track associated with the largest CCS is defined as the main track (Figure S34), and smaller tracks from merges/splits are regarded as parts of the main track when calculating PF and CCF statistics. In the algorithm, we require that a "merge"/"split" track associated with an MCS/IDC event must have a CCS-based lifetime of no more than 5 hours. Otherwise, we treat it as an independent track.

The identification of MCS and IDC is based on the CCS, PF, and CCF statistics of the tracks. Following the definition of MCSs by Feng et al. (2019) (Figure S54), we define a track as an MCS if it satisfies the following criteria: 1) there is at least one pixel of cold cloud core during the whole lifecycle of the track; 2) CCS areas associated with the track surpass 60,000 km^2 for more than six continuous hours; 3) PF major axis length exceeding 100 km and intense convective cell areas of at least 16 km^2 exist for more than five consecutive hours. Considering the lack of a strict and universal the potential impreciseness in the MCS definition (Geerts et al., 2017; Haberlie and Ashley, 2019; Pinto et al., 2015; Prein et al., 2017), we evaluate the impact of different MCS definition criteria on the data product in Section 4.4. For the non-MCS tracks,

we further identify IDC with the following two criteria (Figure ~~S5~~4): 1) a CCS with at least 64 km^2 (4 pixels) is detected; 2) at least 1 hour during the lifecycle of the track when PF and CCF are present (PF and CCF major axis lengths ≥ 4 km). In addition, for each IDC event, the CCS-based lifetime of associated merge and split tracks cannot surpass the lifetime of the IDC event. Here, the IDC criteria denote a low limit in convective signals that we can identify by using the FLEXTRKR algorithm and given source datasets. Potential uncertainties associated with the limit are discussed in Section 4.3.

Note that while we designate the term IDC to differentiate ~~less organized~~smaller convective storms from MCSs, there are sub-categories of deep convection within IDC. For example, multicellular convection systems that do not grow large enough or last long enough to meet our MCS definition are defined as IDC in our study, even though they are not necessarily "isolated." Users of the data product can further separate sub-categories within IDC using the derived CCF statistics information to address specific science questions or research objectives.

Finally, the FLEXTRKR algorithm maps MCS/IDC track information back to the domain pixels. Figures 2f – 2i give an example of the pixel-level MCS/IDC information at 2005-07-04T03:00:00Z. Figure 2f displays the spatial coverages of MCS/IDC tracks at that time at pixel scale and the corresponding unique numbers of these tracks. From Figure 2f, we know whether a pixel belongs to an MCS/IDC track and the number of the track if the pixel belongs to a track. We can further determine whether the track is an MCS or IDC event from Figure 2g, which shows the types (MCS or IDC) of the tracks in Figure 2f at the pixel scale. Figures 2h and 2i are similar to Figures 2f and 2g, respectively. The difference is that Figures 2h and 2i only show pixels with precipitation > 1 mm h^{-1} in that hour. ~~There, one can identify whether a pixel belongs~~

~~to a track; if it does, what is the track number, whether the track is an MCS or IDC event, and whether the pixel has hourly accumulated precipitation > 1 mm or not.~~ Together, the track-based CCS, PF, and CCF statistics of MCS and IDC events and the pixel-level dataset constitute the unified high-resolution MCS/IDC data product we develop in this study. Original T_b (Figure 2a), Stage IV precipitation (Figure 2c), Gridrad Z_H at 2 km (Figure 2d), and Gridrad derived echo-top heights are also archived in the data product.

We run the FLEXTRKR algorithm separately for each year from 2004 to 2017. The starting time of each continuous tracking is 00Z on 1 January, and the ending time is 23Z on 31 December. Because winter has the fewest deep convection events, very few MCS/IDC events extend between two different years based on our investigation. Also, the lifetimes of MCS/IDC events are much shorter compared to our tracking period. Therefore, running FLEXTRKR separately for each year rather than continuously for the whole period has little impact on the MCS/IDC statistics.

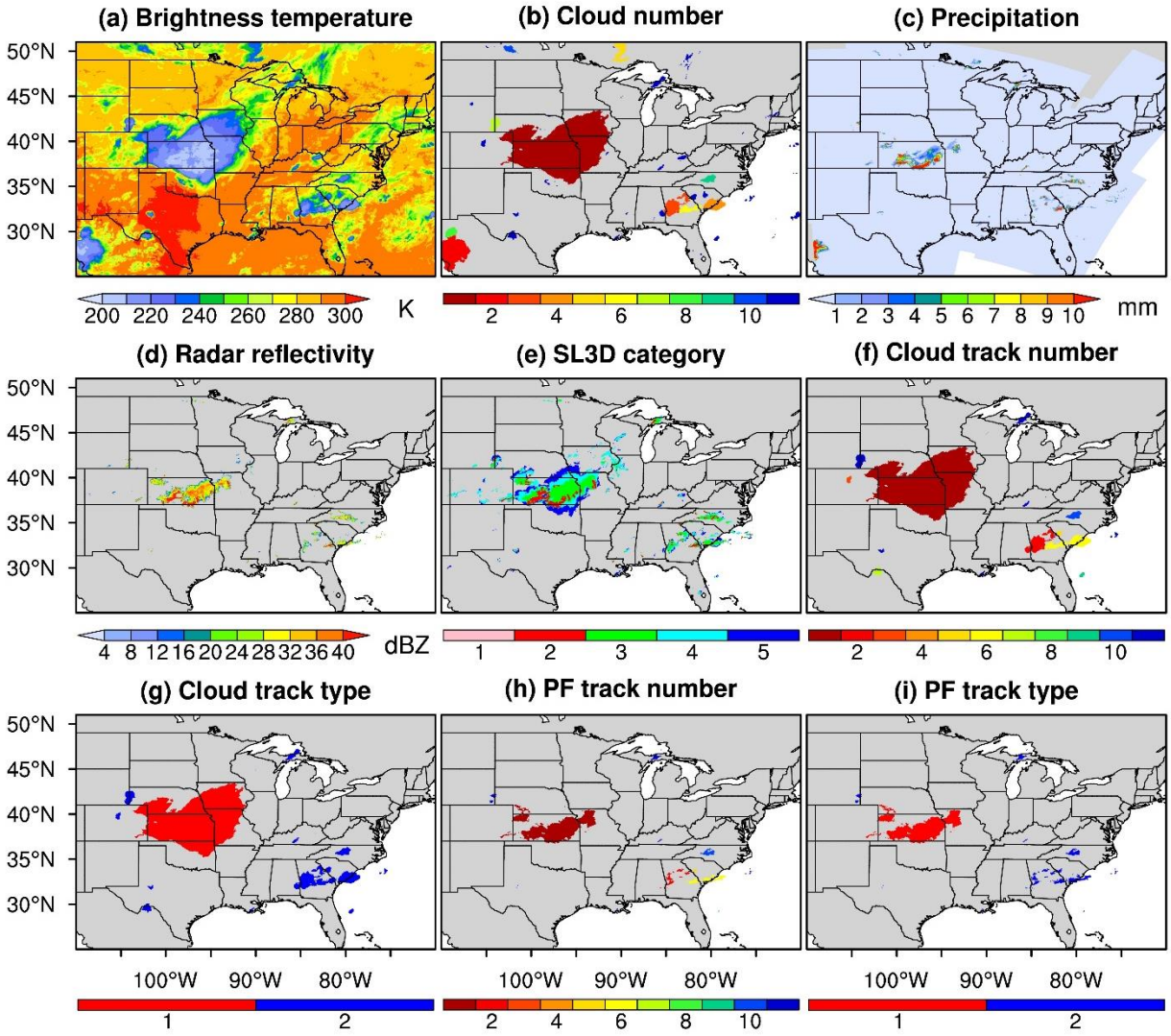

Figure 2. FLEXTRKR pixel-level outputs at 03:00:00Z on July 4, 2005. (a) is satellite T_b. (b) shows identified CCS labels. CCS labels are unique at each hour. (c) is Stage IV hourly accumulated precipitation. (d) is Gridrad Z_H at 2 km (if it is not available, Z_H at 3 km is provided if it is available). (e) is the SL3D classification results: 1, convective updraft; 2, convective; 3, precipitating stratiform; 4, non-precipitating stratiform; 5, anvil. (f) displays the track numbers to which pixels belong. Here, the track numbers are not the real values in the MCS/IDC data product. The track numbers should be unique throughout the whole running period. We adjust the track numbers here to make the figure clear. Similar to "PF track number." (g) gives information on whether the pixels belong to MCS (marked as 1) or IDC (marked as 2) tracks, which correspond to the tracks shown in (f). (h) also displays the track numbers to which the pixels belong, but only for pixels with precipitation > 1 mm h^{-1}. (i) is like (g) but corresponds to (h). All these variables are stored in the FLEXTRKR hourly pixel-level output files.

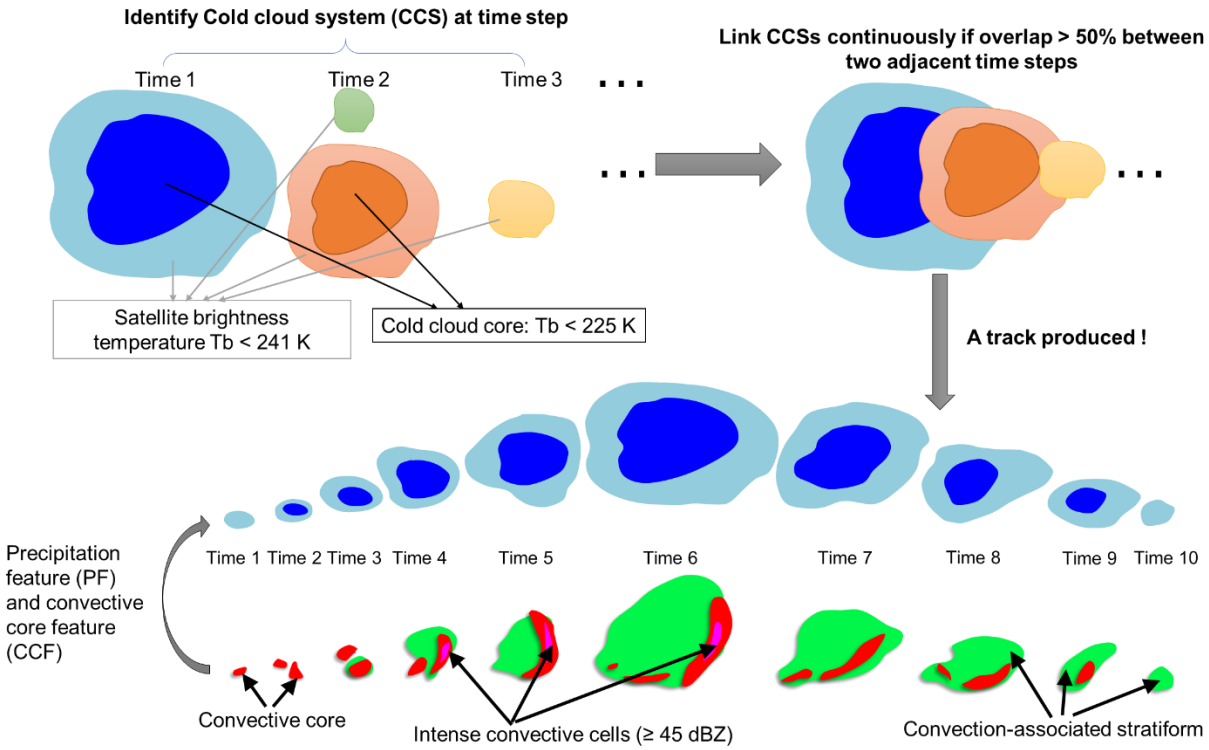

Figure 3. Schematic of the FLEXTRKR algorithm.

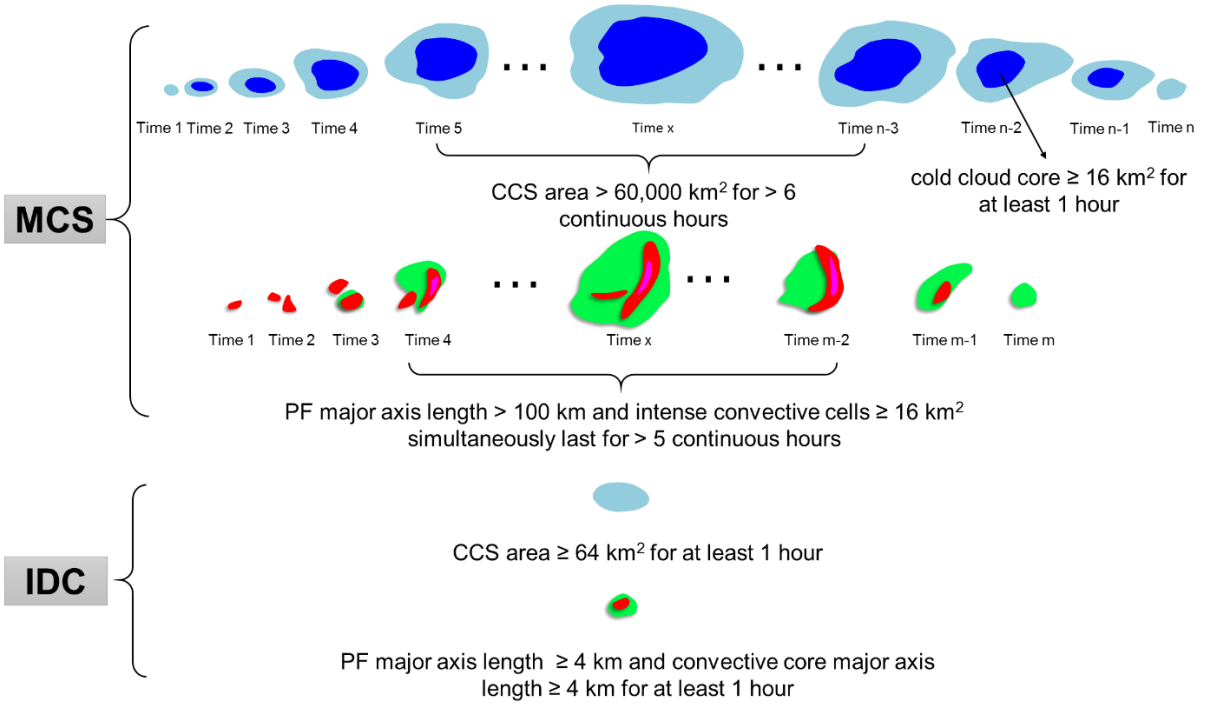

Figure 4. Definition of MCSs and IDC.

3 Results and discussions

3.1 Climatological characteristics of MCS and IDC events

According to the MCS/IDC data product, we identify 45,346 IDC and 454 MCS events each year on average between 2004 and 2017 in our data product domain. Summer (June – August) has the most IDC and MCS events with average numbers of 25,073 and 212, while winter has the least with average quantities of 2,545 and 37. During spring and autumn, there are 8,543 and 9,185 IDC events and 122 and 83 MCSs, respectively. The seasonal feature with the most occurrences of MCSs in winter and the least in summer is consistent with the results of Geerts (1998) in the Southeast US and Haberlie and Ashley (2019) over portions of the CONUS east of the Continental Divide (ECONUS).

We compare the climatological characteristics of MCS and IDC events in Table 1. MCSs have much longer lifetimes than IDC, averaging 21.1 hours (CCS-based) and 18.9 hours (PF-based), compared to 2.1 hours (CCS-based) and 1.7 hours (PF-based) for IDC. Here, PF-based lifetime refers to the lifetime determined by the MCS/IDC PFs. Only those hours with a significant PF present (PF major axis length > 20 km for MCSs; ≥ 4 km for IDC) are counted during the lifecycle of an MCS/IDC event, which represent the active convective period of a storm. We find that MCSs have the longest PF lifetime in winter (21.3 hours) and the shortest in summer (17.9 hours). In comparison, IDC has the longest PF lifetime in winter (1.9 hours), but the summer lifetime (1.7 hours) is comparable to spring and autumn. We examine the seasonal cumulative distribution functions (CDFs) of PF lifetimes for MCS and IDC events for 2004 – 2017 in Figure S4~~6~~. Results show winter has the largest fraction of MCS/IDC events with longer lifetimes than other seasons.

As expected, MCSs are much larger than IDC events in spatial coverage and precipitation area, as shown in Table 1 by the comparisons of CCS area, PF ~~area~~major axis length, PF convective/stratiform ~~precipitation~~ area, ~~etc~~CCF area, and CCF major axis length. Generally, on average, winter MCS/IDC events are the largest in overall spatial coverage (both CCS and PF areas), while summer has the smallest. The larger and longer-lived MCSs in winter than in summer were also observed in the Southeast US in 1994 – 1995 by Geerts (1998). The remarkable seasonal difference in MCS/IDC overall spatial coverage is mainly due to stratiform areas. Convective areas are much smaller than stratiform areas. The PF stratiform area of MCSs in winter is 90,513 km^2, 2.4 times larger than the area of 26,599 km^2 in summer, but the PF convective area of MCSs in winter is 7,293 km^2, 14% smaller than 8,465 km^2 in summer. Similarly, the IDC PF stratiform area in winter is 3,182 km^2, 2.8 times larger than 828 km^2 in summer, while the IDC PF convective area in winter is 528 km^2, slightly larger (9%) than 483 km^2 in summer. Unlike stratiform areas with the largest value in winter, ~~for MCSs,~~ convective activity is ~~summer generally has~~ the most intense ~~convective activity than winter~~ in summer as indicated by ~~a suite of CCF statistics, such as convective precipitation area,~~ PF mean convective 20-dBZ echo-top height~~, major axis length of the largest CCF, etc.~~ in Table 1. ~~While for IDC, convective areas are comparable among all seasons. But for the most intense portion of convective cells, as shown by area with column max reflectivity (Z_{Hmax}) ≥ 45 dBZ, max 30-dBZ echo-top height, and max 40-dBZ echo-top height, summer IDC is still much stronger than those in winter.~~ The ~~more~~ most intense convective activity ~~in summer than winter~~ reflects the ~~stronger~~ strongest atmospheric thermal instability ~~in summer~~ due to ~~stronger~~ the strongest solar radiation in summer. We further confirm this point by investigating the MCS/IDC initiation time. As shown in Figure S5~~7~~, most MCS and IDC events initiate in the afternoon of summer when

atmospheric instability is the strongest, consistent with Geerts (1998), who found warm-season MCSs generally initiated at 12:00 – 14:00 Local Time in the Southeast US.

Although MCSs are much larger than IDC events in spatial coverage, ~~proxies of their mean convective intensities such as~~ their mean convective 20-dBZ echo-top heights, which can be used to represent their mean convective intensities, are similar in Table 1. And their PF mean convective and stratiform rain rates are also comparable. ~~However, for the most intense convective cells, as indicated by the max 30/40-dBZ echo-top heights, MCSs are still much stronger than IDC events.~~ PF mean convective and stratiform rain rates show significant seasonal ~~cycles~~ variations for both MCS and IDC events. Summer MCS and IDC events have the largest rain rates, followed by autumn. Winter has the lowest rain rates compared to other seasons.

The high-resolution nature of the MCS/IDC data product enables a detailed examination of the 3-D evolutions of MCS/IDC events to investigate the relationships between atmospheric environments and MCS/IDC characteristics and to examine the impacts of MCSs and IDC on hydrology, atmospheric chemistry, and severe weather hazards. The data product can also be used to evaluate and improve the representation of MCS/IDC processes in weather and climate models. As an example of the application of the MCS/IDC data product, in Section 3.2, we investigate the contributions of MCS and IDC events to precipitation east of the Rocky Mountains for 2004 – 2017.

Table 1. Annual and seasonal mean characteristics of MCS and IDC events in the data product domain for 2004 – 2017

	MCS					IDC				
	Annual	spring	Summer	autumn	winter	annual	spring	summer	autumn	winter
CCS-based lifetime / hour	21.1	21.5	19.9	22.1	24.3	2.1	2.1	2.0	2.0	2.7
CCS area[1] / km^2	185,436	223,230	130,769	185,246	373,220	6,775	9,400	4,542	6,515	20,902
CCS major axis length / km	693	774	568	726	1,067	99	117	86	100	169
PF-based lifetime[2] / hour	18.9	19.3	17.9	19.7	21.3	1.7	1.7	1.7	1.7	1.9
Major axis length of the largest PF[3] / km	397	426	325	436	620	63	69	56	69	93
PF convective area[4] / km^2	8,273	8,589	8,465	7,752	7,293	494	509	483	502	528
PF stratiform area / km^2	41,336	47,241	26,559	48,376	90,513	1,261	1,610	828	1,583	3,182
PF mean convective rain rate / mm h^{-1}	4.4	3.9	4.7	4.5	3.8	4.2	3.4	4.5	4.3	3.0
PF mean stratiform rain rate /mm h^{-1}	2.6	2.4	2.8	2.6	2.2	2.8	2.5	3.0	2.9	2.3
~~Area with $Z_{Hmax} \geq$ 45 dBZ within the largest PF / km^2~~	~~1,078~~	~~1,147~~	~~1,203~~	~~807~~	~~735~~	~~56~~	~~58~~	~~59~~	~~49~~	~~42~~
PF mean convective 20-dBZ echo-top height / km	6.5	6.2	7.2	6.0	4.9	6.6	6.1	7.0	6.2	5.0
Area of the largest CCF / km^2	2,578	2,515	2,983	2,068	1,606	343	359	339	340	349
Major axis length of the largest CCF / km	109	109	117	100	92	29	30	29	29	31
~~Max 30-dBZ echo-top height of the largest CCF / km~~	~~13.2~~	~~12.8~~	~~14.5~~	~~12.0~~	~~10.0~~	~~7.0~~	~~6.4~~	~~7.6~~	~~6.5~~	~~5.0~~
~~Max 40-dBZ echo-top height of the largest CCF / km~~	~~11.0~~	~~11.0~~	~~12.2~~	~~9.4~~	~~7.7~~	~~5.4~~	~~5.1~~	~~5.9~~	~~5.0~~	~~3.7~~

[1] In this table, for hourly characteristics (all variables except for CCS-based lifetime and PF-based lifetime), we generally first calculate the average values of the characteristics during the duration of each MCS/IDC event except for the max 30/40-dBZ echo-top heights, which are the maximum values of the attributes within the period. Then we calculate the mean values of the characteristics of all MCS/IDC events. For example, an MCS has a CCS-based lifetime of 10 hours. During its duration, it has a CCS at each hour. We calculate the average CCS area during the 10 hours, which is the average CCS area of the MCS. Then, we average all MCSs identified during a period to derive the values shown in this row.

[2] Lifetimes of MCS/IDC events determined by PFs. Only count those hours of an MCS/IDC event with a significant PF present (PF major axis length > 20 km for MCSs; ≥ 4 km for IDC).

[3] There can be multiple PFs and CCFs at a given time for an MCS/IDC event. "Largest" means only the largest PF or CCF is used in the calculation.

[4] There can be multiple PFs and CCFs at a given time for an MCS/IDC event. If not specified, all PFs/CCFs are considered. For example, convective areas of all PFs at a given time are summed to represent the PF convective area of an MCS/IDC event at that time. Similarly, the convective rain rates of all PFs at the given time are averaged to represent the PF mean convective rain rate of the MCS/IDC at that time.

3.2 Precipitation characteristics from different sources

Here we only consider hourly data with precipitation > 1 mm h^{-1} (Feng et al., 2019). At 4 km resolution, precipitation less than 1 mm h^{-1} accounts for less than 19% of the total precipitation, and the uncertainty of radar-derived precipitation at such low rainfall intensity is typically large. Including hourly data with precipitation ≤ 1 mm h^{-1} in the calculation will change the values shown in this study but will neither affect the comparison among MCS, IDC, and ~~stratiform~~ non-convective (NC) precipitation nor their spatial distribution patterns. ~~Stratiform~~ Here, NC precipitation ~~mentioned in this section~~ refers to precipitation ~~areas~~ not associated with any MCS~~s~~ or IDC events and is mainly from stratiform rain. Total precipitation is the sum of MCS, IDC, and ~~stratiform~~ NC precipitation. It is noteworthy that NC precipitation may contain some convection-associated rain due to the limitation of the source datasets and the algorithms used in this study. More relevant details are discussed in Section 3.2.3 and Section 4.

3.2.1 Annual spatial distributions of different types of precipitation

According to the MCS/IDC data product, the annual average total precipitation east of the Rocky Mountains in the US (US grid cells in Figure 1) is 691 mm between 2004 and 2017 with a mean precipitation intensity of 3.6 mm h^{-1}. MCSs contribute the most to the total precipitation with a fraction of 45%, followed by ~~stratiform~~ NC (30%) and IDC (25%). And the mean precipitation intensities of MCSs (4.4 mm h^{-1}) and IDC (3.8 mm h^{-1}) are much larger than ~~stratiform~~ NC (2.7 mm h^{-1}). Our MCS precipitation fraction (45%) is higher than that (~30%) from Haberlie and Ashley (2019) over the ECONUS due to their different algorithms and stricter criteria to track and define MCSs.

Figure ~~3~~ 5 displays the spatial distributions of annual mean precipitation amounts and intensities for different precipitation types for 2004 – 2017. We also calculate the distributions of the fractions of different types of precipitation in Figure ~~4~~6. MCS precipitation strongly affects the whole eastern US (105°W – 70°W, MCS precipitation fractions: 46% ± 12%), especially in the South Central US (MCS precipitation fractions: ~60%). The spatial distribution patterns of MCS annual precipitation amounts and fractions in Figure 5 are similar to those from Haberlie and Ashley (2019), although their MCS precipitation fractions are generally lower than our results. IDC precipitation is concentrated in the SE and NE coastal areas, with peak values in Florida. ~~Stratiform~~ NC precipitation is substantial in the eastern and southern regions with ample moisture supply and contributes over 35% to the total precipitation across most of the NE region. The coastal area near Louisiana, which is significantly affected by all three types of precipitation, has the most total precipitation with annual amounts of over 1,350 mm. The annual total precipitation amounts in most regions of SE also exceed 1,050 mm due to MCS contributions. While the total precipitation amounts in most regions of Florida are also over 1,050 mm, they are mainly attributed to IDC.

The spatial patterns of precipitation intensities are somewhat different from those of precipitation amounts (Figure ~~3~~5). Generally, the southern regions, especially in the coastal areas, have larger precipitation intensities than the northern areas. The MCS precipitation intensities are the largest in Texas, Louisiana, Oklahoma, and Kansas, significantly shifting west compared to MCS precipitation amounts. Unlike IDC precipitation amounts concentrating in the SE and NE coastal areas, IDC precipitation intensities are the largest over the SGP and SE. IDC precipitation intensities over the NE are much smaller compared to the SGP and SE, similar to

~~stratiform~~ NC precipitation intensities. We summarize the annual mean precipitation amounts and intensities of different types of precipitation in the NGP, SGP, SE, and NE in Table S3.

The distributions of MCS/IDC precipitation amounts are mainly determined by the distributions of MCS/IDC hours (Figures ~~3~~ 5 and ~~5~~7). Here, the MCS/IDC hour of a grid cell during a period is the number of hours when any MCS/IDC events produce > 1 mm hourly accumulated rainfall in the grid cell. The distributions of MCS/IDC precipitation intensities, although not the main factor, can also affect the distributions of MCS/IDC precipitation amounts. For example, the maximum MCS hours are located around Missouri (Figures ~~5a~~7a), but the maximum MCS precipitation amount is in the coastal area of Louisiana (Figure 5~~3~~c). The larger MCS precipitation intensities in the southern regions contribute more to the MCS precipitation amount in the southern US. In addition, a large number of IDC events (IDC hours > 60 h yr^{-1}) occur in the NE region along the Appalachian Mountains (Figure ~~5b~~7b), but IDC in that region only contributes to 20% – 30% of the total precipitation amount (Figure ~~4b~~6b) due to the low precipitation intensities (Figure ~~3f~~5f).

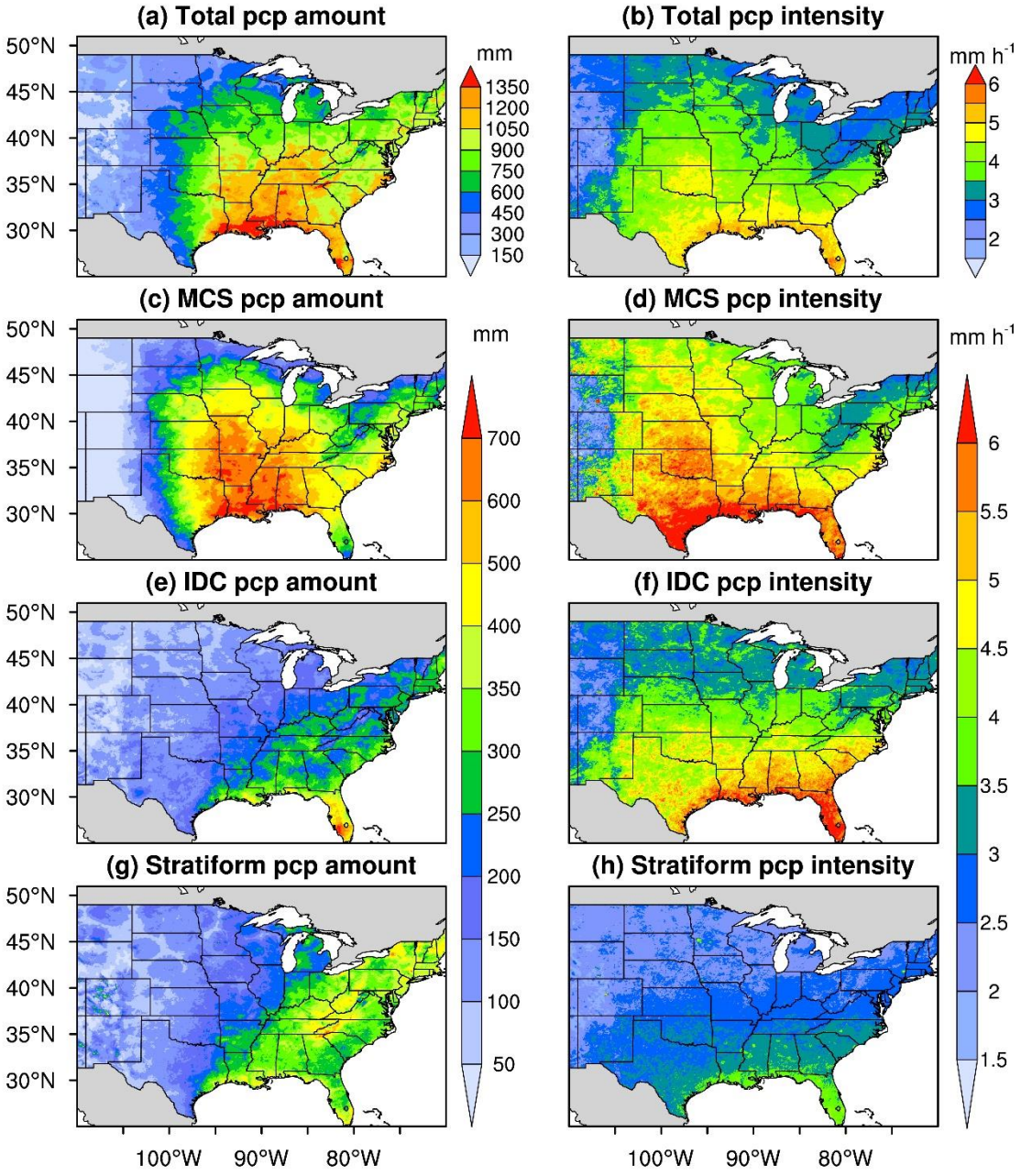
(a) Total pcp amount
(b) Total pcp intensity
(c) MCS pcp amount
(d) MCS pcp intensity
(e) IDC pcp amount
(f) IDC pcp intensity
(g) Stratiform pcp amount
(h) Stratiform pcp intensity
mm
mm h-1
1350
1200
1050
900
750
600
450
300
150
700
500
400
350
250
200
100
50
6
5
4
3
2
5.5
4.5
3.5
2.5
1.5
50°N
45°N
40°N
35°N
30°N
100°W
90°W
80°W

474

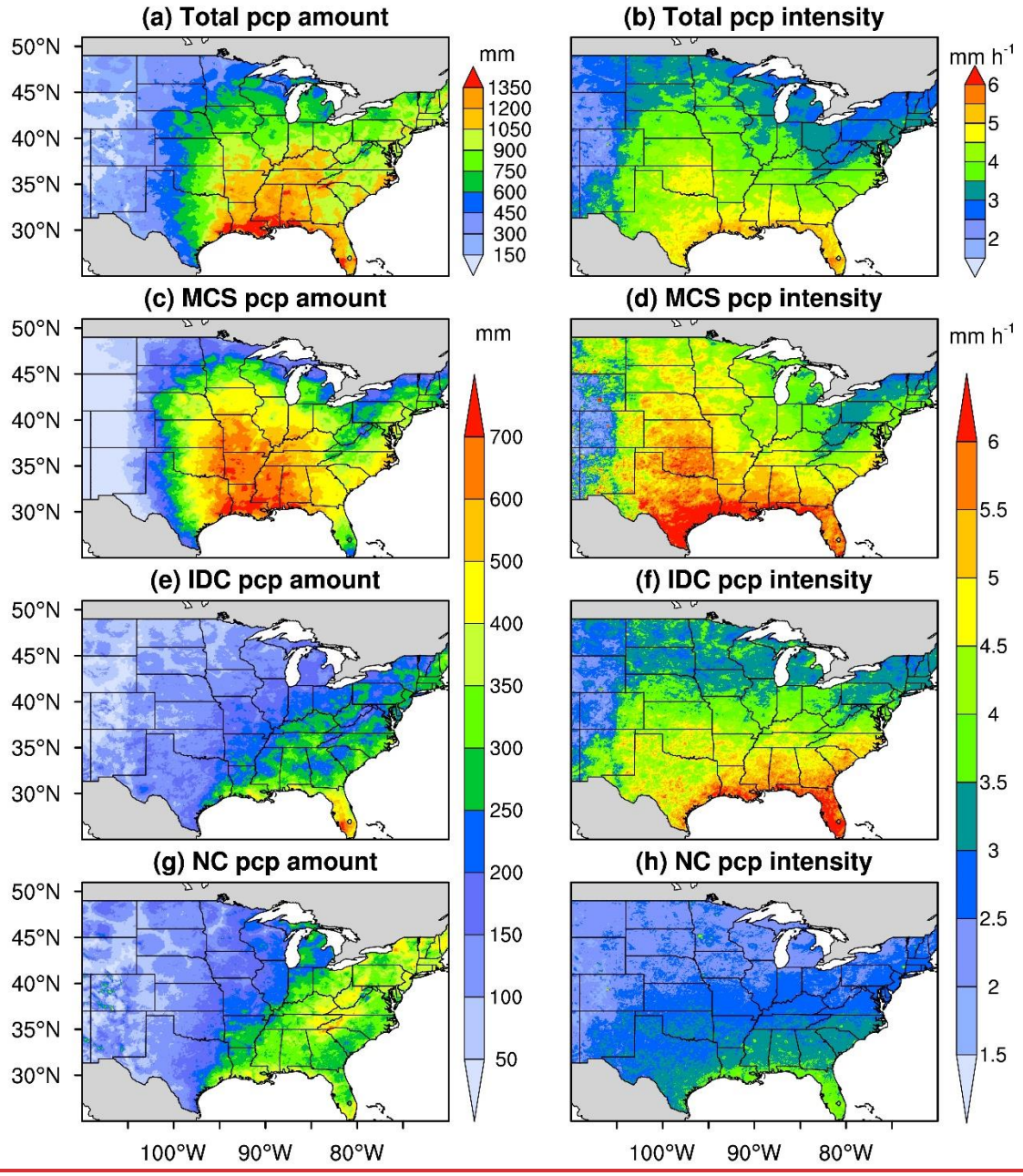

Figure ~~3~~5. Distributions of annual mean precipitation amounts (a, c, e, g) and intensities (b, d, f, h) for different types of precipitation for 2004 – 2017. (a) and (b) are for total precipitation, (c) and (d) are for MCS precipitation, (e) and (f) are for IDC precipitation, and (g) and (h) are for ~~stratiform~~ NC precipitation. We only include hourly data with precipitation > 1 mm h^{-1} in the calculation.

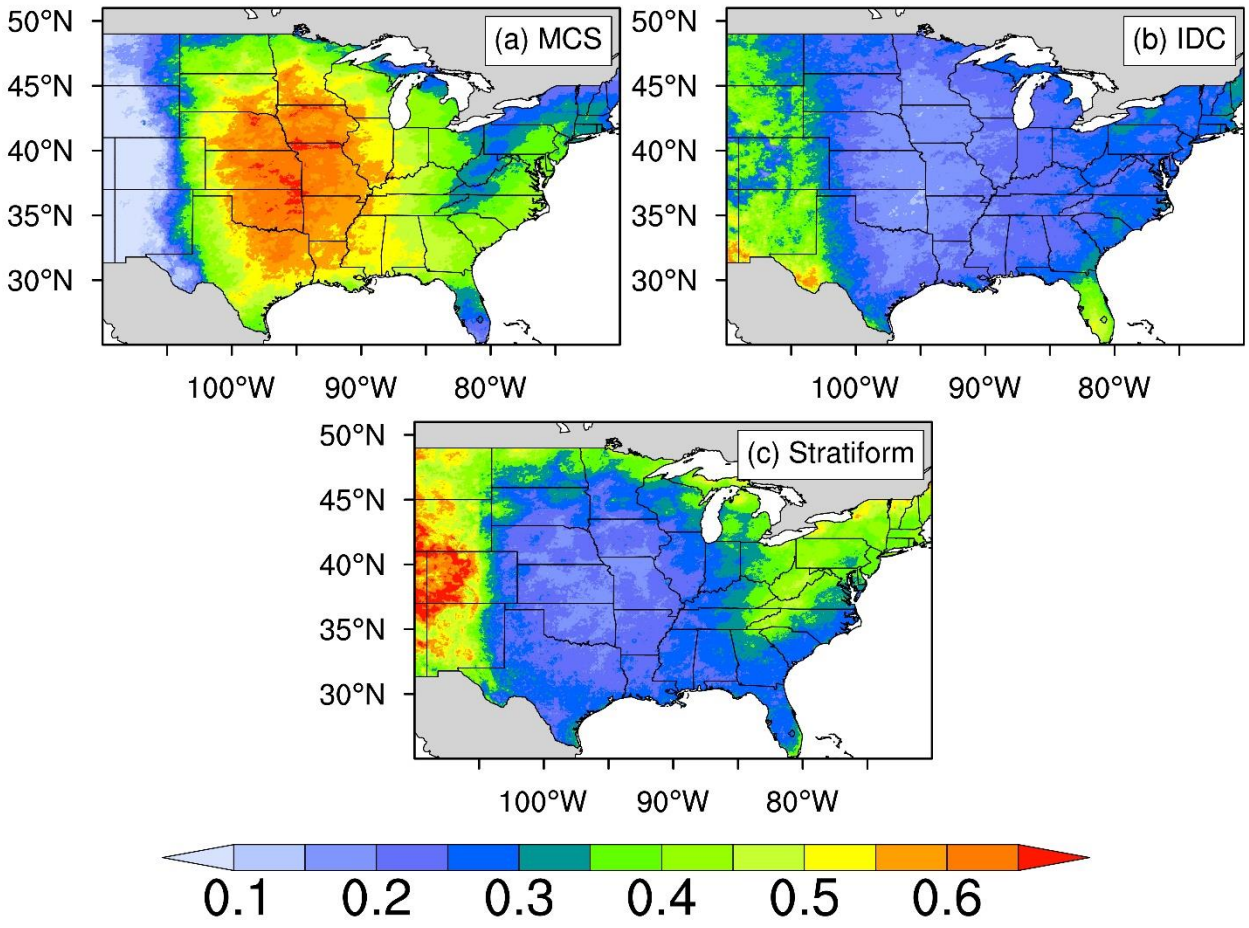
(a) MCS
(b) IDC
(c) Stratiform
50°N
45°N
40°N
35°N
30°N
100°W
90°W
80°W
0.1
0.2
0.3
0.4
0.5
0.6

482

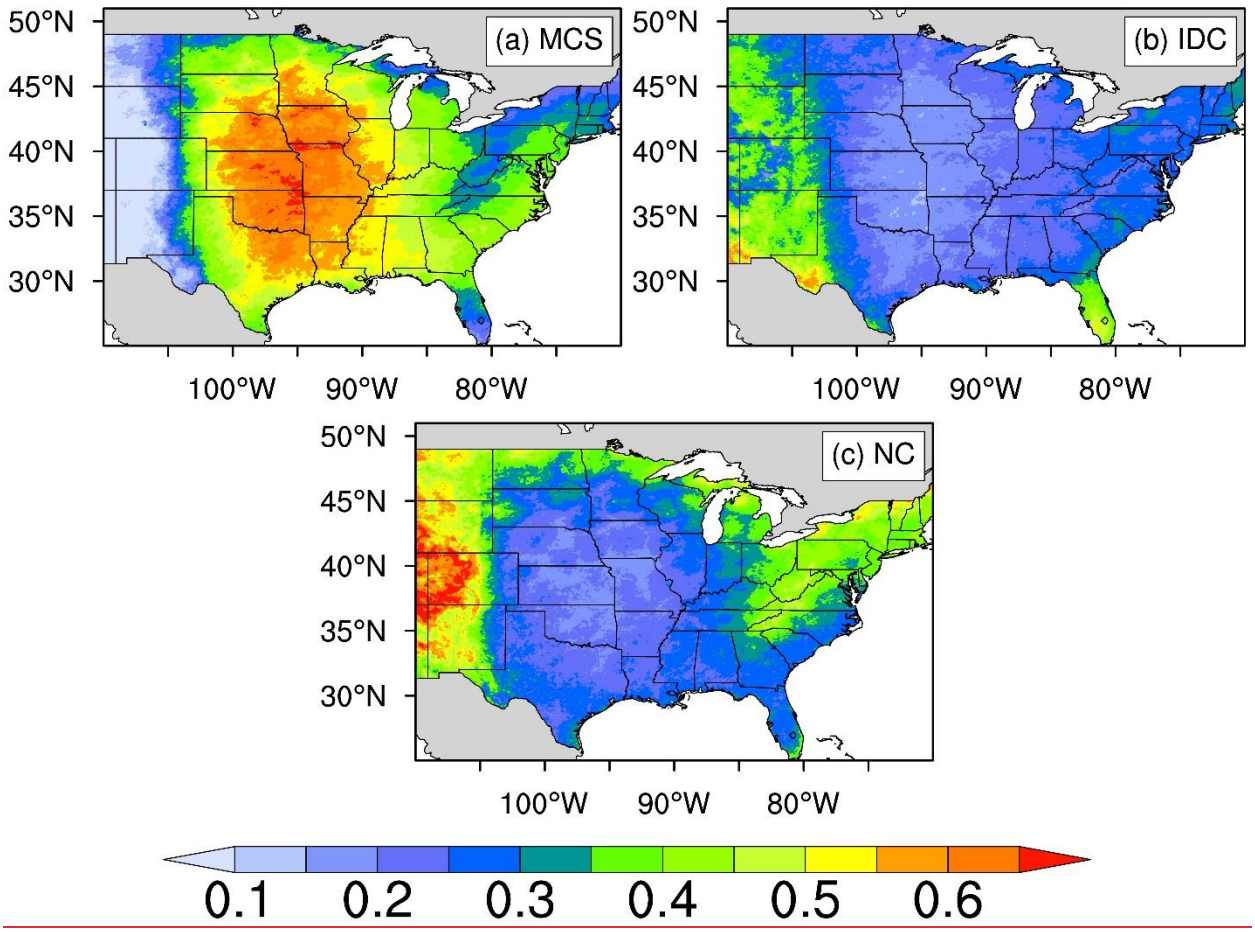

Figure ~~4~~6. Distributions of the fractions of different types of precipitation (MCS, IDC, ~~stratiform~~NC). Here, precipitation refers to annual mean values for 2004 – 2017. We exclude hourly data with precipitation ≤ 1 mm h^{-1} in the calculation.

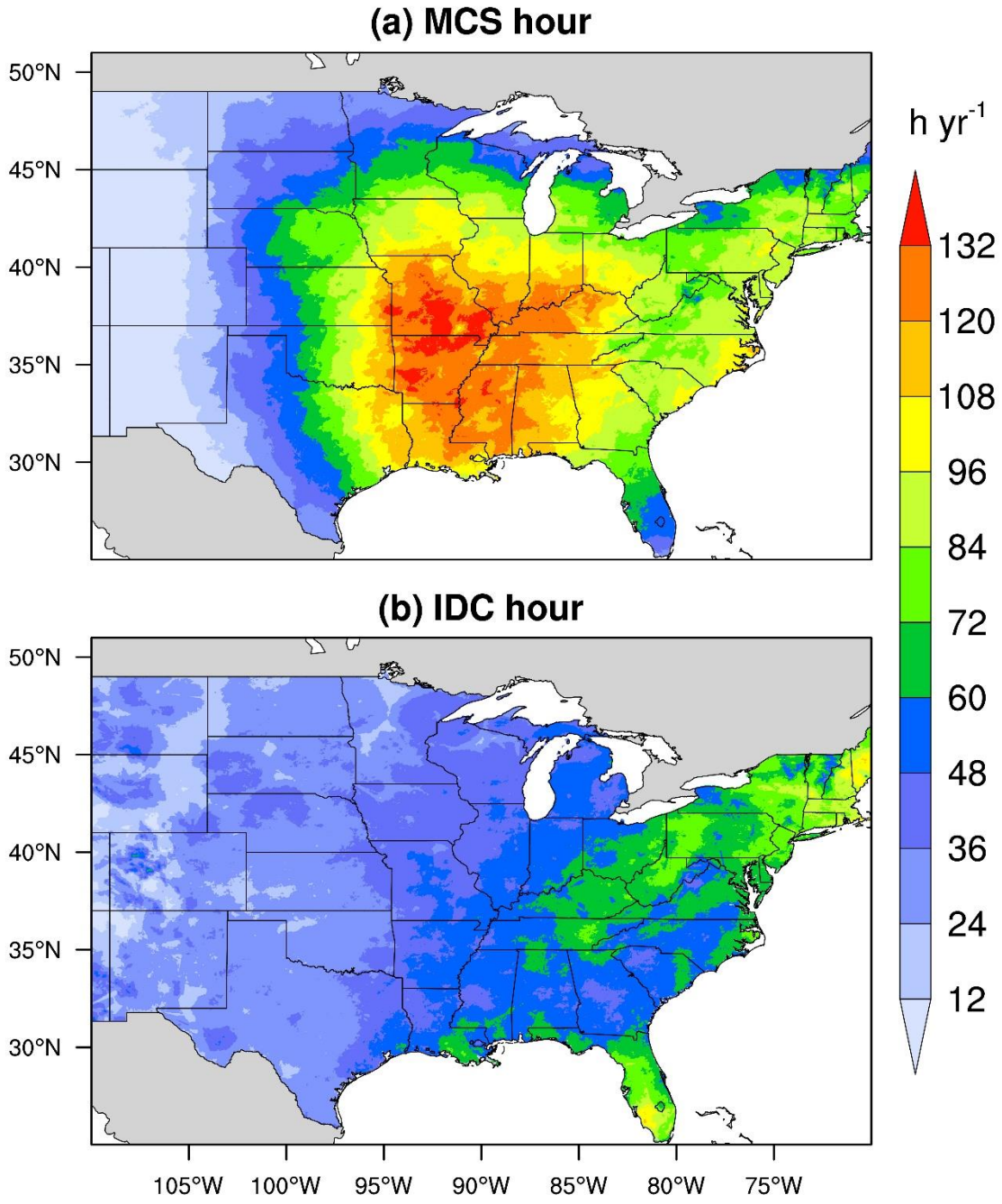

Figure ~~5~~7. Spatial distributions of annual mean MCS/IDC hours for 2004 – 2017. (a) is for MCS, and (b) is for IDC. The annual mean MCS/IDC hour of a grid cell is the number of hours per year when any MCS/IDC events produce > 1 mm hourly accumulated rainfall in the grid cell.

3.2.2 Seasonal spatial distributions of different types of precipitation

Figures ~~6~~8, ~~S8~~S6, and ~~S9~~ S7 display the mean seasonal distributions of precipitation amounts, precipitation fractions, and precipitation intensities for different types of precipitation in 2004 – 2017. The MCS precipitation center migrates northwards from Arkansas in spring to northern Missouri and Iowa in summer, followed by a southward migration to Louisiana in autumn, and finally to Mississippi and Alabama in the Southeast (Figures ~~6e~~ 8e – ~~8~~6h) in winter. The seasonal shift of the MCS precipitation center agrees with the study of Haberlie and Ashley (2019), showing different MCS precipitation distributions between warm and cold seasons over the ECONUS. Spring and summer have much larger MCS precipitation amounts (~100 mm) than autumn (~62 mm) and winter (~50 mm). The mean MCS precipitation amount in spring is close to that in summer. However, the total number of identified MCSs in summer (212) is much higher than that in spring (122), as discussed in Section 3.1; and the mean MCS precipitation intensity in summer (5.2 mm h^{-1}) is also larger than that in spring (4.1 mm h^{-1}) (Figure ~~S9~~S7). The inconsistency is because MCSs in spring occur in more favorable large-scale environments with strong baroclinic forcing and low-level moisture convergence (Feng et al., 2019; Song et al., 2019). As a result, spring MCSs are larger and longer-lasting, and they produce more rainfall per MCS event compared to those in summer (Table 1), compensating for the fewer number of MCS events and lower precipitation intensities in spring. The fractions of MCS precipitation amounts are generally > 35% over the Northern and Southern Great Plains in spring and summer and can reach up to over 70% ~~W~~within the MCS precipitation center (Figures S6a – S6b). The results are roughly consistent with Fritsch et al. (1986), which showed that MCSs accounted for about 30% – 70% of the warm-season (April-September) precipitation over much of the region between the Rocky Mountains and the Mississippi River. The results are also consistent with Haberlie and

Ashley (2019) showing MCS precipitation fractions generally > 30% with a peak > 60% over the Great Plains between May and August. ~~in spring and summer, MCS precipitation accounts for over 70% of the total precipitation amounts (Figures S8a – S8b). And d~~Due to the low precipitation amounts of IDC and ~~stratiform~~NC, the fractions of MCS precipitation amounts in autumn and winter are also large, showing over 50% within the MCS precipitation center (Figures ~~S8c~~ S6c – ~~S8d~~S6d).

The IDC precipitation amounts reach a maximum in summer, centered in the coastal areas of the SE, where IDC precipitation contributes to more than 40% of the total precipitation amounts (Figures ~~6i~~ 8i – 8~~6~~l and S6~~8~~e – S6~~8~~h). Winter has the least IDC precipitation. Areas of high IDC precipitation do not show much seasonal variability, suggesting that IDC is constrained by local conditions such as moisture availability, local solar radiation, and land-atmosphere interactions. The ~~stratiform~~ NC precipitation amount also peaks in summer, followed by autumn, particularly in the NE (Figures ~~6m~~ 8m – 8~~6~~p). However, because both MCS and IDC precipitation amounts are very high in summer, the fraction of the ~~stratiform~~ NC precipitation amount in summer (28%) is smaller than that of winter (32%) (Figures ~~S8i~~ S6i – S6~~8~~l). Winter ~~stratiform~~ NC precipitation center occurs in the SE coastal areas (Figure 8~~6~~p).

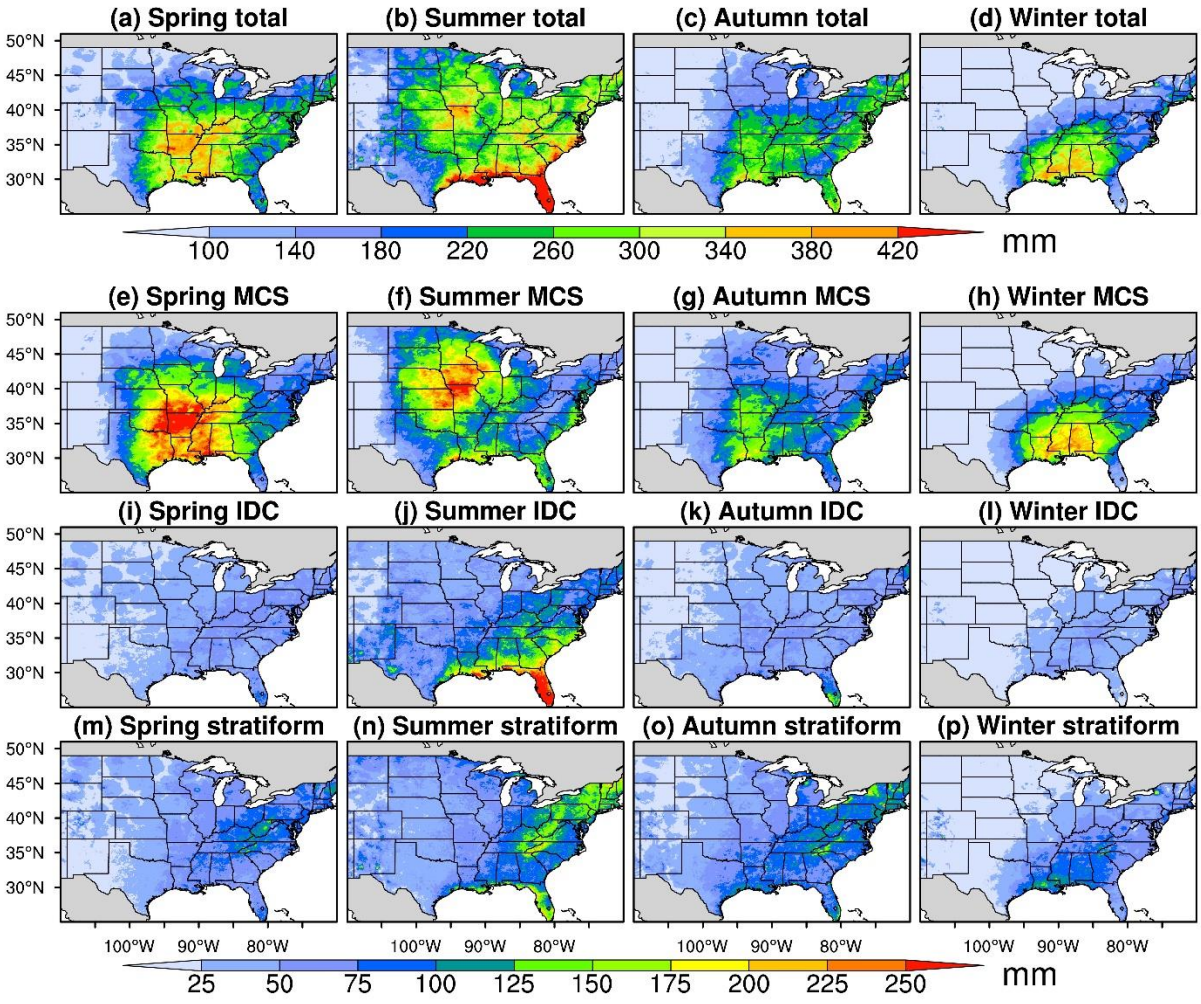
(a) Spring total
(b) Summer total
(c) Autumn total
(d) Winter total
50°N
45°N
40°N
35°N
30°N
100 140 180 220 260 300 340 380 420
mm
(e) Spring MCS
(f) Summer MCS
(g) Autumn MCS
(h) Winter MCS
(i) Spring IDC
(j) Summer IDC
(k) Autumn IDC
(l) Winter IDC
(m) Spring stratiform
(n) Summer stratiform
(o) Autumn stratiform
(p) Winter stratiform
100°W 90°W 80°W
25 50 75 100 125 150 175 200 225 250
mm

531

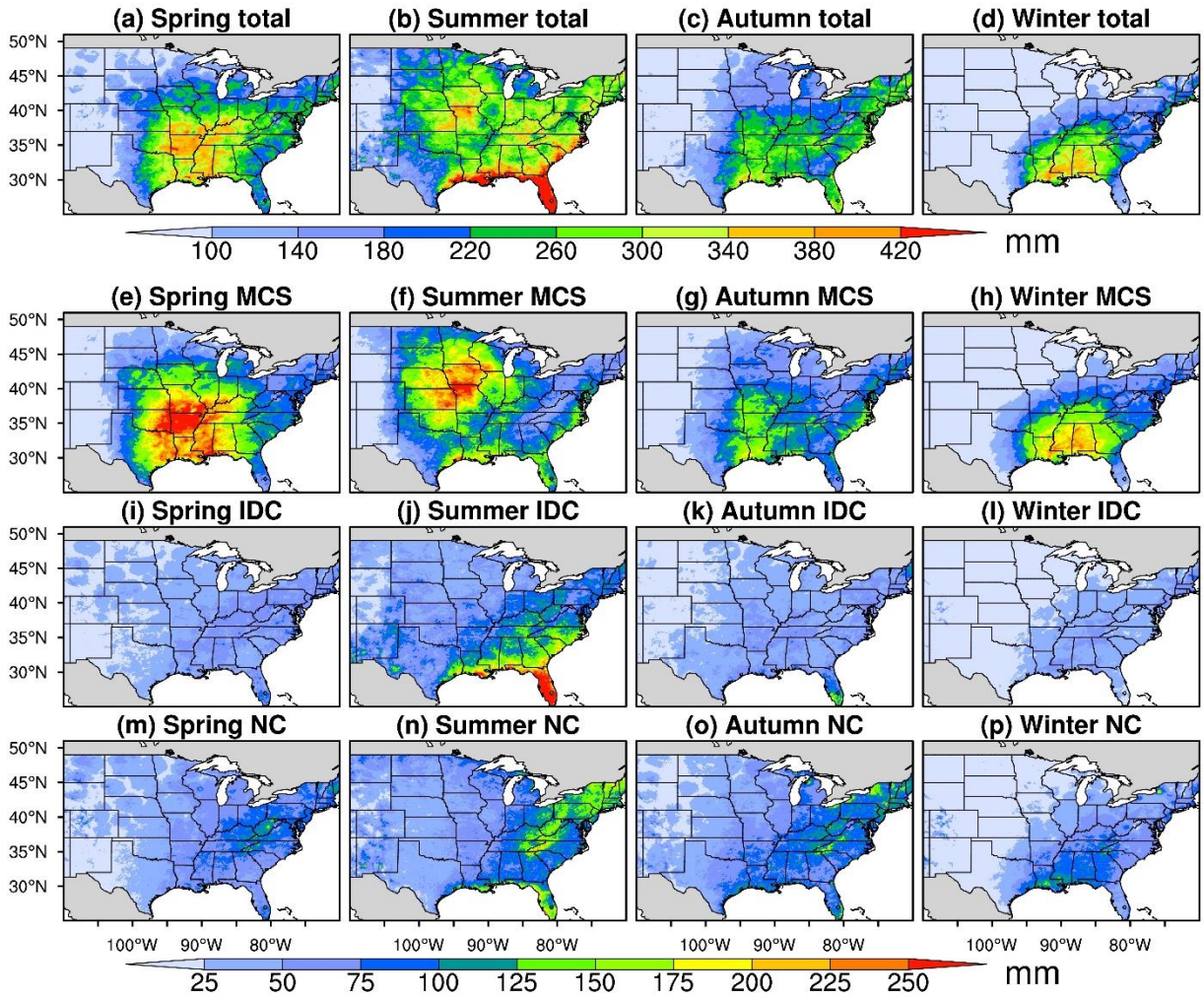

Figure ~~6~~8. Distributions of annual mean seasonal precipitation amounts for different types of precipitation for 2004 – 2017. The first row is for total precipitation, the second for MCS precipitation, the third row for IDC precipitation, and the fourth row for ~~stratiform~~ NC precipitation. The first column shows spring precipitation, the second column for summer, the third column for autumn, and the fourth column for winter. MCS, IDC, and ~~stratiform~~ NC precipitation share the same label bar. We exclude hourly data with precipitation ≤ 1 mm h^{-1} in the calculation.

The precipitation intensities of all three types peak in summer and reach minimums in winter (Figure ~~S9~~S7). In each season, precipitation intensities in the south are larger than those in the north except for MCS precipitation intensities in summer, which maximize in Oklahoma. We summarize the mean seasonal precipitation amounts and intensities of different types of precipitation over the 4 climate regions of Figure 1 in Table S4.

3.2.3 Diurnal cycles of different types of precipitation

Figure ~~7~~ 9 shows the monthly mean diurnal cycles of precipitation amounts from MCSs, IDC, and ~~stratiform~~ NC in the NGP, SGP, SE, and NE, respectively. Generally, MCS precipitation peaks during nighttime in the NGP, SGP, and NE. The seasonal shift of the peaks from spring in the SGP to summer in the NGP reflects the northward migration of the MCS precipitation center in the Great Plains (Figures ~~6e~~ 8e and ~~8~~6f).

The SE has significantly different diurnal cycles of MCS precipitation from other regions. In spring, SE MCS precipitation is mainly located in the western areas (Figure ~~6e~~8e), showing similar diurnal characteristics as the SGP MCS precipitation but with peaks in the early morning and late afternoon (Figures ~~7d~~ 9d and ~~7g~~9g). Besides, the SGP MCS precipitation peaks in May (Figure ~~7d~~9d), while SE peaks in April (Figure ~~7g~~9g), suggesting that the MCS precipitation center first appears in the western SE regions (Alabama, Mississippi, and Louisiana) in April, and then moves northwards to Arkansas in May. In summer, the SE MCS precipitation diurnal cycles are more like those of IDC (Figures ~~7g~~ 9g and ~~7h~~9h), peaking in the late afternoon and much different from those in the Great Plains. The significantly different precipitation diurnal variations between the Great Plains and SE were also identified by Haberlie and Ashley (2019). We find that most summer MCS precipitation over the SE occurs near the coastal areas (Figure ~~6f~~8f), far from the MCS precipitation center in northern Missouri and Iowa, suggesting either a different MCS genesis mechanism in the SE from those in the SGP and NGP (Feng et al., 2019) or long-duration deep convective systems showing MCS characteristics (Geerts, 1998). In autumn, the SE MCS precipitation peaks in the morning (Figure ~~7g~~9g). The diurnal cycle of MCS precipitation in September shows mixed features of summer and autumn with peaks both in

the morning and the afternoon. In winter months, the diurnal cycle of the SE MCS precipitation shifts from the autumn feature to the spring feature, with peaks shifting from the morning to the afternoon. The distinct diurnal cycles of SE MCS precipitation in different seasons in Figure 9g are roughly consistent with the corresponding seasonal diurnal variations of MCS occurrence frequencies from Geerts (1998), where the occurrence time of an MCS was defined as the central time between the initiation and decay of the MCS.

The diurnal cycles of IDC precipitation are consistent in all regions (Figures ~~7b~~9b, 9~~7~~e, 9~~7~~h, and 9~~7~~k), peaking in the late afternoon in summer (Tian et al., 2005), again reflecting the impact of local instability driven by the solar forcing on IDC development. ~~Stratiform~~ NC precipitation (Figures ~~7c~~9c, 9~~7~~f, 9~~7~~i, and 9~~7~~l) shows some diurnal cycle characteristics similar to IDC precipitation. It may be caused by the limitation of the temporal resolution of the datasets used in the FLEXTRKR algorithm. Weak IDC events that are shorter than 1 hour could be missed by Gridrad in identifying CCFs, as Gridrad Z_H only considers reflectivities within ± 3.8 minutes of the analysis time. These weak IDC could be aliased to ~~stratiform~~ NC precipitation, therefore showing some similar diurnal cycles as IDC. Another possible reason is that the FLEXTRKR algorithm may miss some parts of IDC clouds with $T_b \geq 241$ K, which are then classified as ~~stratiform~~NC, so the ~~stratiform~~ NC precipitation exhibits some IDC characteristics.

The monthly diurnal cycles of precipitation intensities for MCSs, IDC, and ~~stratiform~~ NC are generally similar among all regions, peaking in the late afternoon and early morning in the warm season (Figure ~~S10~~S8).

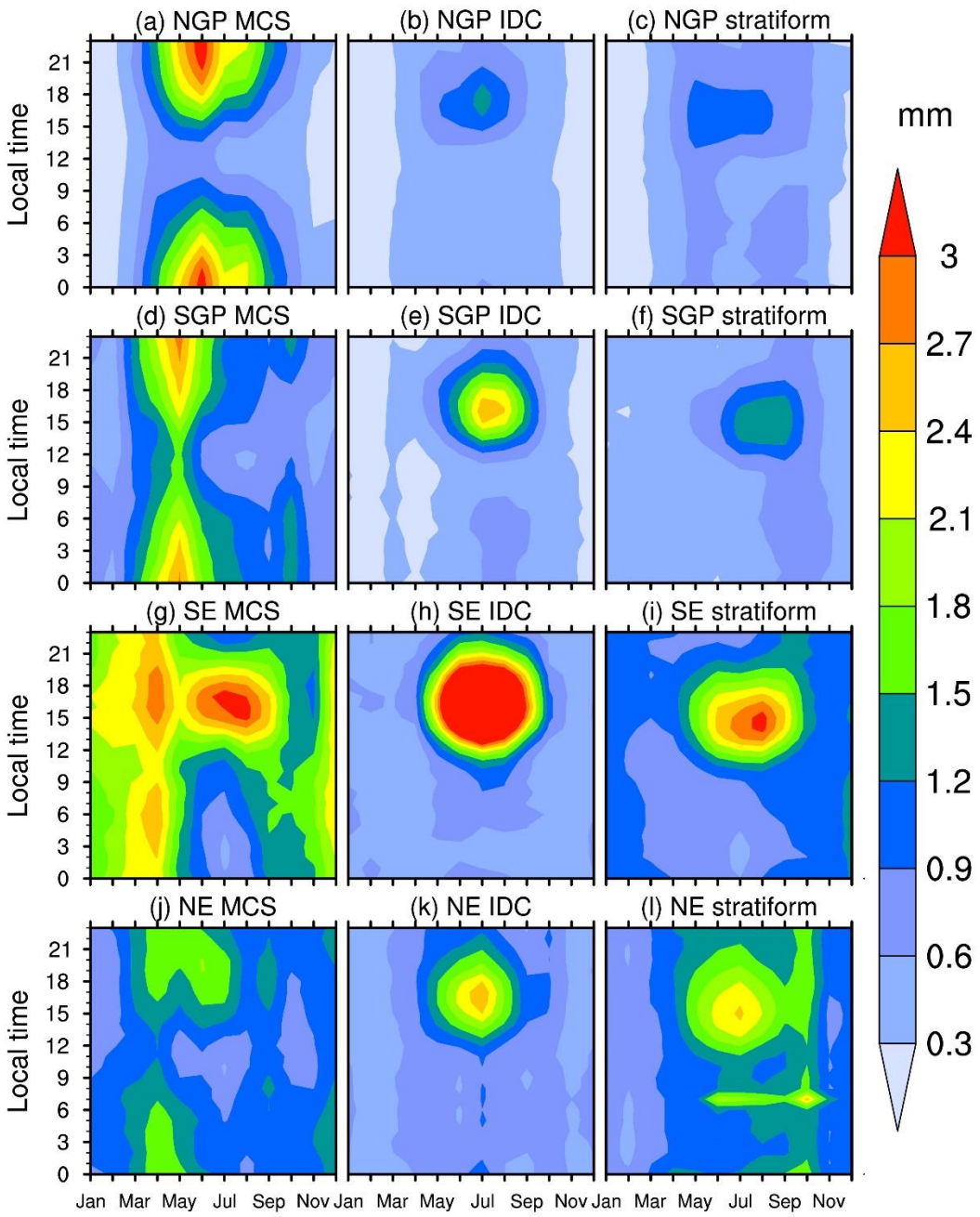
(a) NGP MCS
(b) NGP IDC
(c) NGP stratiform
(d) SGP MCS
(e) SGP IDC
(f) SGP stratiform
(g) SE MCS
(h) SE IDC
(i) SE stratiform
(j) NE MCS
(k) NE IDC
(l) NE stratiform
Local time
0
3
6
9
12
15
18
21
Jan Mar May Jul Sep Nov
mm
3
2.7
2.4
2.1
1.8
1.5
1.2
0.9
0.6
0.3

587

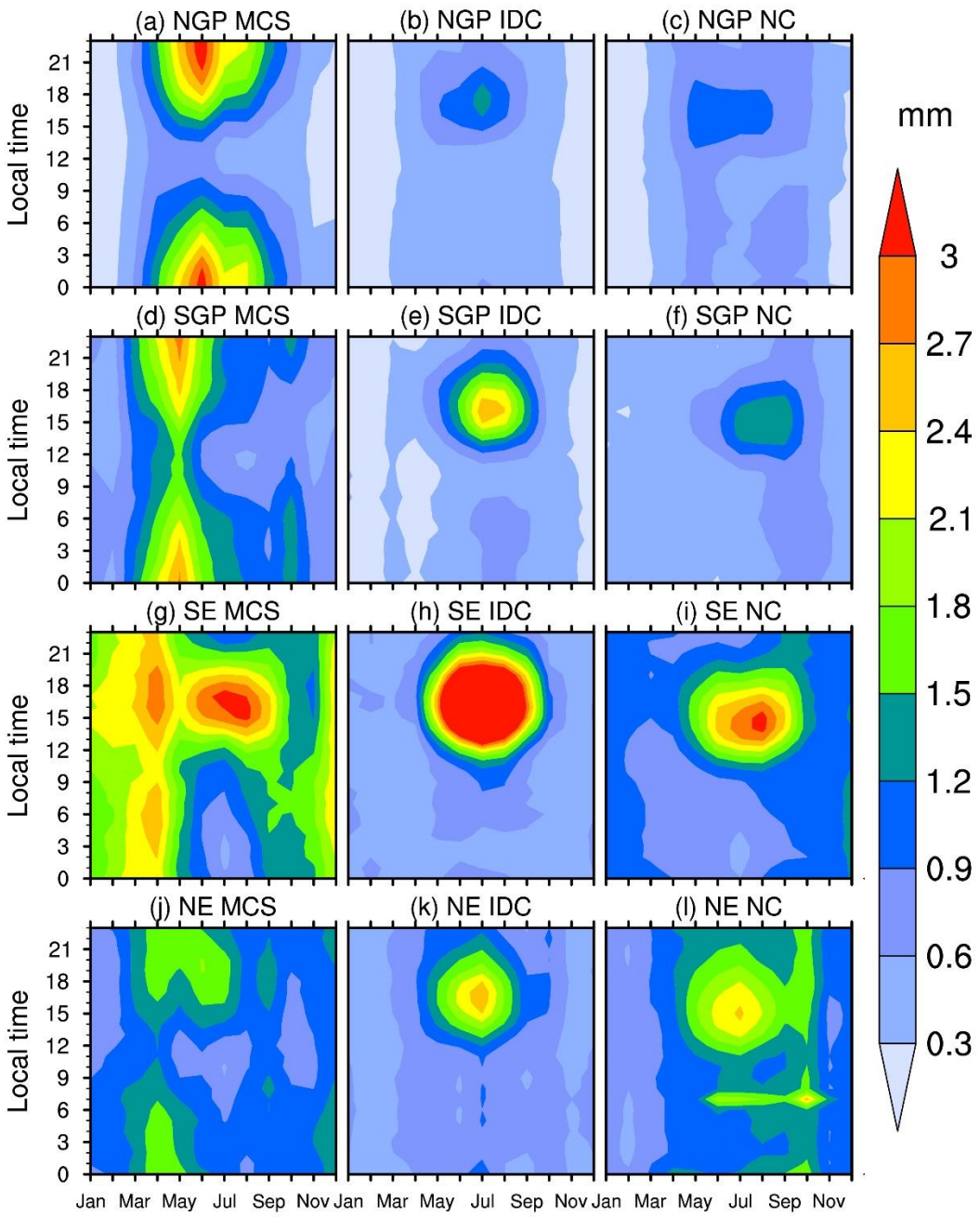

Figure ~~7~~9. Monthly mean diurnal cycles of precipitation amounts from MCSs (a, d, g, j), IDC (b, e, h, k), and ~~stratiform~~ NC (c, f, i, l) in the NGP (a, b, c), SGP (d, e, f), SE (g, h, i), and NE (j, k, l) during 2004 – 2017.

4 Uncertainties of the data product

4.1 Uncertainties from source datasets

The NCEP/CPP L3 4 km Global Merged IR V1 T_b dataset has been view-angle corrected and re-navigated for parallax (Janowiak et al., 2001) to reduce errors. However, the US continent is covered by two series of geostationary IR satellites (GOES-W and GEOS-E). During the production of the T_b dataset, the value with the smaller zenith angle is adopted when duplicate data are available in a grid pixel. Measurements from different satellites may be inconsistent. Janowiak et al. (2001) suggest this type of inconsistency to be considered minor.

For the Gridrad radar dataset, some bad volumes have been removed during the production of Gridrad Z_H. We further filter out potential low-quality observations, scanning artifacts, and non-meteorological echoes from biological scatters and artifacts following the approaches of Homeyer and Bowman (2017). However, there is another source of error from anomalous propagation caused by non-standard refractions of radar signals in the lower atmosphere, which cannot be mitigated during the filtering procedure. Non-standard refractions can result in underestimation or overestimation of the true radar beam altitude, thus affecting the location of radar reflectivity for binning. Estimating the corresponding uncertainties is out of the scope of this study. However, anomalous propagation is typically limited to radar beams traveling long distances in the boundary layer (Homeyer and Bowman, 2017).

Stage IV precipitation is a mosaic of precipitation estimates based on a combination of NEXRAD and gauge data from 12 RFCs. Therefore, the errors of Stage IV are from several sources, such as inherent NEXRAD biases, radar quantitative precipitation estimate (QPE)

algorithm biases, bad gauge data removal inconsistency among different RFCs, multisensory processing algorithm inconsistency among different RFCs, and mosaicking border discontinuities (Nelson et al., 2016). The most severe errors occur in the western US, where NEXRAD data are limited, and a gauge-only rainfall estimation algorithm is used (Nelson et al., 2016; Smalley et al., 2014). Hence our data product has a geographical focus east of the Rocky Mountains, with the best NEXRAD coverage in the US. After regridding the Stage IV precipitation into our 4-km domain, we further manually filter out certain "erroneous precipitation" hours and set all precipitation in those hours to missing values. "Erroneous precipitation" is defined as sudden appearance and disappearance of a large contiguous area (> 4,800 km^2) with intense precipitation (> 40 mm h^{-1}) (Figure ~~S11~~S9), which is physically not possible. There are 40 hours in total in the period 2004 – 2017 containing such "erroneous precipitation."

As the FLEXTRKR algorithm is applied to a combination of three independent types of remote sensing datasets, we identify the most robust MCS/IDC events satisfying all the criteria based on the three datasets. It reduces the potential false classification of tracks as MCSs or IDC based on any single dataset. And to consider the potential error of ERA5 melting level heights, we require $Z_H \geq 45$ dBZ above (Z_{melt} + 1) km for convective classification in the SL3D algorithm (Table S2).

4.2 The impact of missing data

In the CCS identification step of the FLEXTRKR algorithm, we require the fraction of missing satellite T_b in the domain at each hour to be less than 20%. Otherwise, the hour is excluded from our data product. During 2004 – 2017, we excluded 716 hours with missing

satellite T_b data, accounting for less than 0.6% of the total period. The year with the most missing satellite data is 2008, with 206 missing hours (2.3%), followed by 2004 with 154 hours (1.8%). All other years have no more than 57 missing hours. During the link procedure of the FLEXTRKR algorithm, we search the next hour if a missing hour is encountered, as long as the time gap between the two "linked" hours is less than 4 hours. Otherwise, we start new tracks from the next available hour. This method aims to reduce the impact of the missing hours. Considering the high completeness of the satellite T_b data in 2004 – 2017, we conclude that the missing satellite data have little effect on the data product.

We show the distribution of the fractions of valid Stage IV precipitation data in 2004 – 2017 in Figure ~~S12~~S10. The fractions are over 97% for all grid cells of the US in the domain. Most grid cells in the US have less than 2% missing hours, which should have a negligible impact on the data product.

Figure ~~S13~~ S11 shows the fractions of available Gridrad reflectivity data from 2004 to 2017 between 1 km and 12 km ASL. The fractions are relatively high over the majority of the troposphere except for 1 km ASL. Based on the criteria of the SL3D algorithm, Z_H at 1 km is rarely used and can be easily substituted by Z_H at 2 km. Generally, Gridrad has good spatial coverage during the period with most grid cells east of the Rocky Mountains having fractions > 90% between 2 and 9 km and 80% between 10 and 12 km. The completeness of the Gridrad dataset is relatively lower compared to the satellite T_b and Stage IV precipitation datasets, and Gridrad Z_H is a crucial variable in the SL3D classification and MCS/IDC identification. Therefore, the missing data of Gridrad Z_H should have some impacts on our data product.

However, as an advanced long-term high-resolution 3-D radar reflectivity dataset, Gridrad is valuable for constructing a climatological MCS/IDC data product.

4.3 Temporal resolution limitation of the source datasets

As we discussed in Section 3.2.3, the diurnal cycles of ~~stratiform~~ NC precipitation show some possible aliasing from IDC precipitation. Some weak IDC events are so short that the hourly data cannot properly capture their occurrence, especially for Gridrad Z_H, which only includes reflectivities within ± 3.8 minutes of each hour. We calculate the cumulative distribution functions of PF-based lifetimes for MCS and IDC events and their associated precipitation in the data product for 2004 – 2017, as shown in Figure ~~8~~10. About 75% of IDC events have a PF-based lifetime of 1 hour. Therefore, it is almost certain that we miss some IDC events shorter than 1 hour in the data product. Here we give an estimate of the probability *p* that a given IDC event with a convective signal duration of *x* minutes is detected by radar, as expressed below:

$$p = \frac{2 \times 3.8}{60 - x} \quad (1)$$

where the numerator is the time window of Gridrad observation in each hour, and *x* is the duration of the IDC event. The detection probability is only about 25% when $x = 30$ minutes. To obtain a detection probability of 50%, we require $x \geq 45$ minutes. Hence, we cannot assess the distribution of IDC convective signals with durations less than 1 hour using the currently available datasets. Higher-resolution datasets, such as individual NEXRAD radar data, which typically has an update cycle of 4-5 min, are necessary to derive the information. However, as shown in Figure ~~8~~10, we find that precipitation from IDC events with a 1-hour PF lifetime only

accounts for about 10% of the total IDC precipitation. Therefore, IDC events with PF lifetimes less than 1 hour should have a relatively small impact on precipitation.

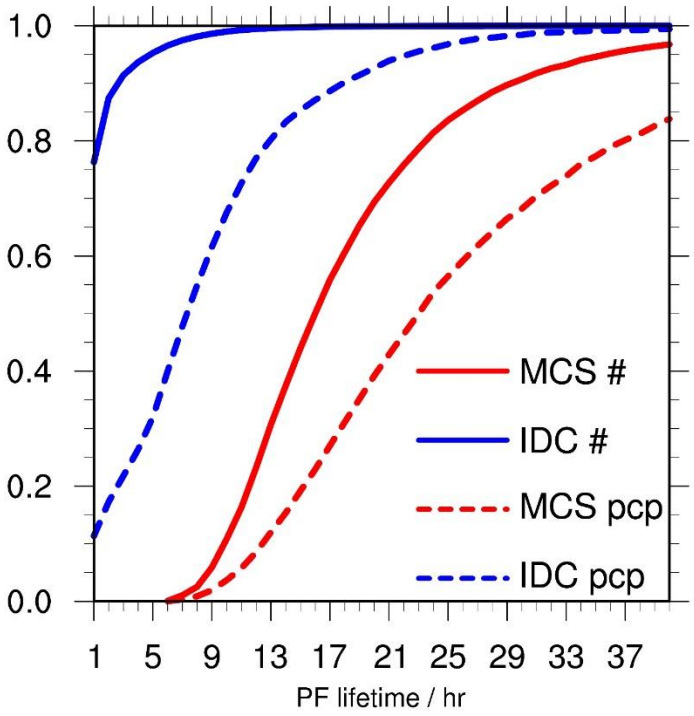

Figure ~~8~~10. Cumulative distribution functions of PF-based lifetimes for MCS and IDC events and their associated precipitation in the data product domain for 2004 – 2017. The red solid line is for the number of MCSs, the red dash line for MCS associated precipitation, the blue solid line for the number of IDC events, and the blue dash line for IDC associated precipitation.

4.4 The impact of MCS and IDC definition criteria

The separation between MCSs and long-lasting IDC events is somewhat fuzzy (Feng et al., 2019; Geerts et al., 2017; Haberlie and Ashley, 2019; Pinto et al., 2015; Prein et al., 2017). Here, we briefly examine the impact of different MCS/IDC definition criteria on the data product. We change the definition of MCSs to relax the CCS and PF size and duration thresholds. Specifically, the second and third criteria listed in Section 2.2.2 are modified as follows: 2) CCS areas associated with the track surpass 40,000 km^2 for more than 4 continuous hours; 3) PF major axis length exceeding 80 km and intense convective cell areas $\geq$ 16 km^2 exist for more

than 3 consecutive hours. And we also require that each merge/split-track associated with MCS/IDC events must have a CCS-based lifetime of no more than 3 hours. We keep the definition of IDC the same as described in Section 2~~3~~.2.2, which is a limit for IDC that we can identify based on the source datasets.

By using the new definition, as expected, the lifetimes and spatial coverages of MCSs are reduced, and those of IDC change little because most IDC events cannot satisfy the new MCS criteria (Tables 1 and S5). The annual number of MCSs identified in 2004 – 2017 increases from 454 to 857. The number increases from 122 to 207 in spring, 212 to 434 in summer, 83 to 151 in autumn, and 37 to 62 in winter. As PF-based lifetimes of MCS/IDC events in summer are the shortest (Table 1), the new definition has the most significant impact in summer. The annual number of IDC decreases from 45,346 to 45,225. Reducing the merge/split lifetime limit retains more independent IDC events, which is the reason why the decrease in the number of IDC events is smaller than the increase in the number of MCSs. Annual mean MCS precipitation east of the Rocky Mountains increases from 313 mm to 353 mm, while IDC precipitation decreases from 170 mm to 130 mm. The fraction of MCS precipitation only increases by 6% (from 45% to 51%), compared to the almost doubling of MCS number (from 454 to 857), suggesting the MCS definition in the original data product is capable of capturing most of the important MCSs with heavy precipitation. Similar to MCS numbers, summer has the most increase in MCS precipitation amount, from 100 mm to 119 mm. And annual mean MCS and IDC precipitation intensities decrease slightly as MCS precipitation intensities are somewhat larger than IDC in most regions (Tables S3, S4, S6, and S7). We summarize the regional precipitation statistics of the NGP, SGP, SE, and NE based on the new definition in Tables S6 and S7.

Although the new definition changes the absolute values of MCS/IDC characteristics, the contrast between MCS and IDC events is still present. The new definition has small impacts on the spatial distribution patterns of MCS/IDC precipitation. And ~~stratiform~~ NC precipitation characteristics are almost the same as before. Therefore, our original definition captures the essential characteristics of MCS and IDC events. In addition, the original data product is complete and flexible. We store all criteria variables of MCS/IDC events in the data product. Users can easily change the definition of MCSs and switch between tracks that are attributed to MCS and IDC without re-running the FLEXTRKR algorithm. There is no need to change the "track" and "merge" lifetime criterion as we do above because they have little impact on the climatological characteristics of MCS and IDC events.

4.5 Recommendations for the usage of the MCS/IDC data product

Considering the limitations and uncertainties mentioned above, we generally recommend using the data product for observational analyses and model evaluations of convection statistics and characteristics over relatively long periods such as a month, a season, or longer to fully take advantage of the long term dataset, although analysis of individual weather events is also possible as supported by the hourly temporal resolution of the data product. In addition, since the completeness and quality of the source radar dataset degrade dramatically beyond the US border and over the Rocky Mountains (Figure ~~S13~~S11), we recommend the usage of the data product within the CONUS east of the Rocky Mountains to alleviate the impact of the termination of MCS/IDC tracks due to poor radar coverage and missing radar data beyond their maximum scan range.

Detailed investigation of a short period or a specific MCS/IDC event is acceptable, but cautions should be taken when encountering missing data around the track during the period. Due to the complexity of the algorithms used to develop the data product, it is difficult to quantify the impact of missing data on the MCS/IDC track. Therefore, we do not recommend examining a specific MCS/IDC track if there are too many missing data (precipitation, T_b, or Z_H) along the track. Users planning to apply the data product for a specific case study should examine the availability of the source data first, which are also stored in the data product except for 3-D Z_H due to the large data volume. Users can access the original 3-D Z_H at https://rda.ucar.edu/datasets/ds841.0/ (Table S1).

Lastly, although our sensitivity test in Section 4.4 shows that precipitation characteristics are similar between two different sets of MCS/IDC definition criteria, we still recommend users conduct further sensitivity tests and examine the impact of different definition criteria on the results if the data product is applied to other studies, such as the effects of MCS and IDC events on atmospheric circulation, environmental conditions associated with the initiation and evolution of MCS and IDC events, and MCS/IDC associated weather hazards.

5 Data availability

The high-resolution (4 km hourly) MCS/IDC data product and the corresponding user guide document are available at http://dx.doi.org/10.25584/1632005 (Li et al., 2020). The original format of the data files is NetCDF-4, and we archive them as compressed files for each year so that the data product is easily accessible. The user guide contains a brief explanation about the approach to develop the data product and a detailed description of the data file content to help users understand the data product.

6 Conclusions

Here we present a unified high-resolution (4 km, hourly) data product that describes the spatiotemporal characteristics of MCS and IDC events from 2004 to 2017 east of the Rocky Mountains over the CONUS. We produce the data product by applying an updated FLEXTRKR algorithm to the NCEP/CPP L3 4 km Global Merged IR V1 T_b dataset, ERA5 melting level heights, the 3-D Gridrad radar reflectivity dataset, and the Stage IV precipitation dataset. Climatological features of the MCS and IDC events from the data product are compared, with a focus on their precipitation characteristics. Consistent with our definitions of MCSs and IDC in the FLEXTRKR algorithm, we find that MCSs have much broader spatial coverage and longer duration than IDC events. While there are many more frequent IDC occurrences than MCSs, the mean convective intensities of IDC events are comparable to those of MCSs. MCS and IDC events both contribute significantly to precipitation east of the Rocky Mountains but with distinct spatiotemporal variabilities. MCS precipitation affects most regions of the eastern US in all seasons, especially in spring and summer. The MCS precipitation center migrates northwards from Arkansas in spring to northern Missouri and Iowa in summer, followed by a southward migration to Louisiana in autumn, and finally to Mississippi and Alabama in the Southeast in winter. IDC precipitation mostly concentrates in the Southeast in summer. IDC precipitation shows a significant diurnal cycle in summer months with a peak around 16:00 – 17:00 Local Time over all regions east of the Rocky Mountains. In contrast, MCS precipitation peaks during nighttime in spring and summer for most regions except for the Southeast, where MCS precipitation peaks in the late afternoon in summer, similar to IDC precipitation. Lastly, we analyze the potential uncertainties of the data product and the sensitivity of the dataset to MCS definitions and give our recommendations for the usage of the data product. The data product

will be useful for investigating the atmospheric environments and physical processes associated with convective systems, quantifying the impacts of convection on hydrology, atmospheric chemistry, severe weather hazards, and other aspects of the energy, water, and biogeochemical cycles, and improving the representation of convective processes in weather and climate models.

Author contributions

JL and ZF updated the FLEXTRKR algorithm and prepared the source datasets. JL ran the SL3D and updated FLEXTRKR algorithms for 2004 – 2017. JL collected and archived the MCS/IDC data product and did the analyses. JL led the writing of the manuscript with input from ZF, YQ, and LRL. YQ and LRL guided the development of the data product. JL, ZF, YQ, and LRL reviewed the manuscript.

Competing interests

The authors declare that they have no conflict of interest.

Acknowledgments

This research was supported by the US Department of Energy Office of Science Biological and Environmental Research as part of the Regional and Global Modeling and Analysis (RGMA) program area through the Integrated Coastal Modeling (ICoM) project. LRL and ZF were also partly supported by the Water Cycle and Climate Extremes Modeling (WACCEM) Scientific Focus Area funded by RGMA. The research used computational resources from the National Energy Research Scientific Computing Center (NERSC), a DOE User Facility supported by the Office of Science under Contract DE-AC02-05CH11231. PNNL is operated for DOE by Battelle

Memorial Institute under Contract DE-AC05-76RL01830. We thank Dr. Cameron R. Homeyer from the University of Oklahoma for helping us understand the Gridrad dataset and Dr. Jingyu Wang from PNNL for identifying the existence of erroneous Stage IV precipitation. We obtain the NCEP/CPP L3 half-hourly 4 km Global Merged IR V1 brightness temperature dataset from https://disc.gsfc.nasa.gov/datasets/GPM_MERGIR_1/summary (last access: Dec 28, 2019). The 3D Gridrad dataset is from https://rda.ucar.edu/datasets/ds841.0/ (last access: Jan 2, 2020). We download hourly Stage IV precipitation data from https://rda.ucar.edu/datasets/ds507.5/ (last access: Dec 28, 2019), and the ERA5 melting level height data was downloaded from https://doi.org/10.24381/cds.adbb2d47 (last access: Jan 24, 2020).

References

Anderson, J. G., Weisenstein, D. K., Bowman, K. P., Homeyer, C. R., Smith, J. B., Wilmouth, D. M., Sayres, D. S., Klobas, J. E., Leroy, S. S., and Dykema, J. A.: Stratospheric ozone over the United States in summer linked to observations of convection and temperature via chlorine and bromine catalysis, Proc. Natl. Acad. Sci. U.S.A., 114, E4905-E4913, https://doi.org/10.1073/pnas.1619318114, 2017.

Andreae, M. O., Artaxo, P., Fischer, H., Freitas, S., Grégoire, J. M., Hansel, A., Hoor, P., Kormann, R., Krejci, R., and Lange, L.: Transport of biomass burning smoke to the upper troposphere by deep convection in the equatorial region, Geophys. Res. Lett., 28, 951-954, https://doi.org/10.1029/2000GL012391, 2001.

Angel, J. R., Palecki, M. A., and Hollinger, S. E.: Storm precipitation in the United States. Part II: Soil erosion characteristics, Journal of Applied Meteorology, 44, 947-959, https://doi.org/10.1175/JAM2242.1, 2005.

Bigelbach, B., Mullendore, G., and Starzec, M.: Differences in deep convective transport characteristics between quasi‐isolated strong convection and mesoscale convective systems using seasonal WRF simulations, J. Geophys. Res.-Atmos., 119, 11,445-411,455, https://doi.org/10.1002/2014JD021875, 2014.

Brooks, H. E., Doswell III, C. A., and Kay, M. P.: Climatological estimates of local daily tornado probability for the United States, Weather and Forecasting, 18, 626-640, https://doi.org/10.1175/1520-0434(2003)018<0626:CEOLDT>2.0.CO;2, 2003.

Carpenter, S. R., Booth, E. G., and Kucharik, C. J.: Extreme precipitation and phosphorus loads from two agricultural watersheds, Limnol. Oceanogr., 63, 1221-1233, https://doi.org/10.1002/lno.10767, 2018.

Changnon, S. A.: Damaging thunderstorm activity in the United States, Bulletin of the American Meteorological Society, 82, 597-608, https://doi.org/10.1175/1520-0477(2001)082<0597:DTAITU>2.3.CO;2, 2001a.

Changnon, S. A.: Thunderstorm rainfall in the conterminous United States, Bulletin of the American Meteorological Society, 82, 1925-1940, https://doi.org/10.1175/1520-0477(2001)082<1925:TRITCU>2.3.CO;2, 2001b.

Choi, S., Joiner, J., Choi, Y., Duncan, B., Vasilkov, A., Krotkov, N., and Bucsela, E.: First estimates of global free-tropospheric NO_2 abundances derived using a cloud-slicing technique applied to satellite observations from the Aura Ozone Monitoring Instrument (OMI), Atmos. Chem. Phys, 14, 10,565-510,588, https://doi.org/10.5194/acp-14-10565-2014, 2014.

Cintineo, J. L., Pavolonis, M. J., Sieglaff, J. M., and Heidinger, A. K.: Evolution of severe and nonsevere convection inferred from GOES-derived cloud properties, Journal of applied meteorology and climatology, 52, 2009-2023, https://doi.org/10.1175/JAMC-D-12-0330.1, 2013.

Davis, C., Brown, B., and Bullock, R.: Object-based verification of precipitation forecasts. Part I: Methodology and application to mesoscale rain areas, Monthly Weather Review, 134, 1772-1784, https://doi.org/10.1175/MWR3145.1, 2006.

Davison, M.: Shallow/Deep Convection: https://www.wpc.ncep.noaa.gov/international/training/deep/index.htm, access: April 9, 2020, 1999.

Derbile, E. K., and Kasei, R. A.: Vulnerability of crop production to heavy precipitation in north-eastern Ghana, International Journal of Climate Change Strategies and Management, https://doi.org/10.1108/17568691211200209, 2012.

Diffenbaugh, N. S., Scherer, M., and Trapp, R. J.: Robust increases in severe thunderstorm environments in response to greenhouse forcing, Proc. Natl. Acad. Sci. U.S.A., 110, 16361-16366, https://doi.org/10.1073/pnas.1307758110, 2013.

Doswell III, C. A., Brooks, H. E., and Maddox, R. A.: Flash flood forecasting: An ingredients-based methodology, Weather and Forecasting, 11, 560-581, https://doi.org/10.1175/1520-0434(1996)011<0560:FFFAIB>2.0.CO;2, 1996.

ECMWF: ERA5 hourly data on single levels from 1979 to present, available at https://cds.climate.copernicus.eu/cdsapp#!/dataset/reanalysis-era5-single-levels?tab=overview, https://doi.org/10.24381/cds.adbb2d47, 2018 (last access: Jan 24, 2020).

Feng, Z., Dong, X., Xi, B., Schumacher, C., Minnis, P., and Khaiyer, M.: Top‐of‐atmosphere radiation budget of convective core/stratiform rain and anvil clouds from deep convective systems, J. Geophys. Res.-Atmos., 116, https://doi.org/10.1029/2011JD016451, 2011.

Feng, Z., Dong, X., Xi, B., McFarlane, S. A., Kennedy, A., Lin, B., and Minnis, P.: Life cycle of midlatitude deep convective systems in a Lagrangian framework, J. Geophys. Res.-Atmos., 117, https://doi.org/10.1029/2012JD018362, 2012.

Feng, Z., Leung, L. R., Houze Jr, R. A., Hagos, S., Hardin, J., Yang, Q., Han, B., and Fan, J.: Structure and evolution of mesoscale convective systems: Sensitivity to cloud microphysics in convection‐permitting simulations over the United States, Journal of Advances in Modeling Earth Systems, 10, 1470-1494, https://doi.org/10.1029/2018MS001305, 2018.

Feng, Z., Houze Jr, R. A., Leung, L. R., Song, F., Hardin, J. C., Wang, J., Gustafson Jr, W. I., and Homeyer, C. R.: Spatiotemporal characteristics and large-scale environments of mesoscale convective systems east of the Rocky Mountains, J. Clim., 32, 7303-7328, https://doi.org/10.1175/JCLI-D-19-0137.1, 2019.

Folger, P., and Reed, A.: Severe thunderstorms and tornadoes in the United States, Congressional Research Service, 2013.

French, A. J., and Parker, M. D.: The initiation and evolution of multiple modes of convection within a meso-alpha-scale region, Weather and forecasting, 23, 1221-1252, https://doi.org/10.1175/2008WAF2222136.1, 2008.

Fritsch, J. M., Kane, R. J., and Chelius, C. R.: The contribution of mesoscale convective weather systems to the warm-season precipitation in the United States, Journal of Applied Meteorology and Climatology, 25, 1333-1345, https://doi.org/10.1175/1520-0450(1986)025<1333:TCOMCW>2.0.CO;2, 1986.

Futyan, J. M., and Del Genio, A. D.: Deep convective system evolution over Africa and the tropical Atlantic, J. Clim., 20, 5041-5060, https://doi.org/10.1175/JCLI4297.1, 2007.

Geerts, B.: Mesoscale convective systems in the southeast United States during 1994–95: A survey, Weather and Forecasting, 13, 860-869, https://doi.org/10.1175/1520-0434(1998)013<0860:MCSITS>2.0.CO;2, 1998.

Geerts, B., Parsons, D., Ziegler, C. L., Weckwerth, T. M., Biggerstaff, M. I., Clark, R. D., Coniglio, M. C., Demoz, B. B., Ferrare, R. A., and Gallus Jr, W. A.: The 2015 plains elevated convection at night field project, Bulletin of the American Meteorological Society, 98, 767-786, https://doi.org/10.1175/BAMS-D-15-00257.1, 2017.

Giangrande, S. E., Krause, J. M., and Ryzhkov, A. V.: Automatic designation of the melting layer with a polarimetric prototype of the WSR-88D radar, Journal of Applied Meteorology and Climatology, 47, 1354-1364, https://doi.org/10.1175/2007JAMC1634.1, 2008.

Gourley, J. J., Hong, Y., Flamig, Z. L., Wang, J., Vergara, H., and Anagnostou, E. N.: Hydrologic evaluation of rainfall estimates from radar, satellite, gauge, and combinations on Ft. Cobb basin, Oklahoma, Journal of Hydrometeorology, 12, 973-988, https://doi.org/10.1175/2011JHM1287.1, 2011.

Grewe, V.: Impact of climate variability on tropospheric ozone, Sci. Total Environ., 374, 167-181, https://doi.org/10.1016/j.scitotenv.2007.01.032, 2007.

Groisman, P. Y., Knight, R. W., Karl, T. R., Easterling, D. R., Sun, B., and Lawrimore, J. H.: Contemporary changes of the hydrological cycle over the contiguous United States: Trends derived from in situ observations, Journal of hydrometeorology, 5, 64-85, https://doi.org/10.1175/1525-7541(2004)005<0064:CCOTHC>2.0.CO;2, 2004.

Haberlie, A. M., and Ashley, W. S.: A radar-based climatology of mesoscale convective systems in the United States, J. Clim., 32, 1591-1606, https://doi.org/10.1175/JCLI-D-18-0559.1, 2019.

Hersbach, H., Bell, B., Berrisford, P., Horányi, A., Sabater, J. M., Nicolas, J., Radu, R., Schepers, D., Simmons, A., and Soci, C.: Global reanalysis: goodbye ERA-Interim, hello ERA5, in: ECMWF Newsl, 159, 17-24, https://doi.org/10.21957/vf291hehd7, 2019.

Hodges, K. I., and Thorncroft, C.: Distribution and statistics of African mesoscale convective weather systems based on the ISCCP Meteosat imagery, Monthly Weather Review, 125, 2821-2837, https://doi.org/10.1175/1520-0493(1997)125<2821:DASOAM>2.0.CO;2, 1997.

Homeyer, C. R., and Bowman, K. P.: Algorithm Description Document for Version 3.1 of the Three-Dimensional Gridded NEXRAD WSR-88D Radar (GridRad) Dataset, available at http://gridrad.org/pdf/GridRad-v3.1-Algorithm-Description.pdf, 23, 2017.

Houze Jr, R. A.: Mesoscale convective systems, Rev. Geophys., 42, https://doi.org/10.1029/2004RG000150, 2004.

Houze Jr, R. A., Wang, J., Fan, J., Brodzik, S., and Feng, Z.: Extreme convective storms over high - latitude continental areas where maximum warming is occurring, Geophys. Res. Lett., 46, 4059-4065, https://doi.org/10.1029/2019GL082414, 2019.

Hu, H., Leung, L. R., and Feng, Z.: Observed Warm - Season Characteristics of MCS and Non - MCS Rainfall and Their Recent Changes in the Central United States, Geophys. Res. Lett., 47, e2019GL086783, https://doi.org/10.1029/2019GL086783, 2020.

Janowiak, J., Joyce, B., and Xie, P.: NCEP/CPC L3 half hourly 4 km global (60 S–60 N) merged IR V1, available at https://disc.gsfc.nasa.gov/datasets/GPM_MERGIR_1/summary, https://doi.org/10.5067/P4HZB9N27EKU, 2017 (last access: Dec 28, 2019).

Janowiak, J. E., Joyce, R. J., and Yarosh, Y.: A real-time global half-hourly pixel-resolution infrared dataset and its applications, Bulletin of the American Meteorological Society, 82, 205-218, https://doi.org/10.1175/1520-0477(2001)082<0205:ARTGHH>2.3.CO;2, 2001.

Kalinga, O. A., and Gan, T. Y.: Estimation of rainfall from infrared - microwave satellite data for basin - scale hydrologic modelling, Hydrological processes, 24, 2068-2086, https://doi.org/10.1002/hyp.7626, 2010.

Koehler, T. L.: Cloud-to-Ground Lightning Flash Density and Thunderstorm Day Distributions over the Contiguous United States Derived from NLDN Measurements: 1993–2018, Monthly Weather Review, 148, 313-332, https://doi.org/10.1175/MWR-D-19-0211.1, 2020.

Li, J., Feng, Z., Qian, Y., and Leung, L. R.: MCSs and IDC in the US for 2004 – 2017, available at https://data.pnnl.gov/dataset/13218, http://dx.doi.org/10.25584/1632005, 2020 (last access: Jun 18, 2020).

Lin, Y., and Mitchell, K. E.: 1.2 the NCEP stage II/IV hourly precipitation analyses: Development and applications, 19th Conf. Hydrology, American Meteorological Society, San Diego, CA, USA, 2005,

Liu, C., Zipser, E. J., and Nesbitt, S. W.: Global distribution of tropical deep convection: Different perspectives from TRMM infrared and radar data, J. Clim., 20, 489-503, https://doi.org/10.1175/JCLI4023.1, 2007.

Lopez, P.: Direct 4D-Var assimilation of NCEP stage IV radar and gauge precipitation data at ECMWF, Monthly Weather Review, 139, 2098-2116, https://doi.org/10.1175/2010MWR3565.1, 2011.

Machado, L., Rossow, W., Guedes, R., and Walker, A.: Life cycle variations of mesoscale convective systems over the Americas, Monthly Weather Review, 126, 1630-1654, https://doi.org/10.1175/1520-0493(1998)126<1630:LCVOMC>2.0.CO;2, 1998.

Motew, M., Booth, E. G., Carpenter, S. R., Chen, X., and Kucharik, C. J.: The synergistic effect of manure supply and extreme precipitation on surface water quality, Environmental Research Letters, 13, 044016, https://doi.org/10.1088/1748-9326/aaade6, 2018.

Nearing, M., Pruski, F., and O'neal, M.: Expected climate change impacts on soil erosion rates: a review, Journal of soil and water conservation, 59, 43-50, 2004.

Nelson, B. R., Prat, O. P., Seo, D.-J., and Habib, E.: Assessment and implications of NCEP Stage IV quantitative precipitation estimates for product intercomparisons, Weather and Forecasting, 31, 371-394, https://doi.org/10.1175/WAF-D-14-00112.1, 2016.

Piani, C., Durran, D., Alexander, M., and Holton, J.: A numerical study of three-dimensional gravity waves triggered by deep tropical convection and their role in the dynamics of the QBO, Journal of the atmospheric sciences, 57, 3689-3702, https://doi.org/10.1175/1520-0469(2000)057<3689:ANSOTD>2.0.CO;2, 2000.

Pinto, J. O., Grim, J. A., and Steiner, M.: Assessment of the High-Resolution Rapid Refresh model's ability to predict mesoscale convective systems using object-based evaluation, Weather and Forecasting, 30, 892-913, https://doi.org/10.1175/WAF-D-14-00118.1, 2015.

Prein, A. F., Liu, C., Ikeda, K., Bullock, R., Rasmussen, R. M., Holland, G. J., and Clark, M.: Simulating North American mesoscale convective systems with a convection-permitting climate model, Climate Dynamics, 1-16, https://doi.org/10.1007/s00382-017-3993-2, 2017.

Rosenzweig, C., Tubiello, F. N., Goldberg, R., Mills, E., and Bloomfield, J.: Increased crop damage in the US from excess precipitation under climate change, Global Environ. Change, 12, 197-202, https://doi.org/10.1016/S0959-3780(02)00008-0, 2002.

Rowe, A. K., Rutledge, S. A., and Lang, T. J.: Investigation of microphysical processes occurring in isolated convection during NAME, Monthly weather review, 139, 424-443, https://doi.org/10.1175/2010MWR3494.1, 2011.

Rowe, A. K., Rutledge, S. A., and Lang, T. J.: Investigation of microphysical processes occurring in organized convection during NAME, Monthly weather review, 140, 2168-2187, https://doi.org/10.1175/MWR-D-11-00124.1, 2012.

Seeley, J. T., and Romps, D. M.: The effect of global warming on severe thunderstorms in the United States, J. Clim., 28, 2443-2458, https://doi.org/10.1175/JCLI-D-14-00382.1, 2015.

Sieglaff, J. M., Hartung, D. C., Feltz, W. F., Cronce, L. M., and Lakshmanan, V.: A satellite-based convective cloud object tracking and multipurpose data fusion tool with application to developing convection, Journal of Atmospheric and Oceanic Technology, 30, 510-525, https://doi.org/10.1175/JTECH-D-12-00114.1, 2013.

Smalley, M., L'Ecuyer, T., Lebsock, M., and Haynes, J.: A comparison of precipitation occurrence from the NCEP Stage IV QPE product and the CloudSat Cloud Profiling Radar, Journal of hydrometeorology, 15, 444-458, https://doi.org/10.1175/JHM-D-13-048.1, 2014.

Song, F., Feng, Z., Leung, L. R., Houze Jr, R. A., Wang, J., Hardin, J., and Homeyer, C. R.: Contrasting spring and summer large-scale environments associated with mesoscale convective systems over the US Great Plains, J. Clim., 32, 6749-6767, https://doi.org/10.1175/JCLI-D-18-0839.1, 2019.

Starzec, M., Homeyer, C. R., and Mullendore, G. L.: Storm labeling in three dimensions (SL3D): A volumetric radar echo and dual-polarization updraft classification algorithm, Monthly Weather Review, 145, 1127-1145, https://doi.org/10.1175/MWR-D-16-0089.1, 2017.

Steiner, M., Houze Jr, R. A., and Yuter, S. E.: Climatological characterization of three-dimensional storm structure from operational radar and rain gauge data, Journal of Applied Meteorology, 34, 1978-2007, https://doi.org/10.1175/1520-0450(1995)034<1978:CCOTDS>2.0.CO;2, 1995.

Stensrud, D. J.: Effects of persistent, midlatitude mesoscale regions of convection on the large-scale environment during the warm season, Journal of the atmospheric sciences, 53, 3503-3527, https://doi.org/10.1175/1520-0469(1996)053<3503:EOPMMR>2.0.CO;2, 1996.

Stensrud, D. J.: Upscale effects of deep convection during the North American monsoon, Journal of the atmospheric sciences, 70, 2681-2695, https://doi.org/10.1175/JAS-D-13-063.1, 2013.

Taszarek, M., Allen, J. T., Púčik, T., Hoogewind, K. A., and Brooks, H. E.: Severe convective storms across Europe and the United States. Part II: ERA5 environments associated with lightning, large hail, severe wind, and tornadoes, J. Clim., 33, 10263-10286, https://doi.org/10.1175/JCLI-D-20-0346.1, 2020.

Thompson, A. M., Tao, W.-K., Pickering, K. E., Scala, J. R., and Simpson, J.: Tropical deep convection and ozone formation, Bulletin of the American Meteorological Society, 78, 1043-1054, https://doi.org/10.1175/1520-0477(1997)078<1043:TDCAOF>2.0.CO;2, 1997.

Tian, B., Held, I. M., Lau, N. C., and Soden, B. J.: Diurnal cycle of summertime deep convection over North America: A satellite perspective, J. Geophys. Res.-Atmos., 110, https://doi.org/10.1029/2004JD005275, 2005.

Tippett, M. K., Allen, J. T., Gensini, V. A., and Brooks, H. E.: Climate and hazardous convective weather, Current Climate Change Reports, 1, 60-73, https://doi.org/10.1007/s40641-015-0006-6, 2015.

Twohy, C. H., Clement, C. F., Gandrud, B. W., Weinheimer, A. J., Campos, T. L., Baumgardner, D., Brune, W. H., Faloona, I., Sachse, G. W., and Vay, S. A.: Deep convection as a source of new particles in the midlatitude upper troposphere, J. Geophys. Res.-Atmos., 107, AAC 6-1-AAC 6-10, https://doi.org/10.1029/2001JD000323, 2002.

Walker, J. R., MacKenzie Jr, W. M., Mecikalski, J. R., and Jewett, C. P.: An enhanced geostationary satellite–based convective initiation algorithm for 0–2-h nowcasting with object tracking, Journal of Applied Meteorology and Climatology, 51, 1931-1949, https://doi.org/10.1175/JAMC-D-11-0246.1, 2012.

Wang, P. K.: Moisture plumes above thunderstorm anvils and their contributions to cross‐tropopause transport of water vapor in midlatitudes, J. Geophys. Res.-Atmos., 108, https://doi.org/10.1029/2002JD002581, 2003.

Yang, Q., Houze Jr, R. A., Leung, L. R., and Feng, Z.: Environments of long‐lived mesoscale convective systems over the central United States in convection permitting climate simulations, J. Geophys. Res.-Atmos., 122, 13,288-213,307, https://doi.org/10.1002/2017JD027033, 2017.

Yuan, H., McGinley, J. A., Schultz, P. J., Anderson, C. J., and Lu, C.: Short-range precipitation forecasts from time-lagged multimodel ensembles during the HMT-West-2006 campaign, Journal of Hydrometeorology, 9, 477-491, https://doi.org/10.1175/2007JHM879.1, 2008.

Zhang, K., Randel, W. J., and Fu, R.: Relationships between outgoing longwave radiation and diabatic heating in reanalyses, Climate Dynamics, 49, 2911-2929, https://doi.org/10.1007/s00382-016-3501-0, 2017.

1030

Supporting information for

A high-resolution unified observational data product of mesoscale convective systems and isolated deep convection in the United States for 2004 – 2017

Jianfeng Li[1*], Zhe Feng[1], Yun Qian[1*], L. Ruby Leung[1]

[1] Atmospheric Sciences and Global Change Division, Pacific Northwest National Laboratory, Richland, Washington

* *Correspondence to* Jianfeng Li (jianfeng.li@pnnl.gov) and Yun Qian (yun.qian@pnnl.gov)

Table captions

Table S1. Summary of source datasets used to develop the MCS/IDC data product

Table S2. The classification criteria of the Storm Labeling in Three Dimensions (SL3D) algorithm in this study

Table S3. Annual mean precipitation amounts and intensities for different types of precipitation in different regions of the US for 2004 – 2017

Table S4. Annual mean seasonal precipitation amounts and intensities for different types of precipitation in different regions of the US for 2004 – 2017

Table S5. Annual and seasonal mean characteristics of MCS and IDC events in the data product domain for 2004 – 2017 by using the new MCS definition

Table S6. Annual mean precipitation amounts and intensities for different types of precipitation in different regions of the US for 2004 – 2017 by using the new MCS definition

Table S7. Annual mean seasonal precipitation amounts and intensities for different types of precipitation in different regions of the US for 2004 – 2017 by using the new MCS definition

Figure captions

~~**Figure S1.** Schematic of the FLEXTRKR algorithm.~~

Figure S1~~2~~. Schematic of CCS merging and splitting.

Figure S2~~3~~. An example of CCS merging and splitting from 2005-05-07T4:00:00Z – T9:00:00Z. Cloud 1 and Cloud 2 at 5:00:00Z merged into Cloud 1 at 6:00:00Z. And Cloud 1 at 7:00:00Z at least split to Cloud 1 and Cloud 3 at 8:00:00Z.

Figure S3~~4~~. Schematic of "merge" tracks and "split" tracks.

~~**Figure S5.** Definition of MCSs and IDC.~~

Figure S4~~6~~. Seasonal cumulative distribution functions (CDFs) of PF-based lifetimes for (a) MCSs and (b) IDC in the data product domain for 2004 – 2017. Red lines denote spring, blue lines denote summer, green lines denote autumn, and black lines denote winter.

Figure S5~~7~~. Annual mean monthly diurnal cycles of initiated MCS (left panel) and IDC (right panel) numbers in the data product domain for 2004 – 2017. Here, we define that an MCS or IDC event initiates when the first PF appears. Therefore, we can derive the initiated time of all MCS and IDC events, which is the basis of this figure. For example, on average, more than 7 MCSs initiated at 14:00 Local Time (LT) every June between 2004 and 2017.

Figure S6~~8~~. Distributions of the fractions of different types of precipitation in each season. Here, precipitation refers to annual mean seasonal amounts for 2004 – 2017. We exclude hourly data with precipitation $\leq$ 1 mm h^{-1} in the calculation. The first row is for total precipitation, the second for MCS precipitation, the third for IDC precipitation, and the fourth for ~~stratiform~~ NC precipitation. The first column shows spring precipitation, the second for summer, the third for autumn, and the fourth for winter.

Figure S7~~9~~. Distributions of annual mean seasonal precipitation intensities for different types of precipitation for 2004 – 2017. The first row is for total precipitation, the second for MCS precipitation, the third for IDC precipitation, and the fourth for ~~stratiform~~ NC precipitation. The first column shows spring precipitation, the second for summer, the third for autumn, and the fourth for winter. We exclude hourly data with precipitation $\leq$ 1 mm h^{-1} in the calculation.

Figure ~~S10~~S8. Monthly mean diurnal cycles of precipitation intensities for MCSs (a, d, g, j), IDC (b, e, h, k), and ~~stratiform~~ NC (c, f, i, l) in the NGP (a, b, c), SGP (d, e, f), SE (g, h, i), and NE (j, k, l) during 2004 – 2017.

Figure ~~S11~~S9. An example of Stage IV erroneous precipitation. Stage IV shows a large area of intense precipitation suddenly appearing at 2011-05-02T12:00:00Z, which then

unexpectedly disappears at 13:00:00Z, comes back abruptly at 14:00:00Z, and finally goes away immediately at 17:00:00Z.

Figure S102. Distribution of the fraction of valid Stage IV precipitation data for 2004 – 2017. Here, "valid" means that precipitation data are available and reasonable. The erroneous precipitation discussed in the main manuscript is unreasonable and invalid.

Figure S113. Distributions of the fractions of available radar reflectivity data for 2004 – 2017 at different vertical levels. As long as radars scan a grid cell, we think it as "available" even though there is no echo.

73 **Table S1.** Summary of source datasets used to develop the MCS/IDC data product

Dataset name	NCEP/CPP L3 half-hourly 4 km Global Merged IR	Three-dimensional Gridded NEXRAD Radar (Gridrad)	NCEP Stage IV precipitation	ERA5 melting level
Dataset version	V 1	V 3.1	V 1.0	
DOI	10.5067/P4HZB9N27EKU	10.5065/D6NK3CR7	10.5065/D69Z93M3	10.24381/cds.adbb2d47
URL	https://disc.gsfc.nasa.gov/datasets/GPM_MERGIR_1/summary	https://rda.ucar.edu/datasets/ds841.0/	https://rda.ucar.edu/datasets/ds507.5/	https://cds.climate.copernicus.eu/cdsapp#!/dataset/reanalysis-era5-single-levels?tab=overview
Last access	Dec 28, 2019	Jan 2, 2020	Dec 28, 2019	Jan 24, 2020
Initial spatial resolution	Horizontal: ~ 4 km	Horizontal: 0.02° Vertical: 1 km	Horizontal: ~ 4 km	Horizontal: 0.25°
Initial temporal resolution	0.5 hours	1 hour	1 hour	1 hour

74

Table S2. The classification criteria of the Storm Labeling in Three Dimensions (SL3D) algorithm in this study

SL3D category	Criteria
convective	Z_H[1] = 25 dBZ echo-top height ≥ 10 km; or Z_H ≥ 45 dBZ above (Z_{melt}[2] + 1) km; or Z_H peakedness[3] exceeding thresholds[4] in at least 30% of the echo column between surface and 9 km. After the above filtering, exclude isolated convective grid points. Finally, grid points that have Z_{Hmax}[5] ≥ 25 dBZ and are immediately adjacent to other convective grid points are classified as convective.
precipitating stratiform	Z_H ≥ 20 dBZ at 3 km; or Z_H ≥ 10 dBZ at 1 km or 2 km
non-precipitating stratiform	no echo or Z_H < 20 dBZ at 3 km, and echo presents above 3 km. If no echo at 3 km – 5 km, but echo presents above 5 km, classified as an anvil.
anvil	No echo at 3 km – 5 km, but echo presents above 5 km
convective updraft	convective grid points satisfy: (1) Z_{Hmax} ≥ 40 dBZ, and (2) $\frac{\partial Z_H}{\partial z} \geq 8$ dBZ km^{-1} with echoes in at least six of eight horizontally adjacent grid volumes presents between the surface and 7 km.

[1] Z_H: logarithmic radar reflectivity.

[2] Z_{melt}: melting level height. If temperatures at different vertical levels within a grid column are all below zero, there is no melting level. In this situation, we set Z_{melt} = -2.

[3] Peakedness is the difference between the Z_H of the grid point being evaluated and the median Z_H of a horizontal 12-km radius around the point.

[4] $threshold = \max\left(4.0\,dBZ, 10.0 - \frac{Z_H^2}{337.5}\,dBZ\right)$.

[5] Z_{Hmax} denotes column max reflectivity.

Table S3. Annual mean precipitation amounts and intensities for different types of precipitation in different regions of the US for 2004 – 2017

	Precipitation amount / mm				Precipitation intensity / mm h^{-1}			
	Total	MCS	IDC	~~Stratiform~~NC	Total	MCS	IDC	~~Stratiform~~NC
NGP	515	254	116	145	3.3	4.3	3.3	2.4
SGP	613	308	149	156	4.1	5.2	4.4	2.9
SE	1,156	526	303	327	4.5	5.2	5.3	3.3
NE	889	324	228	337	3.2	3.7	3.6	2.6

Table S4. Annual mean seasonal precipitation amounts and intensities for different types of precipitation in different regions of the US for 2004 – 2017

		Precipitation amount / mm				Precipitation intensity / mm h^{-1}			
		Total	MCS	IDC	~~Stratiform~~NC	Total	MCS	IDC	~~Stratiform~~NC
NGP	spring	150	78	31	40	2.9	3.6	2.8	2.2
	summer	214	117	47	50	4.2	5.0	4.5	3.0
	autumn	109	43	27	39	2.9	3.9	3.1	2.3
	winter	42	15	11	15	1.9	2.4	1.9	1.7
SGP	spring	176	119	27	30	4.2	5.2	3.9	2.9
	summer	200	83	71	47	4.7	5.5	5.3	3.2
	autumn	150	62	36	52	4.1	5.3	4.6	3.0
	winter	87	44	16	27	2.8	3.6	2.6	2.2
SE	spring	275	157	52	66	4.6	5.3	4.8	3.3
	summer	367	112	156	99	5.2	5.7	6.1	3.7
	autumn	249	109	55	85	4.6	5.4	5.5	3.5
	winter	265	147	40	78	3.8	4.7	3.7	2.8
NE	spring	230	97	56	78	2.9	3.5	3.2	2.4
	summer	276	80	85	111	4.2	4.9	5.0	3.3
	autumn	218	75	49	94	3.2	3.8	3.6	2.6
	winter	165	72	39	55	2.4	2.9	2.4	2.1

Table S5. Annual and seasonal mean characteristics of MCS and IDC events in the data product domain for 2004 – 2017 by using the new MCS definition[1]

	MCS					IDC				
	annual	spring	summer	autumn	winter	annual	spring	summer	autumn	winter
CCS-based lifetime / hour	17.1	17.6	16.0	18.2	20.0	2.0	2.1	2.0	2.0	2.6
CCS area / km^2	135,541	172,517	93,828	139,837	295,931	6,657	9,379	4,314	6,352	21,484
CCS major axis length / km	579	667	475	615	935	99	117	85	99	173
PF-based lifetime / hour	15.0	15.6	14.1	15.8	17.1	1.6	1.6	1.6	1.6	1.8
Major axis length of the largest PF / km	321	357	264	357	518	63	69	55	68	93
PF convective area / km^2	6,119	6,468	6,091	5,897	5,697	477	496	463	487	520
PF stratiform area / km^2	28,570	34,718	17,997	34,607	67,902	1,205	1,559	774	1,517	3,113
PF mean convective rain rate / mm h^{-1}	4.5	4.0	4.8	4.6	3.9	4.1	3.4	4.5	4.3	3.0
PF mean stratiform rain rate /mm h^{-1}	2.7	2.4	2.8	2.7	2.3	2.8	2.5	3.0	2.9	2.3
~~Area with $Z_{Hmax} \geq$ 45 dBZ within the largest PF / km^2~~	~~791~~	~~862~~	~~850~~	~~617~~	~~563~~	~~54~~	~~56~~	~~57~~	~~47~~	~~42~~
PF mean convective 20-dBZ echo-top height / km	6.6	6.2	7.2	6.1	5.0	6.5	6.1	7.0	6.2	5.0
Area of the largest CCF / km^2	2,094	2,081	2,317	1,754	1,392	339	355	333	337	347
Major axis length of the largest CCF / km	95	96	99	88	82	29	30	28	29	30
~~Max 30-dBZ echo-top height of the largest CCF / km~~	~~12.7~~	~~12.2~~	~~13.9~~	~~11.6~~	~~9.4~~	~~7.0~~	~~6.4~~	~~7.6~~	~~6.5~~	~~5.0~~
~~Max 40-dBZ echo-top height of the largest CCF / km~~	~~10.4~~	~~10.2~~	~~11.4~~	~~8.9~~	~~7.1~~	~~5.4~~	~~5.0~~	~~5.9~~	~~5.0~~	~~3.7~~

[1] Refer to Section 4.4 in the main manuscript for the new MCS definition.

Table S6. Annual mean precipitation amounts and intensities for different types of precipitation in different regions of the US for 2004 – 2017 by using the new MCS definition

	Precipitation amount / mm				Precipitation intensity / mm h^{-1}			
	Total	MCS	IDC	~~Stratiform~~NC	Total	MCS	IDC	~~Stratiform~~NC
NGP	515	280	89	145	3.3	4.2	3.2	2.4
SGP	613	344	113	156	4.1	5.1	4.4	2.9
SE	1,156	602	227	327	4.5	5.3	5.3	3.3
NE	889	371	181	337	3.2	3.7	3.5	2.6

Table S7. Annual mean seasonal precipitation amounts and intensities for different types of precipitation in different regions of the US for 2004 – 2017 by using the new MCS definition

		Precipitation amount / mm				Precipitation intensity / mm h^{-1}			
		Total	MCS	IDC	~~Stratiform~~NC	Total	MCS	IDC	~~Stratiform~~NC
NGP	spring	150	83	26	41	2.9	3.5	2.8	2.2
	summer	214	130	34	50	4.2	5.0	4.5	3.0
	autumn	109	50	20	39	2.9	3.8	3.0	2.3
	winter	42	17	9	16	1.9	2.4	1.9	1.7
SGP	spring	176	126	20	30	4.2	5.0	3.9	2.9
	summer	200	102	51	47	4.7	5.5	5.2	3.2
	autumn	150	70	28	52	4.1	5.2	4.5	3.0
	winter	87	47	13	27	2.8	3.5	2.6	2.2
SE	spring	275	170	39	66	4.6	5.2	4.8	3.3
	summer	367	153	115	99	5.2	5.8	6.1	3.7
	autumn	249	122	42	85	4.6	5.4	5.5	3.5
	winter	265	156	31	78	3.8	4.6	3.7	2.8
NE	spring	230	108	44	78	2.9	3.5	3.1	2.4
	summer	276	99	66	111	4.2	4.9	5.0	3.3
	autumn	218	85	39	94	3.2	3.8	3.5	2.6
	winter	165	79	31	55	2.4	2.9	2.3	2.1

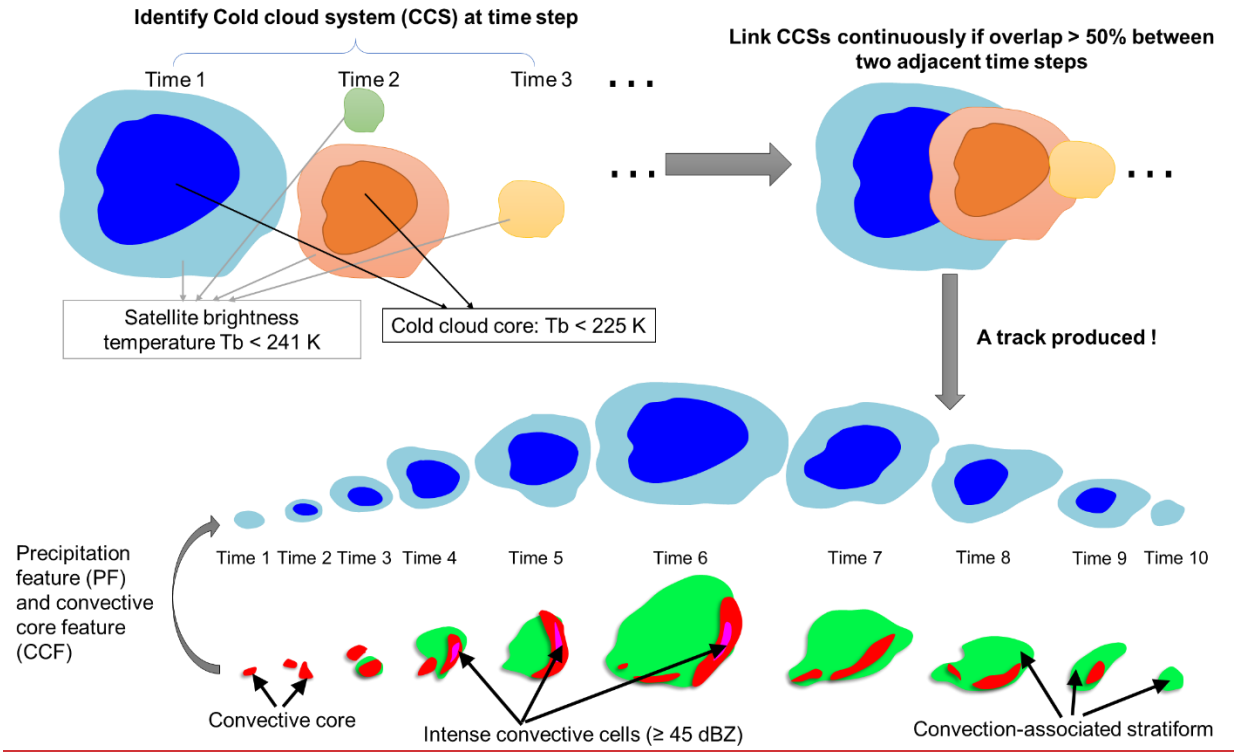

~~Figure S1.~~ ~~Schematic of the FLEXTRKR algorithm.~~

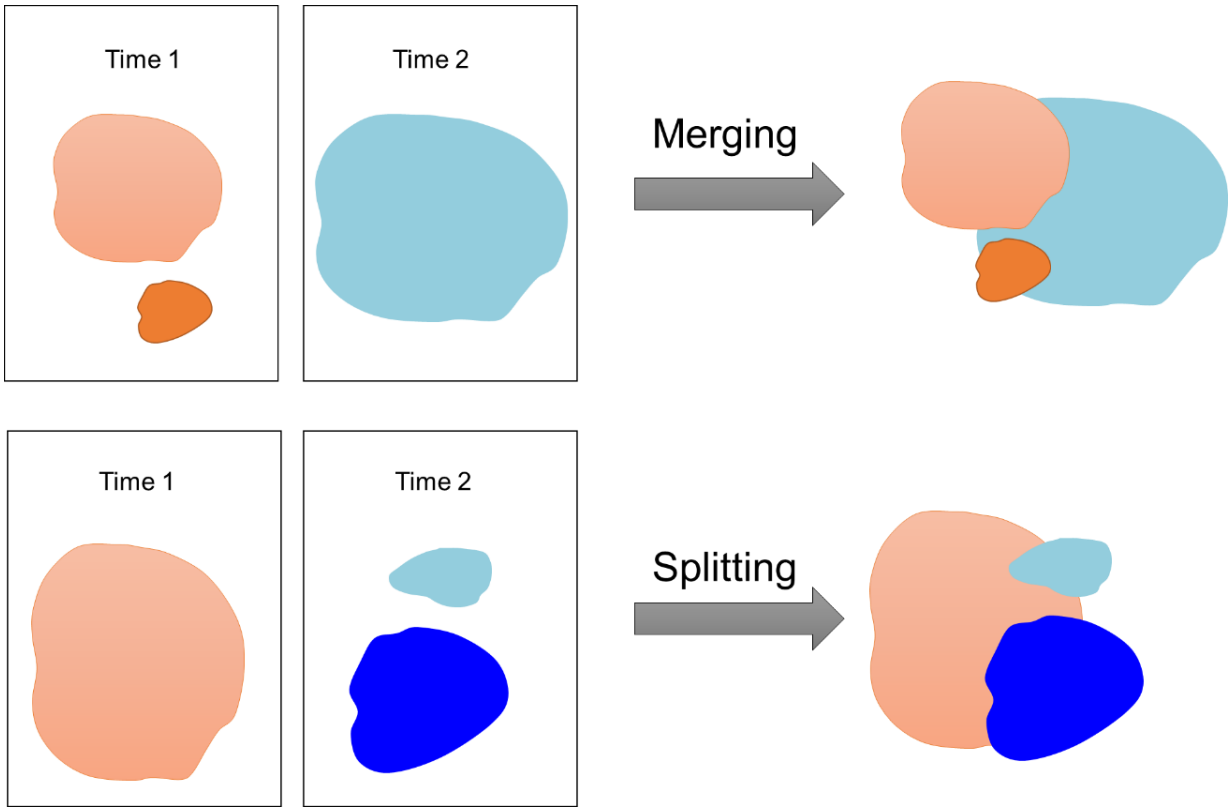

Figure ~~S2~~S1. Schematic of CCS merging and splitting.

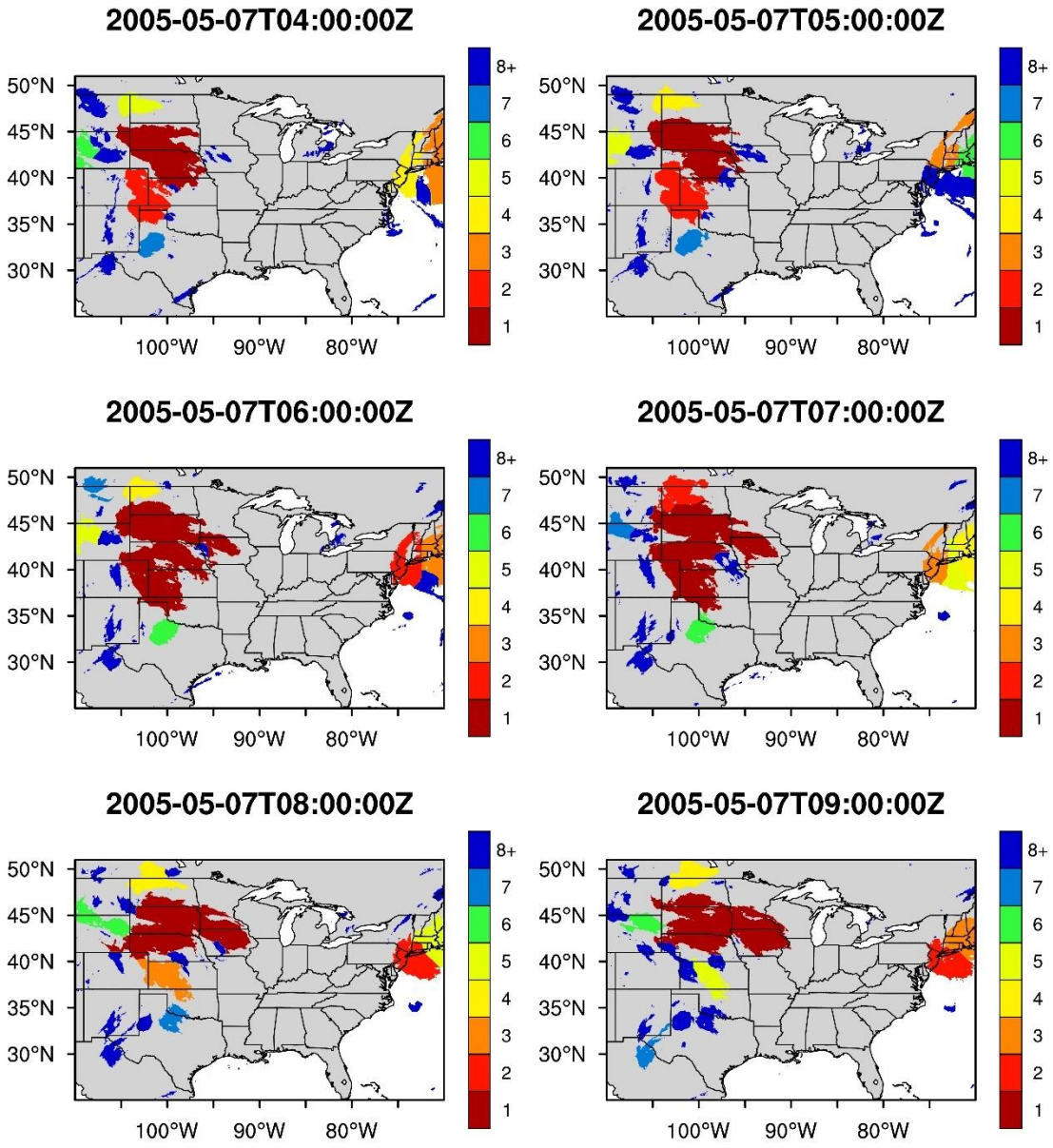

Figure ~~S3~~S2. An example of CCS merging and splitting from 2005-05-07T4:00:00Z – T9:00:00Z. Cloud 1 and Cloud 2 at 5:00:00Z merged into Cloud 1 at 6:00:00Z. And Cloud 1 at 7:00:00Z at least split to Cloud 1 and Cloud 3 at 8:00:00Z.

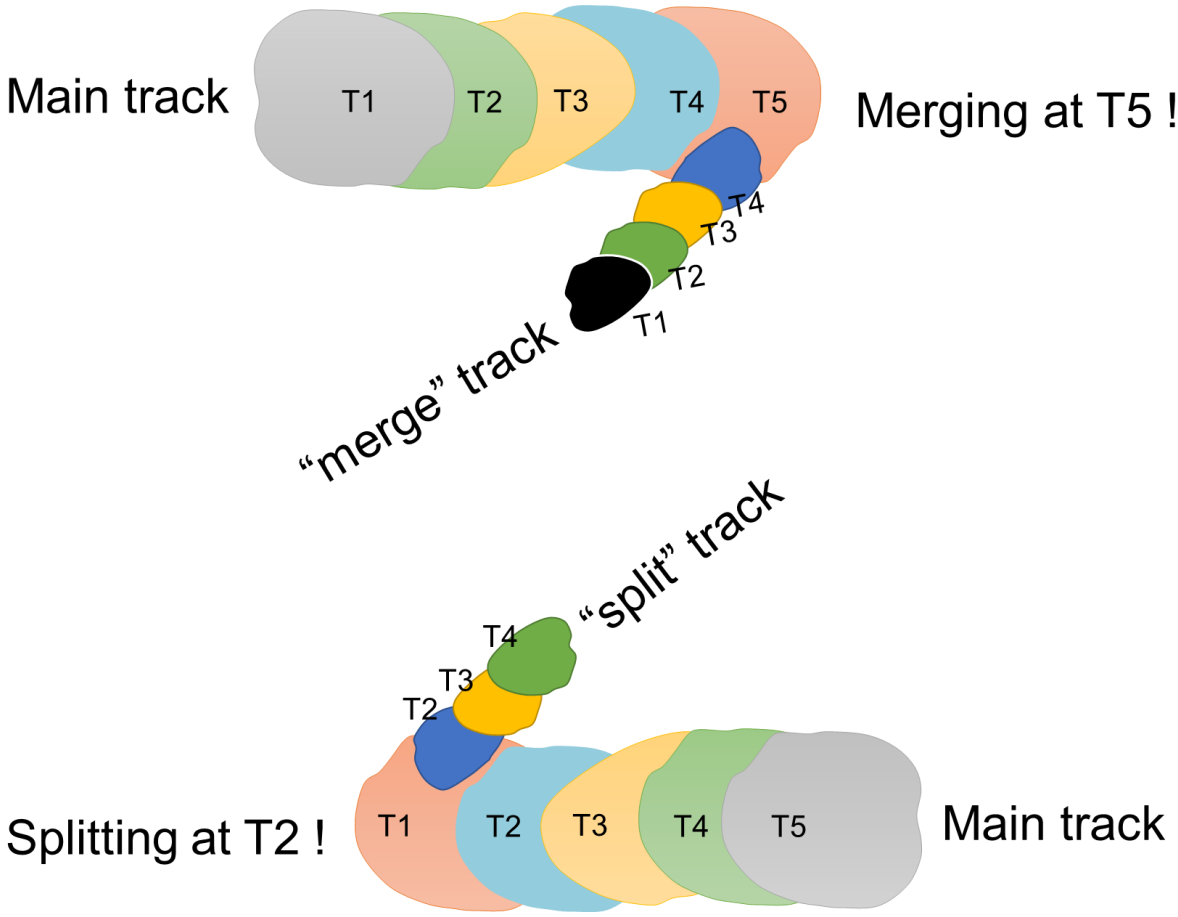

107

108 **Figure ~~S4~~S3.** Schematic of “merge” tracks and “split” tracks.

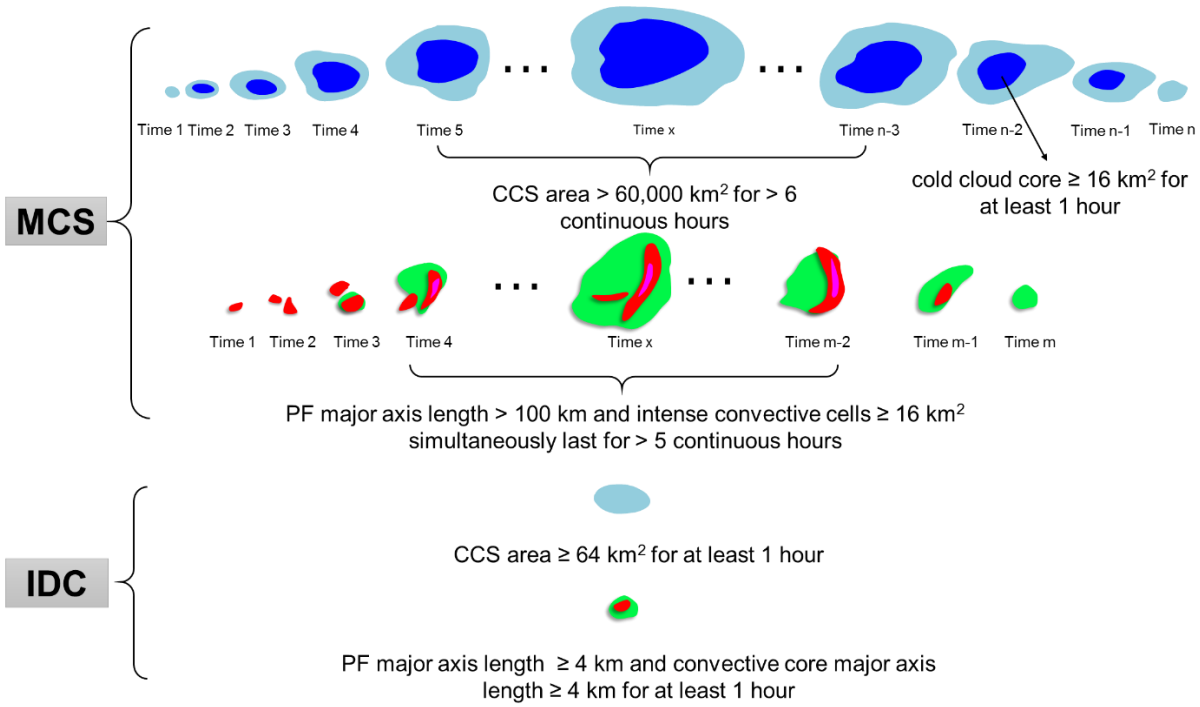

~~Figure S5.~~ ~~Definition of MCSs and IDC.~~

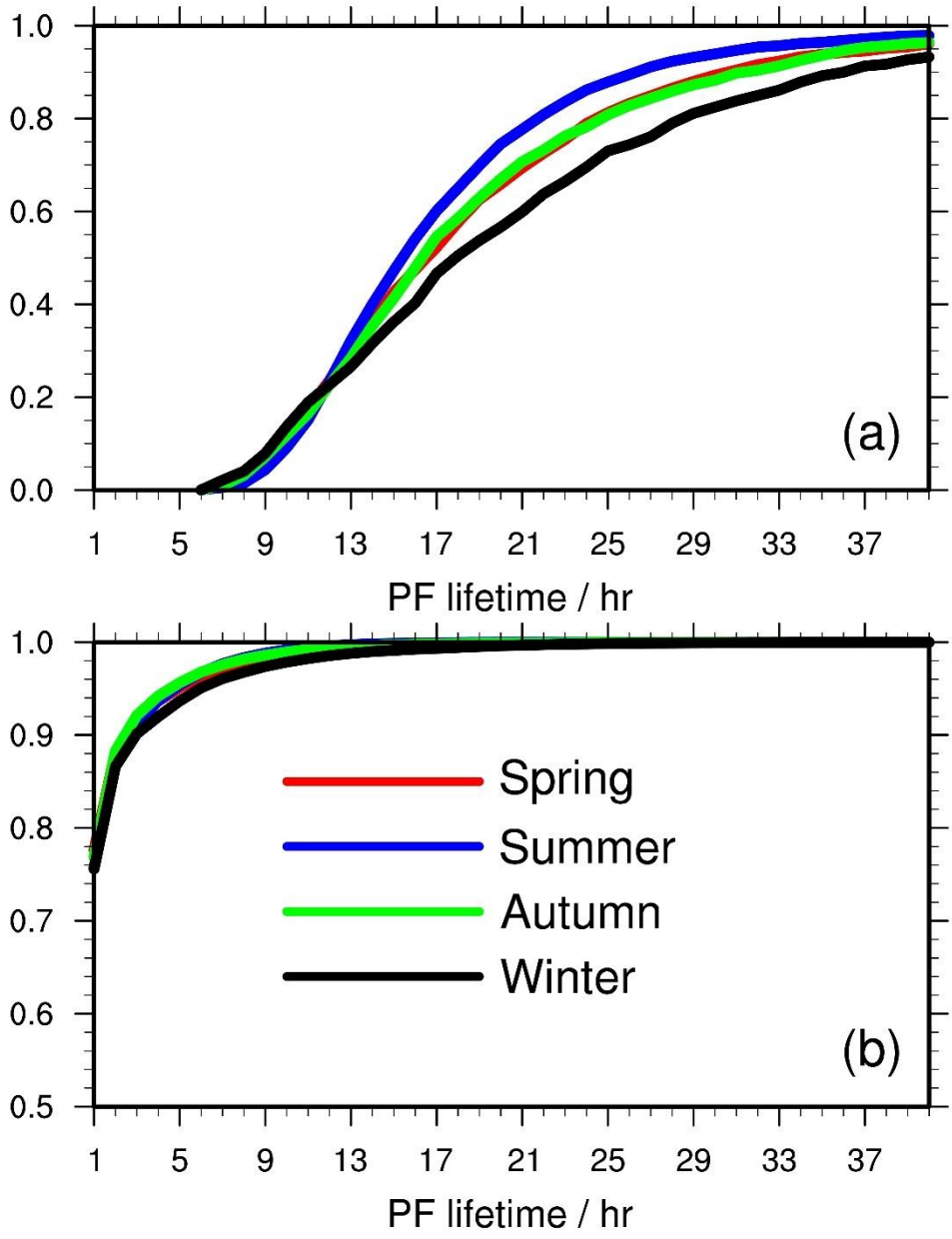

Figure ~~S6~~S4. Seasonal cumulative distribution functions (CDFs) of PF-based lifetimes for (a) MCSs and (b) IDC in the data product domain for 2004 – 2017. Red lines denote spring, blue lines denote summer, green lines denote autumn, and black lines denote winter.

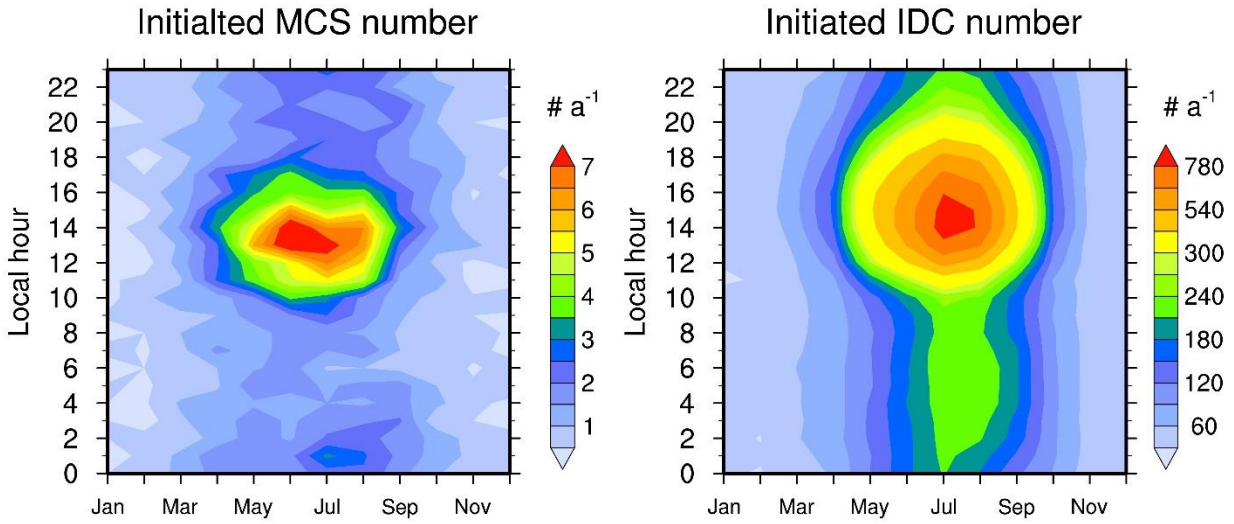

Figure ~~S7~~S5. Annual mean monthly diurnal cycles of initiated MCS (left panel) and IDC (right panel) numbers in the data product domain for 2004 – 2017. Here, we define that an MCS or IDC event initiates when the first PF appears. Therefore, we can derive the initiated time of all MCS and IDC events, which is the basis of this figure. For example, on average, more than 7 MCSs initiated at 14:00 Local Time (LT) every June between 2004 and 2017.

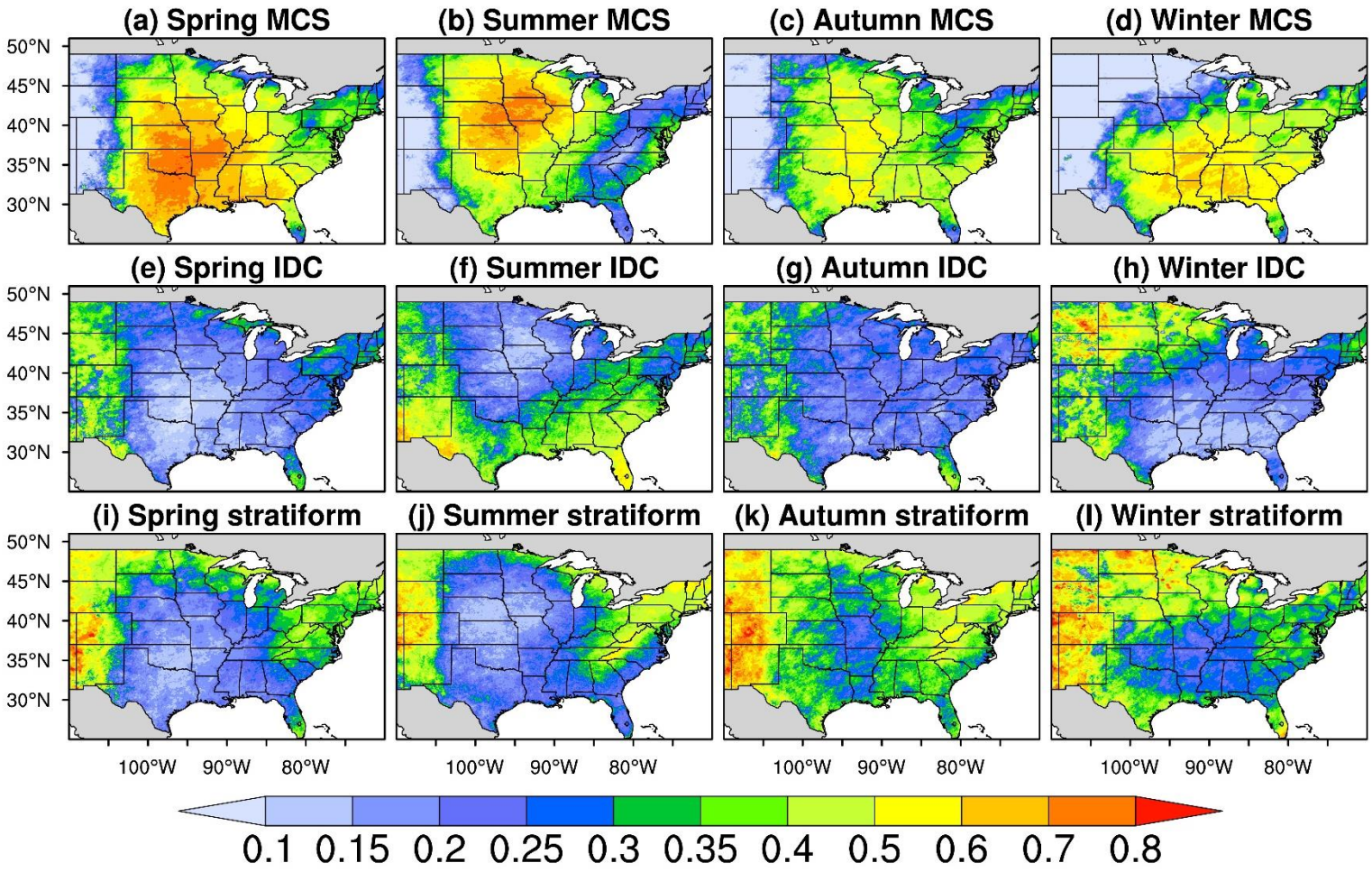
(a) Spring MCS
(b) Summer MCS
(c) Autumn MCS
(d) Winter MCS
(e) Spring IDC
(f) Summer IDC
(g) Autumn IDC
(h) Winter IDC
(i) Spring stratiform
(j) Summer stratiform
(k) Autumn stratiform
(l) Winter stratiform
50°N
45°N
40°N
35°N
30°N
100°W
90°W
80°W
0.1 0.15 0.2 0.25 0.3 0.35 0.4 0.5 0.6 0.7 0.8

123

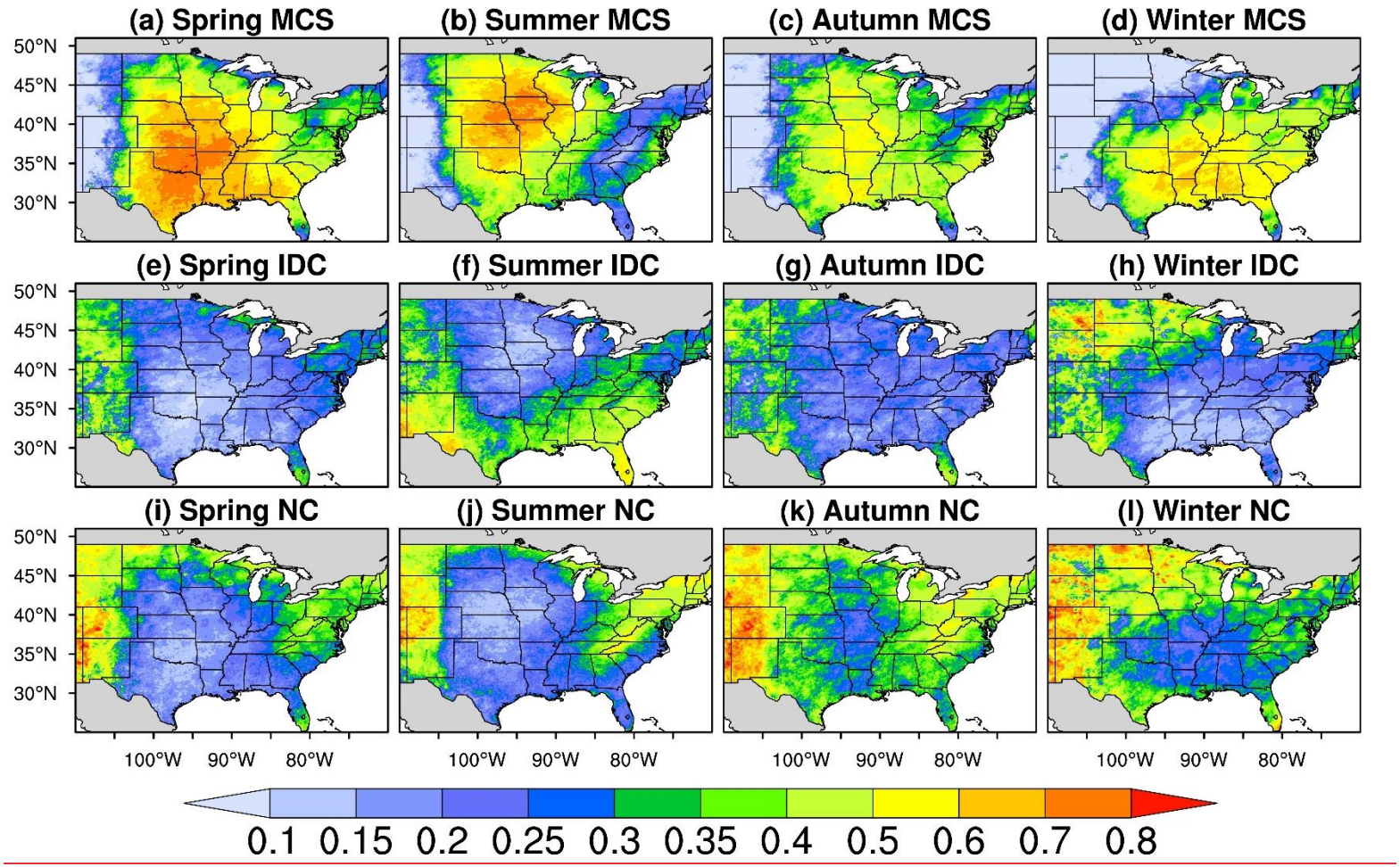

Figure ~~S8~~S6. Distributions of the fractions of different types of precipitation in each season. Here, precipitation refers to annual mean seasonal amounts for 2004 – 2017. We exclude hourly data with precipitation ≤ 1 mm h^{-1} in the calculation. The first row is for total precipitation, the second for MCS precipitation, the third for IDC precipitation, and the fourth for ~~stratiform~~ NC precipitation. The first column shows spring precipitation, the second for summer, the third for autumn, and the fourth for winter.

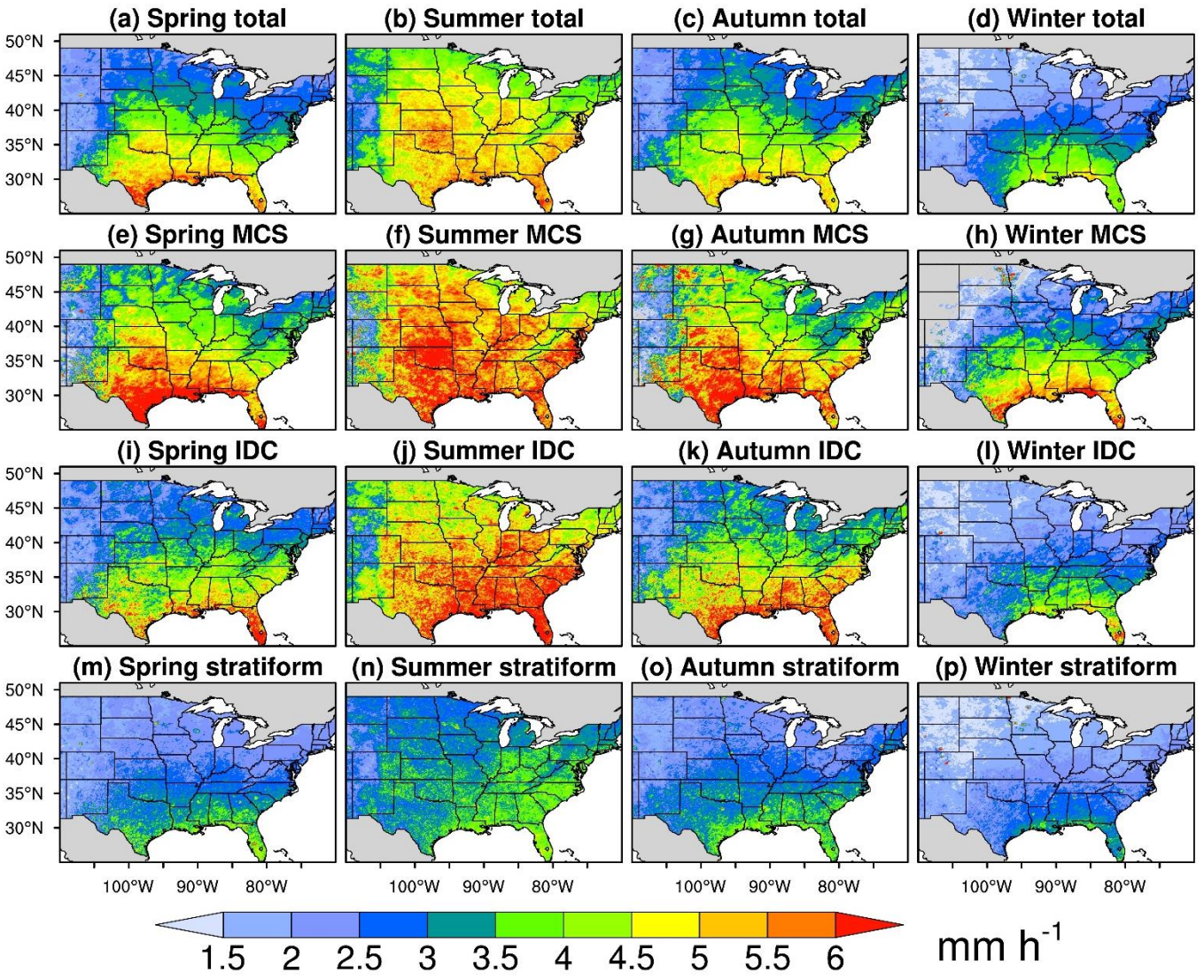
(a) Spring total
(b) Summer total
(c) Autumn total
(d) Winter total
(e) Spring MCS
(f) Summer MCS
(g) Autumn MCS
(h) Winter MCS
(i) Spring IDC
(j) Summer IDC
(k) Autumn IDC
(l) Winter IDC
(m) Spring stratiform
(n) Summer stratiform
(o) Autumn stratiform
(p) Winter stratiform
50°N
45°N
40°N
35°N
30°N
100°W
90°W
80°W
1.5
2
2.5
3
3.5
4
4.5
5
5.5
6
mm h-1

130

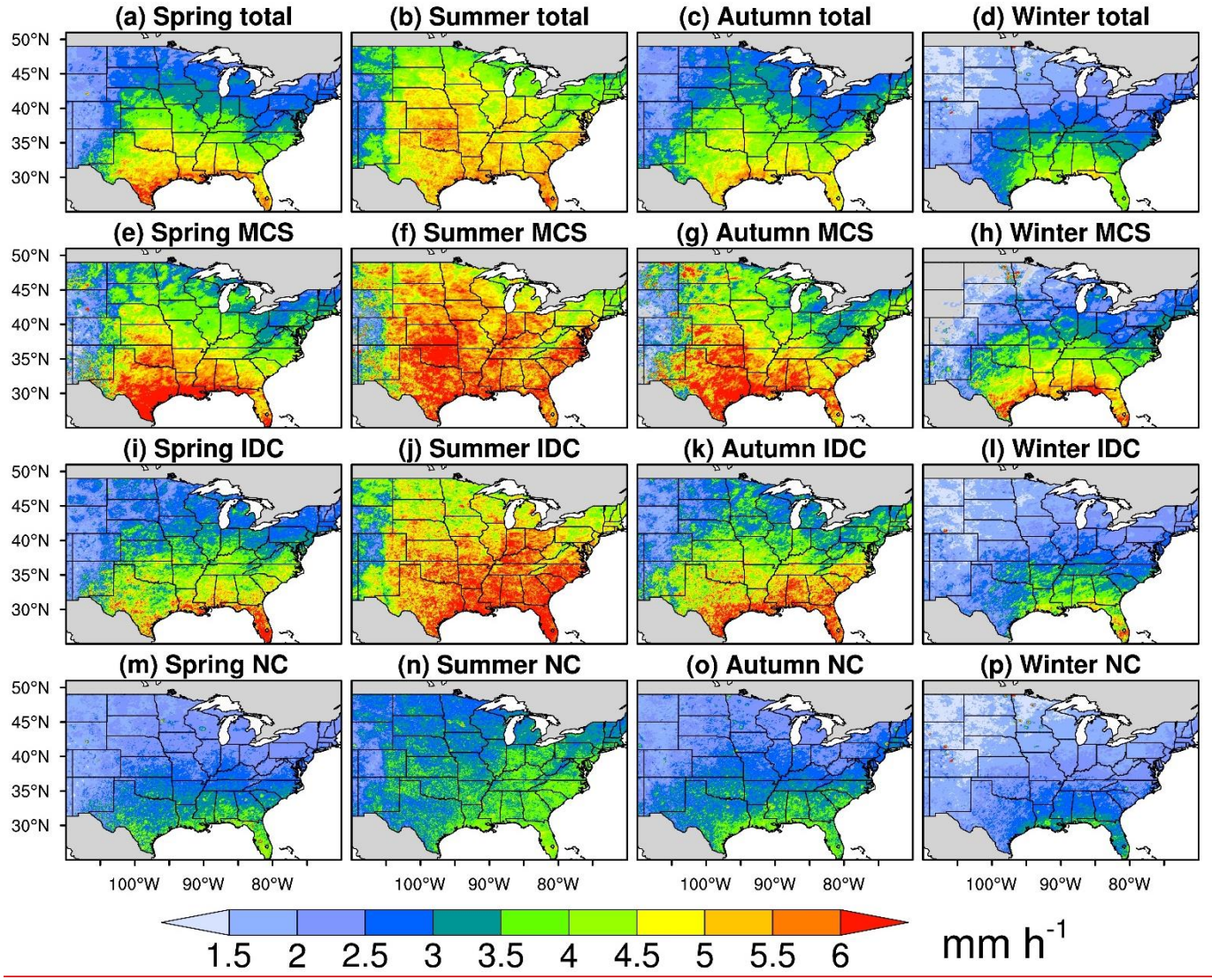

Figure ~~S9~~S7. Distributions of annual mean seasonal precipitation intensities for different types of precipitation for 2004 – 2017. The first row is for total precipitation, the second for MCS precipitation, the third for IDC precipitation, and the fourth

for ~~stratiform~~ NC precipitation. The first column shows spring precipitation, the second for summer, the third for autumn, and the fourth for winter. We exclude hourly data with precipitation ≤ 1 mm h^{-1} in the calculation.

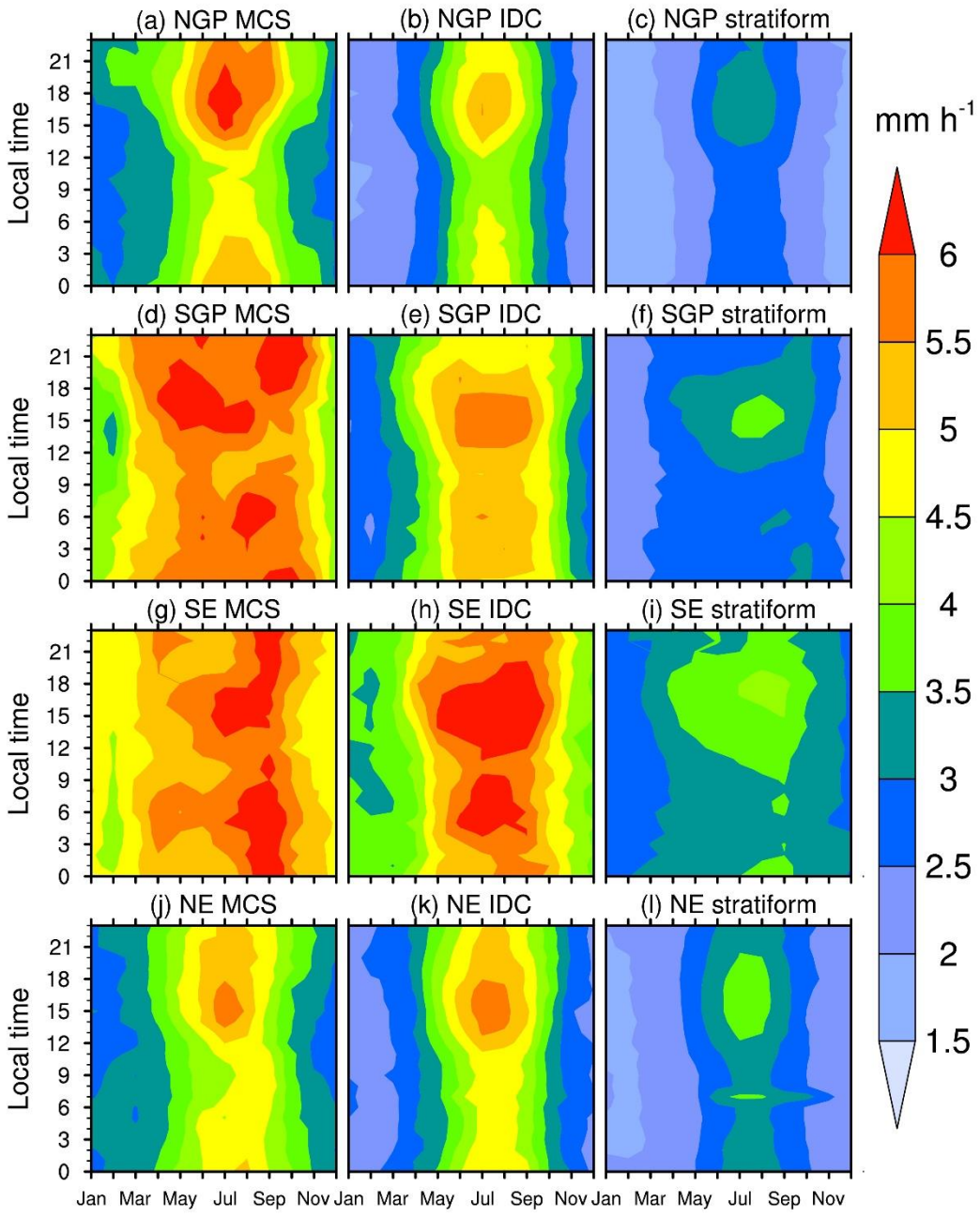
(a) NGP MCS
(b) NGP IDC
(c) NGP stratiform
(d) SGP MCS
(e) SGP IDC
(f) SGP stratiform
(g) SE MCS
(h) SE IDC
(i) SE stratiform
(j) NE MCS
(k) NE IDC
(l) NE stratiform
Local time
0
3
6
9
12
15
18
21
Jan Mar May Jul Sep Nov
mm h-1
6
5.5
5
4.5
4
3.5
3
2.5
2
1.5

136

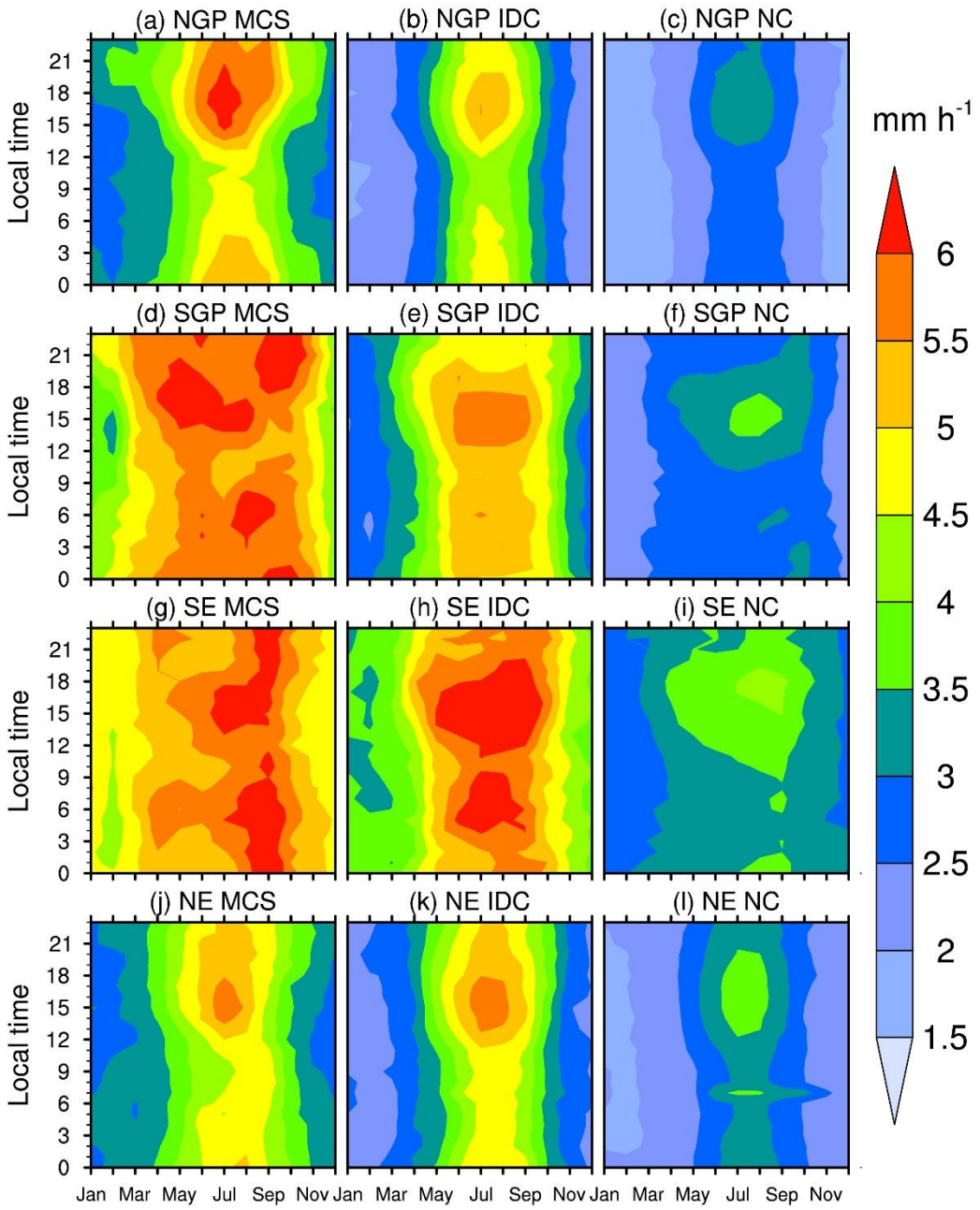

Figure ~~S10~~S8. Monthly mean diurnal cycles of precipitation intensities for MCSs (a, d, g, j), IDC (b, e, h, k), and ~~stratiform~~ NC (c, f, i, l) in the NGP (a, b, c), SGP (d, e, f), SE (g, h, i), and NE (j, k, l) during 2004 – 2017.

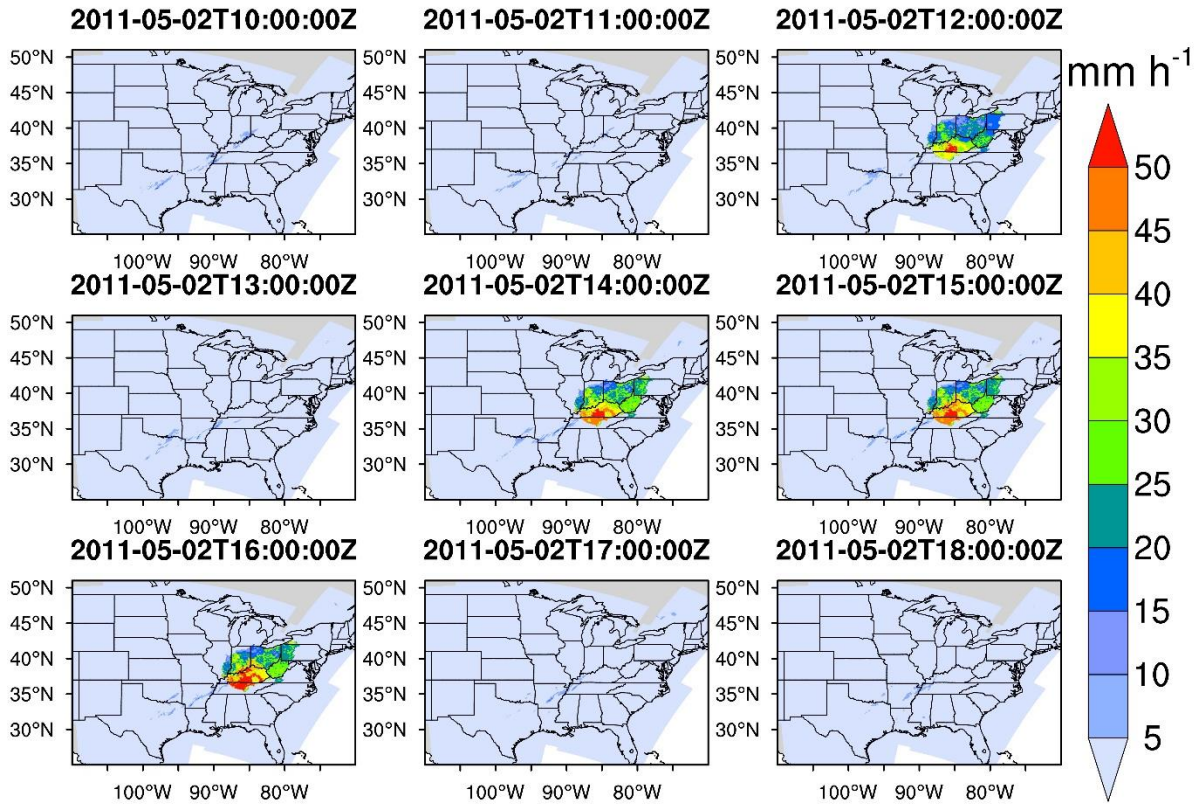

Figure ~~S11~~S9. An example of Stage IV erroneous precipitation. Stage IV shows a large area of intense precipitation suddenly appearing at 2011-05-02T12:00:00Z, which then unexpectedly disappears at 13:00:00Z, comes back abruptly at 14:00:00Z, and finally goes away immediately at 17:00:00Z.

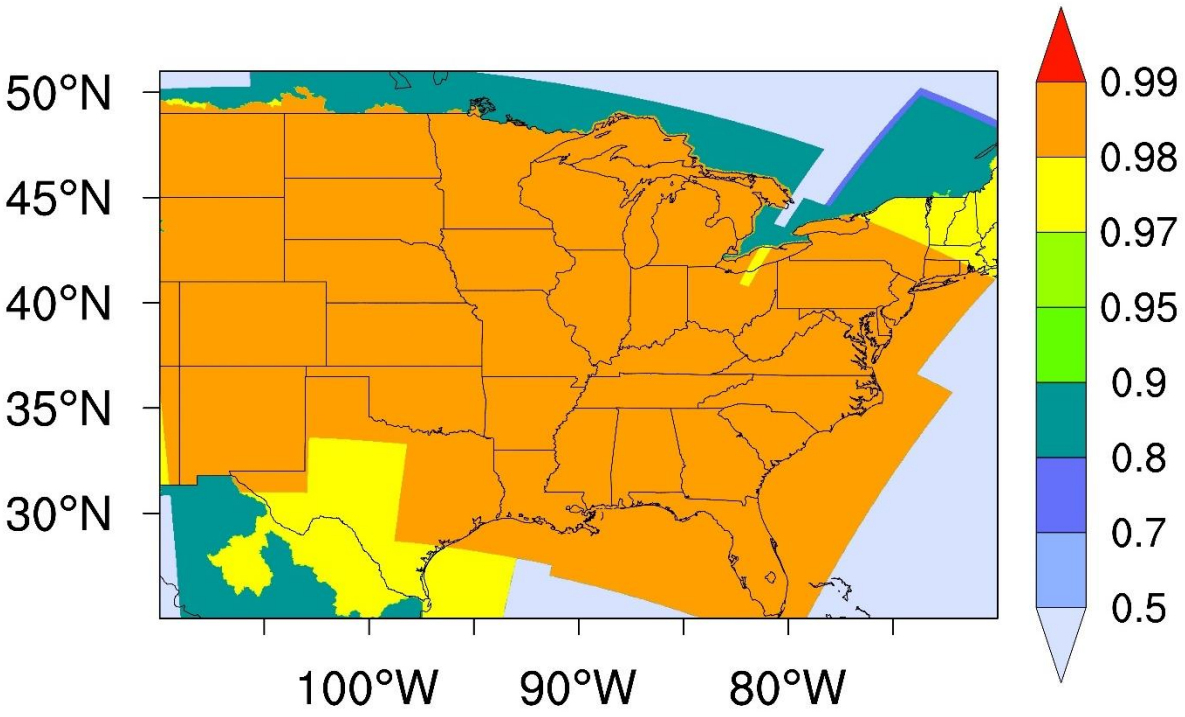

Figure ~~S12~~S10. Distribution of the fraction of valid Stage IV precipitation data for 2004 – 2017. Here, "valid" means that precipitation data are available and reasonable. The erroneous precipitation discussed in the main manuscript is unreasonable and invalid.

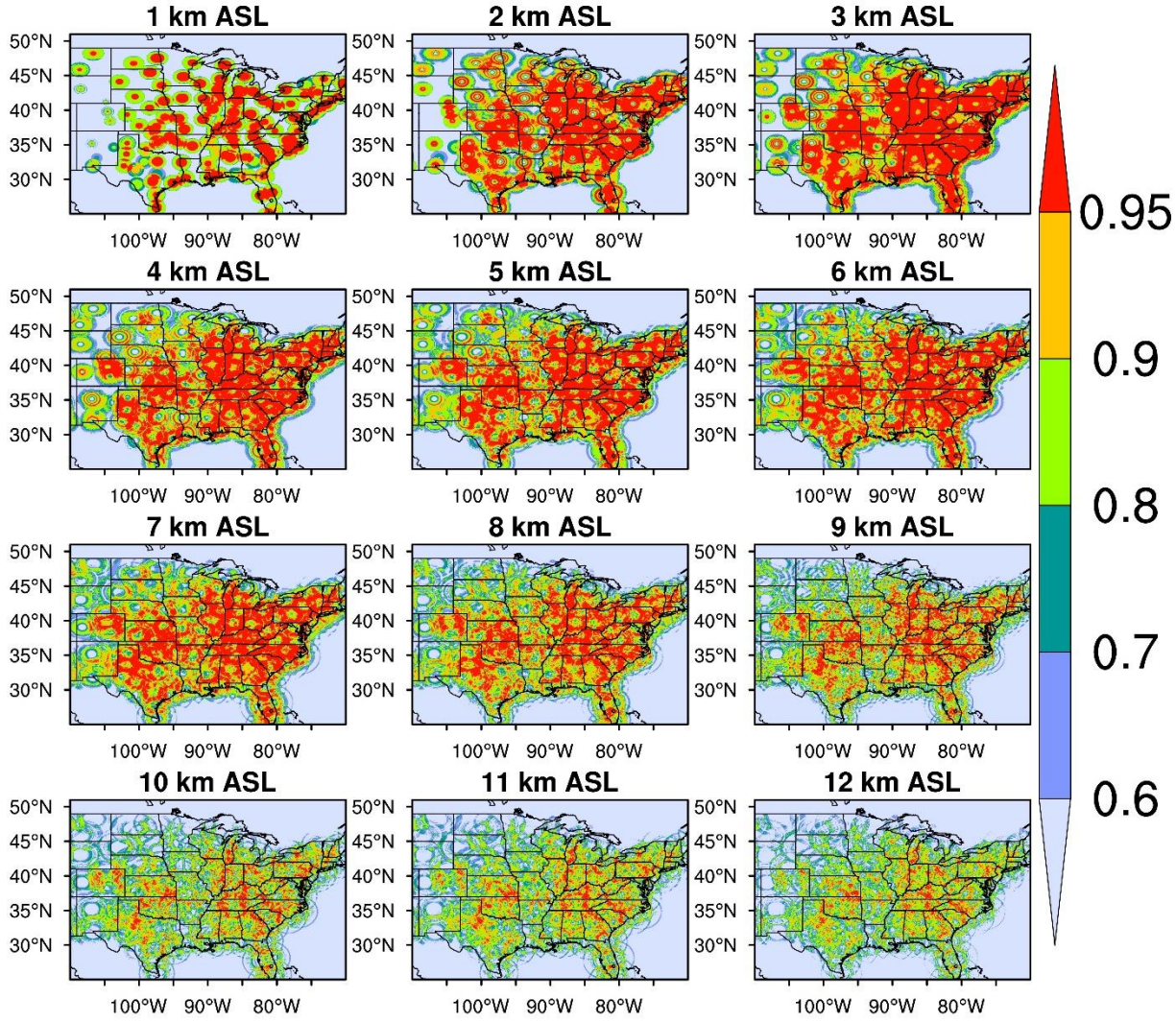

Figure ~~S13~~S11. Distributions of the fractions of available radar reflectivity data for 2004 – 2017 at different vertical levels. As long as radars scan a grid cell, we think it as "available" even though there is no echo.